

University of Alberta

Observation and modeling of ice jam release
events on the Hay River, NWT

by

David Watson

A thesis submitted to the Faculty of Graduate Studies and Research
in partial fulfillment of the requirements for the degree of

Master of Science

in

Water Resources Engineering

Department of Civil and Environmental Engineering

©David Watson
Spring 2011
Edmonton, Alberta

Permission is hereby granted to the University of Alberta Libraries to reproduce single copies of this thesis and to lend or sell such copies for private, scholarly or scientific research purposes only. Where the thesis is converted to, or otherwise made available in digital form, the University of Alberta will advise potential users of the thesis of these terms.

The author reserves all other publication and other rights in association with the copyright in the thesis and, except as herein before provided, neither the thesis nor any substantial portion thereof may be printed or otherwise reproduced in any material form whatsoever without the author's prior written permission.

Examining Committee

Dr. Faye Hicks, Civil and Environmental Engineering

Dr. Mark Loewen, Civil and Environmental Engineering

Dr. Paul Myers, Earth and Atmospheric Science

Abstract

The Town of Hay River experiences significant threats to life and property each spring as ice jam release events from upstream bring waves of ice and water to the town. The development of a forecasting tool for ice jam release events has been limited by insufficient data, especially regarding the speed of ice runs associated with ice jam release events. The purpose of this research was to document and analyze ice jam release events to provide the town warning of their potential timing and magnitude, and to contribute to general knowledge on ice jam release. Comprehensive field programs were undertaken from 2007 to 2009, and this new data was used to assess the *RiverID* ice jam release forecasting model. Although the model showed reasonable approximations for wave arrival times for flood forecasting purposes, the predicted speeds and arrival times of ice runs did not agree very well with field observations.

Acknowledgments

This study was the result of a collaboration between the University of Alberta, The Town of Hay River and Indian and Northern Affairs Canada. A major source of funding for this research was provided by the Natural Sciences and Engineering Research Council of Canada (NSERC) through the Strategic Grants program. This funding provided funds for the field program as well as stipends for graduate students and was greatly appreciated.

The author would like to thank Dr. Faye Hicks for her support and guidance. The entire river ice team is thanked for all their help: Robyn Andrishak, Brett Howard and Wendy Howard. The Hay River research team are also thanked for their tireless work and long hour in the field: Michael Brayall, Nadia Kovachis, Chris Krath, Joshua Maxwell, Janell Morley, Jennifer Nafziger, Liming Zhao and research partners Shawne Kokelj and Meg McCluskie, from the Department of Indian Affairs and Northern Development.

The author acknowledges Dr. Mark Loewen from the Water Resources group and Dr. Paul Myers from the Earth and Atmospheric Sciences group. Their participation on such short notice is greatly appreciated.

1.0	Introduction.....	1
2.0	Site Description and Field Program.....	6
2.1	Reach Description	6
2.2	Geometric Data.....	7
2.2.1	Survey Data	7
2.2.2	Map Data	8
2.2.2.1	Bed Profile.....	8
2.2.2.2	Top Widths	9
2.2.3	Channel Roughness	9
2.3	Hydrometric Data	9
2.3.1	Water Survey of Canada.....	10
2.3.2	The Town of Hay River Emergency Measures Operations.....	12
2.3.3	Discharge.....	16
2.4	Field Investigations and Progression of Breakup.....	16
2.4.1	Methods	17
2.4.1.1	Observational Flights.....	17
2.4.1.2	Time-Lapse Camera Stations.....	18
2.4.1.3	Identification of Ice Jam Release Events.....	21
2.4.2	2007 Breakup Observations and Analysis.....	22
2.4.2.1	2007 General Progression of Breakup.....	22
2.4.2.2	2007 Observed Water Waves and Ice Runs	23
2.4.3	2008 Breakup Observations and Analysis.....	28
2.4.3.1	2008 General Progression of Breakup.....	28
2.4.3.2	2008 Observed Water Waves and Ice Runs	29
2.4.4	2009 Breakup Observations and Analysis.....	32
2.4.4.1	2009 General Progression of Breakup.....	33
2.4.4.2	2009 Observed Water Waves and Ice Runs	33
2.4.5	Summary of Breakup Analysis 2007-2009	41
2.5	Observed Ice Jam Release Events	42
2.5.1	Ice Jam Release Event 1 - 2007.....	42
2.5.2	Ice Jam Release Event 2 - 2007.....	43

2.5.3	Ice Jam Release Event 3 - 2008.....	45
2.5.4	Ice Jam Release Event 4 – 2008.....	48
2.5.5	Ice Jam Release Event 5 - 2009.....	49
2.5.6	Ice Jam Release Event 6 – 2009.....	50
2.5.7	Summary of Ice Jam Release Events.....	52
3.0	<i>River1D</i> Modeling of Ice Jam Release Events.....	53
3.1	Previous Ice Jam Release Event Modeling.....	53
3.2	Model Description and Setup.....	57
3.2.1	Model Formulation.....	57
3.2.1.1	Ice Jam Formation: Steady Flow Analysis Modelling.....	57
3.2.1.2	Ice Jam Release: Unsteady Flow Modelling.....	62
3.2.2	Model Geometry and Discretization.....	63
3.2.3	Boundary Conditions.....	64
3.2.4	Initial Conditions.....	64
3.3	Selection of Model Parameters.....	65
3.3.1	Ice Jam Formation Parameters.....	65
3.3.2	Ice Jam Release Parameters.....	66
3.4	Model Validation for Hay River Data.....	67
3.5	Model Application.....	68
3.5.1	<i>River1D</i> Modeling of Ice Jam Release Events.....	99
4.0	Summary.....	109
5.0	References.....	112

Appendices:

Note: All appendices are found in the attached CD.

Appendix A: Surveyed cross sections on the Hay River

Appendix B: Data set for top widths and bed profile for the Hay River

Appendix C: Hay River WSC and THR-EMO hydrometric data

Appendix D: Data set of observed ice conditions used to compile flightmaps

Appendix E: Detailed summary of ice conditions observed by Time-Lapse Camera Stations, 2007-2009

List of Tables

Table 2.1: Period of record for high frequency data for the WSC-Border and WSC-HR.....	12
Table 2.2: Period and frequency of data measurement for the EMO-AF gauge, 2004 to 2009	13
Table 2.3: Period and frequency of data measurement for the EMO-PG gauge, 2004 to 2009	14
Table 2.4: Period and frequency of data measurement for the EMO-PPB gauge, 2004 to 2009.....	15
Table 2.5: 2007 Period of record and frequency of data collection for the Time-Lapse Camera Stations.....	19
Table 2.6: 2008 Period of record and frequency of data collection for the Time-Lapse Camera Stations.....	20
Table 2.7: 2009 Period of record and frequency of data collection for the Time-Lapse Camera Stations.....	21
Table 2.8: 2007 documented wave events and observed speeds	25
Table 2.9: 2007 documented ice run events and observed speeds.....	26
Table 2.10: 2007 lag-times of ice run features to associated wave features.....	27
Table 2.11: 2007 normalized lag-times of ice features to the associated front of wave, expressed in minutes-per-kilometre-travelled.....	28
Table 2.12: 2008 documented wave events.....	30
Table 2.13: 2008 Observed ice runs associated with water waves.....	31
Table 2.14: 2008 lag-times of ice run features to associated wave features and normalized lag-times for ice run features and the front of the associated wave.....	32
Table 2.15: 2009 observations of wave features.....	34
Table 2.16: 2009 travel times and speeds of wave features.....	35
Table 2.17: 2009 observations of ice run features	37
Table 2.18: 2009 travel times and speeds of ice run features.....	38
Table 2.19: 2009 lag-times of ice run features to associated wave features.....	39
Table 2.20: 2009 normalized lag-times of ice features to the front of associated wave features, expressed in minutes-per-kilometre-traveled	40

Table 2.21: Observed ice run features and speeds for Ice Jam Release Event 2.	44
Table 2.22: Features and speeds of observed ice run from Ice Jam Release Event 3, as observed from during the observation flight of 4-May at 14:35	46
Table 2.23: Estimated time release for Ice Jam Release 3, and average observed propagation speed.....	47
Table 2.24: Front and back of the 100% concentration from the observed ice run resulting from Ice Jam Release Event 6.	51
Table 2.25: Summary of all documented Ice Jam Release Events between 2007 and 2009.....	52
Table 3.1: Estimated periods of open water between the EMO-AF and EMO- PG used for River1D validation.....	97
Table 3.2: Comparison of River1D simulations to observed ice jam release events	100

List of Figures

Figure 1.1: Showing a typical ice jam (adapted from Ashton, 1986)	4
Figure 1.2: Showing extent of ice jam related flooding during the 2008 breakup season at the Town of Hay River.....	5
Figure 2.1: Hay River basin showing study reach	53
Figure 2.2: Study reach and locations of interest.....	54
Figure 2.3: Available surveyed data within the study reach.....	55
Figure 2.4: Bed profile of equivalent rectangular channel for the Hay River (adapted from Hicks <i>et al.</i> 1992)	56
Figure 2.5: Top widths (smoothed and un-smoothed) of the Hay River (adapted from Hicks <i>et al.</i> 1992)	57
Figure 2.6: WSC provided rating curve for WSC gauge (07OB008) Hay River near ALTA/NWT Boundary	58
Figure 2.7: WSC provided rating curve for WSC gauge (07OB001) Hay River near Hay River	59
Figure 2.8: Rating curve for the EMO Alexandra Falls gauge as provided by THE-EMO.....	60
Figure 2.9: Improved EMO-Alexandra Falls gauge rating curve with original curve from THR-EMO.....	61
Figure 2.10: Flightmap showing the observed ice conditions during the 2007 breakup season	62
Figure 2.11: 2007 hydrographs showing progression of wave events and ice conditions.....	63
Figure 2.12: Flightmap showing the observed ice conditions during the 2008 breakup season	64
Figure 2.13: 2008 hydrographs showing progression of wave events and ice conditons	65
Figure 2.14: Flightmap showing the observed ice conditions during the 2009 breakup season	66
Figure 2.15: 2009 Hydrographs showing progression of wave events and ice conditions.....	67
Figure 2.16: Normalized lag-times for all ice run features matched to the front of waves from 2007 to 2009.	68

Figure 2.17: Observation of the ice jam corresponding to Ice Jam Release Event 1 during the 25-Apr-07 observation flight at 19:00.....	69
Figure 2.18: Observations of the ice jams corresponding to Ice Jam Release Event 2 during the 26-Apr-07 at 11:00.....	70
Figure 2.19: Estimated time of release and discharge of Ice Jam Release Event 2 using the WSC-Border and EMO-AF gauges.....	71
Figure 2.20: Observation of ice run from Ice Jam Release Event 2 during the 27-Apr-07 observation flight at 19:00.....	72
Figure 2.21: Observations of the ice jam corresponding to Ice Jam Release Event 3 during the 3-May-08 observation flight at 14:35.....	73
Figure 2.22: Flightmap for 2-May-08 at 14:35 tracking individual ice pieces and the release of Ice Jam Release Event 3.....	74
Figure 2.23: Tracking the front of the 100% concentration point in the ice run resulting from Ice Jam Release Event 3.....	75
Figure 2.24: Tracking particle 'A' in the ice run resulting from Ice Jam Release Event 3.....	76
Figure 2.25: Tracking particle 'B' in the ice run resulting from the Ice Jam Release Event 3.....	77
Figure 2.26: Tracking the back of the 100% concentration point in the ice run resulting from Ice Jam Release Event 3.....	78
Figure 2.27: Observation of ice jam corresponding to Ice Jam Release Event 4 during the 4-May-08 observation flight at 20:00.....	79
Figure 2.28: Observation of the ice jam corresponding to Ice Jam Release Event 4 during the 5-May-09 observation flight at 14:00.....	80
Figure 2.29: Estimation of time of release and discharge for Ice Jam Release Event 5 using the WSC-Border and EMO-AF.....	81
Figure 2.30: Observations of ice jams corresponding to Ice Jam Release Event 6 during the 5-May-09 observation flight at 14:00.....	82
Figure 3.1: <i>RiverID</i> validation using estimated 2004 open water periods, $k = 0.2$ m.....	102
Figure 3.2: <i>RiverID</i> validation using estimated 2005 open water periods, $k = 0.2$ m.....	102
Figure 3.3: <i>RiverID</i> validation using estimated 2006 open water periods, $k = 0.2$ m.....	103

Figure 3.4: <i>RiverID</i> validation using estimated 2007 open water periods, k = 0.2 m	103
Figure 3.5: Observed and simulated <i>RiverID</i> ice runs from Ice Jam Release Event 3, with varying parameters of λ_1 and λ_2	104
Figure 3.6: <i>RiverID</i> simulation of released wave 'B' from Ice Jam Release Event 1	105
Figure 3.7: <i>RiverID</i> simulation of released wave 'E' from Ice Jam Release Event 2	106
Figure 3.8: <i>RiverID</i> simulation of released wave 'D' from Ice Jam Release Event 3	107
Figure 3.9: <i>RiverID</i> simulation of released wave 'E' from Ice Jam Release Event 4	107
Figure 3.10: <i>RiverID</i> simulation of released wave 'G' from Ice Jam Release Event 5	108
Figure 3.11: <i>RiverID</i> simulation of released wave 'H' from Ice Jam Release Event 6	108

List of Symbols

A	total area of the cross-section under the water surface (m^2)
B	width of the accumulation (m)
C_f	is generally used to incorporate the effects of freezing cohesion between ice particles, and is generally considered to be zero in breakup ice jams.
C_o	$\tan \phi$
C^*	Chezy's resistance factor (<i>dimensionless</i>)
e	porosity of the ice accumulation (<i>dimensionless</i>)
g	acceleration due to gravity (m^2/s)
H	depth of flow under the water surface (m)
k	bed roughness height (m)
K_x	passive pressure coefficient
Q	total discharge, including both water and ice flow (m^3/s)
R	hydraulic radius (m)
S_f	friction slope (<i>dimensionless</i>)
S_o	river bed slope (<i>dimensionless</i>)
t_i	thickness of the ice jam accumulation (m)
V	average flow velocity (m/s)
V_{max}	maximum erosion velocity (m/s)
x	longitudinal co-ordinate (km)
y	flow depth (m)
z	bed elevation (m)
λ_1	bank resistance coefficient (<i>dimensionless</i>)

λ_2	observed diffusion of ice runs coefficient (<i>dimensionless</i>)
μ	jam strength parameter
ρ	density of water (kg/m^3)
ρ_i	density of ice (kg/m^3)
τ	shear stress of flow on underside of accumulation (N/m^2)
ϕ	angle of internal friction of the ice accumulation ($^\circ$)

1.0 Introduction

The Hay River, NWT experiences ice jams every year during spring breakup. As it is a north flowing river, snowmelt from the headwaters pushes through the ice cover, creating a cascade of ice jam formation and release events, ultimately pushing over 150 km of river ice into the Hay River delta at the Town of Hay River. When intact ice on the Great Slave Lake holds back the ice runs, flooding results.

Figure 1.1 illustrates a typical ice jam. Ice jams form when ice floes from a broken ice cover arrest in the channel (Figure 1.1 shows the ice floes were trapped behind an intact ice cover although ice jams can form in open water conditions as well), and impede incoming ice floes which begin to accumulate behind the stopped ice floe. If enough ice floes are added to this accumulation, the downslope component of ice weight can cause the ice accumulation to consolidate and thicken into an ice jam. An ice jam is a channel obstruction, and as such the flow of water is impeded, and water backs up behind the ice jam. During an ice jam release event, the ice jam is unable to physically support itself anymore: the water that was held behind the intact ice jam is released, and the water wave and ice mass propagate downstream which in turn can trigger the release of other ice jams. These ice jams may also shove or slide before releasing. Shoving events are consolidation events, and are caused when the head of an ice jam advances downstream (often due to incoming ice floes and/or water waves) while the toe of the ice jam remains stationary. A sliding event occurs when the toe of the ice jam mobilizes for a brief period before the ice jam re-stabilizes slightly downstream of its original position.

Previous investigations of ice jam release events (Doyle and Andres, 1979; Beltaos et al, 1994, Kowalczyk and Hicks, 2003) indicated that it is not uncommon for these events to have wave speeds of ~3 m/s and stage changes of up to 4 m. These drastic speeds and stage changes

associated with ice jam release events pose a significant threat to life and property for any downstream communities, as is the case with the Town of Hay River, NWT. The Town of Hay River has experienced serious ice jam related flooding as recently as 2008, during which major property damage occurred but thankfully no one was injured. Figure 1.2 shows the extent of flooding and damage caused by the flooding at the Town of Hay River during the 2008 breakup season. It is clear that the ability to forecast ice jam release events would provide an excellent and much needed tool for communities affected by ice jam release events and the risk of flooding associated with the released water wave and ice mass.

Previous research has been conducted on the hydraulic modeling of ice jam release events (which are summarized in section 3.1), but the available documentation of ice jam release events available to validate proposed models is extremely limited. As a result of this limited data, the importance of ice effects on the propagation of the released wave was unresolved and more detailed documentation of ice jam release events is needed in order to refine current modeling techniques. The annual occurrence of ice jam release events on the Hay River and the amount of available hydrometric data (as discussed in section 2.3) made it an excellent site to study such events. The objectives of this study were:

- to document these ice jam release events on the Hay River, NWT in an effort to provide the town warning of their potential timing and magnitude; and
- to use the data collected on ice jam water wave and ice run propagation in this study to test the applicability of a currently available ice jam release event forecasting model, specifically the University of Alberta's hydrodynamic *RiverID* ice jam release event model developed by She and Hicks (2006).

Chapter 2 provides a site description and the details of all of the available data, including details of all of the ice jam release events that were documented in this study. Chapter 3 presents the details of the model application. Chapter 4 presents the summary and conclusions of this study. In addition, five data appendices present details of the river geometry, hydrometric data, and breakup observations assembled as part of this study.

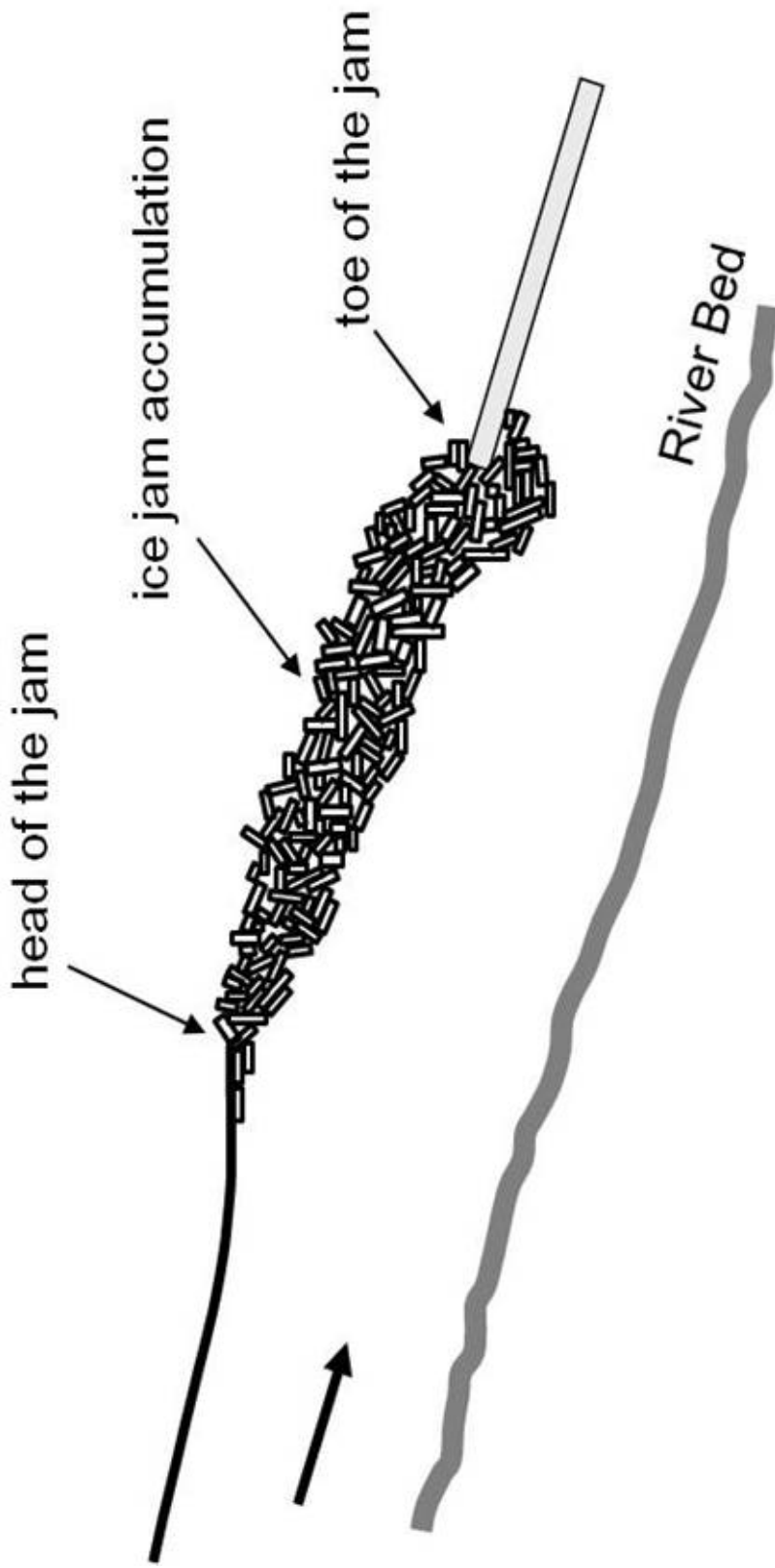


Figure 1.1, Showing a typical ice jam (adapted from Ashton, 1986).



Figure 1.2, Showing extent of ice jam related flooding during the 2008 breakup season at the Town of Hay River.

2.0 Site Description and Field Program

2.1 Reach Description

The following description comes from Gerard and Stanley (1988). The Hay River Basin, shown in Figure 2.1, has a catchment area of approximately 48,100 km². It is comprised of three sub-catchments: the Chinchaga River, the Upper Hay River and the Lower Hay River basins. The Chinchaga River basin is the upper (southern) portion of the Hay River catchment and comprises 23% of its area. The Upper Hay River basin is 42% of the catchment area, is dominated by lowlands and contains Zama Lake, which is the only significant lake storage in the catchment. The Lower Hay River basin is the remaining 35% of the catchment area and terrain consists of mainly low-relief muskeg.

The river runs generally through flat muskeg regions in the upper reach before encountering Alexandra Falls (33m high) and Louise Falls (15m high). Downstream of the waterfalls, the river flows through a steep and narrow gorge. The sides of the gorge gradually diminish in height and the river flattens out as the river runs toward Great Slave Lake. At the Town of Hay River, the river splits around Vale Island, flowing down the East and West Channels to Great Slave Lake.

The upper portion of the river is steep with an average slope of 0.001 for the first 400 km. After this, the reach flattens out to an average slope of 0.00045. The 200 km of river above the falls are very mild with a slope of only 0.0001. After the falls, the river has a very steep reach, with an average slope of 0.003 which gradually decreases to a slope of 0.0001 in the delta (Gerard and Stanley, 1988).

Gerard and Stanley (1988) established a river stationing system along the reach by digitizing the plan view of the Hay River on a 1:50,000 National Topographic Series (NTS) maps (Gerard and Stanley, 1988). They took the source of the river, and origin of the stationing as UTM 311280/6379670, as it is the greatest river distance from the river's mouth at the Great Slave Lake. This stationing system was digitally updated in 2009 using electronic maps and a Geographic Information System (GIS). Figure 2.2 illustrates the study reach of interest here, which begins at the boundary between the Northwest Territories (NWT) and Alberta (945.17) and extends all the way to the Great Slave Lake (1114.24 km).

2.2 Geometric Data

Various geometric data is available along the lower Hay River from past investigations (e.g. Gerard and Stanley, 1988; Gerard et al., 1990) and Indian and Northern Affairs Canada (INAC). For portions of the study reach for which no data was available, geometric information was determined from NTS map data. This section details all of the available geometric data in the study reach.

2.2.1 Survey Data

Figure 2.3 shows the locations of the known surveyed cross sections in the study reach. Thirty-two cross-sections were measured on the Hay River by University of Alberta researchers between July 6 and 22, 1987 (Gerard and Stanley, 1988). These cross-sections were completed in the lower reach of the Hay River, between stations 1094.428 km and 1113.608 km. A Ratheon DE-719B Fathometer was mounted to the side of a boat in order to measure the depth of water across the channel. A 'Topofil' was used to measure distances across the channel. Bank profiles were measured using a rod and level.

An additional 17-cross-sections were surveyed by INAC in 2001, between stations 1089.19 km and 1095.675 km. Eight of these cross-sections do not have bank profile information: data is limited to water elevation and bed profile measurements. Figure 2.3 shows the available cross-sections data from previous field investigations is limited to the lower portions of the study reach, and all surveyed cross sections are presented in Appendix A. This lack of cross-section data resulted in the use of NTS maps for additional geometric information.

2.2.2 Map Data

To augment the limited survey data of the Hay River that was available for hydraulic modeling, previous researchers (Gerard et al. 1990; Hicks et al. 1992) used 1:50,000 NTS maps to obtain water surface slopes and channel width along the river. Using this data, they determined the bed profile and top widths of an equivalent rectangular channel for the Hay River.

2.2.2.1 Bed Profile

To obtain a bed profile for an equivalent rectangular channel of the Hay River, average bed elevation points were first obtained for the surveyed reaches. These bed elevation points were calculated by determining a reach-averaged mean depth for a reference discharge, then subtracting these depths from the geodetic water level elevation for the reference discharge. The bed profile between the bed elevation points was interpolated using the water slopes determined from NTS maps. This process, including the determination of the reference discharge is discussed in more detail in Gerard et al. 1990 and Hicks et al. 1992. The resulting bed profile is shown in Figure 2.4 and the corresponding data are provided in Appendix B.

2.2.2.2 Top Widths

The top width of the equivalent rectangular channel was taken to be the width of the water surface at bank full discharge. Throughout reaches of the Hay River without surveyed cross-sections, this top width was interpolated at one kilometer intervals using NTS maps and aerial photos. These top widths were also smoothed to decrease computation time during hydraulic modeling of the Hay River (Hicks et al., 1992), and it was found that the smoothed top widths did not significantly affect model results. The top widths and smoothed data set are shown in Figure 2.5 adapted from Hicks et al. (1992). The corresponding data are provided in Appendix B.

2.2.3 Channel Roughness

Hydraulic roughness heights were calibrated along the Hay River using surveyed cross-sections in conjunction with Water Survey of Canada (WSC) discharge data from the dates of survey, as described in Hicks et al. 1992. The analysis yielded bed roughness heights ranging from 0.05 to 0.55 m, and they deemed a value of $k = 0.2$ m was acceptable and consistent with the bed material for the entire reach. The authors tested their assumption by producing rating curves for the WSC Hay River at Hay River (07OB001) gauge using the value of $k = 0.27$ m (as measured by the WSC during their discharge measurements) and the assumed value of $k = 0.2$ m. When these rating curves were compared to the rating curve determined by the Water Survey of Canada for this site, only negligible differences in stage were found, and the value of $k = 0.2$ m was adopted for the entire reach.

2.3 Hydrometric Data

There are two sources for hydrometric data within the study reach, the WSC and the Town of Hay River Emergency Measures Operations (THR-EMO). In total there are seven gauged sites

within the study reach, four of which are operated by the THR-EMO and the remaining three are operated by the WSC. The information that is available from these sites and how they aid the monitoring of breakup is discussed in this section. The hydrometric data from the WSC and THR-EMO used in this study are found in Appendix C.

2.3.1 Water Survey of Canada.

The WSC Hay River near ALTA/NWT Boundary (07OB008) is located at river station 945.6 km and is referred to as WSC-Border. The WSC Hay River near Hay River (07OB001) is located at river station 1095.3 km and is referred to as WSC-HR. The WSC Great Slave Lake (07OB001) is located at the mouth of the Hay River at station 1114.24 km and is referred to as WSC-GSL.

The first WSC gauge within the study reach is the WSC Hay River near ALTA/NWT Boundary gauge 07OB008 (WSC-Border) located at 945.6 km. The WSC-Border hydrometric station was installed in 1986 and has a gross drainage area of 48,800 km². The WSC provides real-time water levels at the WSC-Border site which is monitored during breakup. Water levels are archived as daily averaged water levels and are publically available from the WSC website.¹

The stage measurements at the WSC-Border are often affected by an ice cover or ice jams during the breakup season. Because of these ice effects, water waves are rarely captured at the WSC-Border site. The approximate time of release for some ice jams in the vicinity of this hydrometric station can be estimated from the WSC-Border hydrographs.

The WSC Hay River Near Hay River gauge 07OB001 (WSC-HR) is located at river station 1095.3 km. This hydrometric station has a gross drainage area of approximately 51,700 km² and

¹ <http://www.wateroffice.ec.gc.ca>

has been operational since 1963. Similar to the WSC-Border gauge, water levels are available in real time for this gauge site. The data for the WSC-HR gauge is archived in the form of daily averaged discharge, which is available from the WSC website.² The discharge data available from the WSC-HR station could not be used as the station is typically affected by ice jams, making the determination of discharge unreliable.

The final WSC hydrometric station within the study reach is the WSC Great Slave Lake gauge 07OB002 (WSC-GSL) and is located at the mouth of the Hay River at the Great Slave Lake (1114.24 km). The WSC-GSL station has been operational since 1959 and has a gross drainage area of 51,900 km². This gauge is not monitored during breakup, but the archived daily averaged stage measurements are available for use as a downstream boundary condition when modeling the study reach.

The publicly available data for the WSC gauged sites within the study reach was insufficient for the purposes of identifying waves from released ice jams, as the data is presented as daily averages. Higher frequency data, with stage measurements every 15 minutes, was provided by the WSC to augment the publicly available data.³ Table 2.1 contains the periods of record for which high frequency data was made available for the WSC-Border and WSC-HR. It is noted that waves captured by WSC gauges are limited by this 15 minute resolution, meaning that the arrival time for wave features (front and peak) are accurate to approximately ± 7 minutes.

² <http://www.wateroffice.ec.gc.ca>

³ Personal communication, R. Pilling, WSC (Yellowknife), October 2008.

Table 2.1, Period of record for high frequency data for the WSC-Border and WSC-HR.

Year	Start of Period	End of Period
2004	26-Apr	08-May
2005	19-Apr	20-Apr
2006	22-Apr	02-May
2007	23-Apr	03-May
2008	01-May	08-May
2009	30-Apr	09-May

2.3.2 The Town of Hay River Emergency Measures Operations

The most upstream gauge station operated by the THR-EMO is the Alexandra Falls gauge which is actually located 2 km upstream of Alexandra Falls at river station 1032.0 km; it will be referred to as EMO-AF. Here, the water level is measured by a DCU-1104 Ultrasonic Sensor which is suspended over the river on a cantilever boom. This location was chosen as a gauge site since this reach often becomes, and remains, free of ice early in the progression of breakup and the water surface is hydraulically controlled by Alexandra Falls, which makes this gauge site ideal for estimating the discharge of the Hay River at this location. Table 2.2 shows the dates for which water levels are available from THR-EMO as well as the frequency of data collection. It is noted that although the manufacturer's specifications state accuracy of measurements of approximately 0.25%, the use of a cantilever beam introduces greater uncertainty, as the structure will oscillate in the presence of wind, which may further impact stage measurements by ± 0.1 m (estimated based on the noise in the data for steady, open water conditions).

Table 2.2, Period and frequency of data measurement for the EMO-AF gauge, 2004 to 2009.

Year	Start of Period	End of Period	Frequency of Data Measurement
2004	17-Apr	26-Apr	10 minutes
	26-Apr	08-May	1 minute
	08-May	07-May	10 minutes
2005	11-Apr	19-Apr	10 minutes
	19-Apr	06-May	1 minute
	06-May	07-Aug	10 minutes
2006	08-Apr	24-Apr	10 minutes
	24-Apr	30-Apr	1 minute
	30-Apr	11-Jun	10 minutes
2007	13-Apr	24-Apr	10 minutes
	24-Apr	07-May	1 minute
	07-May	19-Jun	10 minutes
2008	14-Apr	02-May	10 minutes
	02-May	09-May	1 minute
	09-May	11-Jun	10 minutes
2009	22-Apr	29-Apr	10 minutes
	29-Apr	07-May	1 minute

The next downstream gauge operated by the THR-EMO is at Paradise Gardens (1067.5 km) and is referred to as the EMO-PG. The stage measurements here are recorded by an acoustic sensor (DCU-1104 Ultrasonic Sensor, accurate to 0.25%) which is suspended over the river by a cantilever boom in a similar fashion to the EMO-AF gauge. This location often experiences ice jams, and a gauge at this location allows the THR-EMO to remotely monitor any such jams. The periods for which water levels are available and the frequency of the measurements are shown in Table 2.3. Similar to the EMO-AF gauge, the use of a cantilever beam to suspend the sensor over the river can introduce uncertainties of water level measurement of up to ± 0.1 m when wind causes the structure to oscillate.

Table 2.3, Period and frequency of data measurement for the EMO-PG gauge, 2004 to 2009.

Year	Start of Period	End of Period	Frequency of Data Measurement
2004	17-Apr	26-Apr	10 minutes
	26-Apr	08-May	1 minute
	08-May	10-May	10 minutes
2005	11-Apr	19-Apr	10 minutes
	19-Apr	06-May	1 minute
	06-May	04-Jul	10 minutes
2006	05-Apr	24-Apr	10 minutes
	24-Apr	30-Apr	1 minute
	30-Apr	11-Jun	10 minutes
2007	17-Apr	24-Apr	10 minutes
	24-Apr	07-May	1 minute
	07-May	19-Jun	10 minutes
2008	15-Apr	03-May	10 minutes
	03-May	10-May	1 minute
	10-May	12-Jun	10 minutes
2009	20-Apr	29-Apr	10 minutes
	29-Apr	07-May	1 minute

The third gauge operated by the THR-EMO is located just 2.7 km downstream of the WSC-HR at river station 1098.0 km at the Pine Point Bridge and is referred to as the EMO-PPB. Here, the DCU-1104 Ultrasonic Sensor is mounted directly to the Pine Point Bridge. This location also experiences ice jams, possibly due to the channel constriction caused by the bridge piers. This gauged location is used to monitor ice jams at this location during breakup, and is also the final gauged location on the study reach before the Town of Hay River and the last place events can be observed as a warning to THR. The periods for which water levels are available and the frequency of the measurements are shown in Table 2.4. As the sensor is mounted directly to the

bridge at this location (and is not subject to the oscillations associated with using a cantilever beam, as discussed for the EMO-AF and EMO-PG), the measurement are assumed to be accurate within 0.25% as per manufacturers specifications.

Table 2.4, Period and frequency of data measurement for the EMO-PPB gauge, 2004 to 2009.

Year	Start of Period	End of Period	Frequency of Data Measurement
2004	17-Apr	26-Apr	10 minutes
	26-Apr	08-May	1 minute
	08-May	10-May	10 minutes
2005	11-Apr	19-Apr	10 minutes
	19-Apr	06-May	1 minute
	06-May	04-Jul	10 minutes
2006	05-Apr	24-Apr	10 minutes
	24-Apr	30-Apr	1 minute
	30-Apr	11-Jun	10 minutes
2007	17-Apr	24-Apr	10 minutes
	24-Apr	07-May	1 minute
	07-May	19-Jun	10 minutes
2008	15-Apr	03-May	10 minutes
	03-May	10-May	1 minute
	10-May	12-Jun	10 minutes
2009	20-Apr	29-Apr	10 minutes
	29-Apr	07-May	1 minute

The final gauge operated by the THR-EMO is within the Town of Hay River and is located in the West Chanel at station 1108.3 km, just downstream of the flow split around Vale Island. The DCU-1104 Ultrasonic Sensor is suspended directly from the West Channel Bridge at this location, and the station will be referred to as the EMO-WCB. Since this gauge is located in the delta where ice jams form, it was not of particular interest to this study.

2.3.3 Discharge

As discussed in section 2.3.1, the only direct discharge data within the study reach is not available in real-time, but as archived daily discharges from the WSC-HR gauge. Rating curves for the WSC-Border and WSC-HR were provided by the WSC. A rating curve for the EMO-AF gauge was provided by THR-EMO.

The rating curves for the WSC-HR and WSC-Border can be seen in Figures 2.6 and 2.7, respectively. The rating curve at the WSC-HR was determined empirically from discharge surveys conducted by the WSC. The rating curve at the WSC-Border was interpolated by assuming a one day travel time between the WSC-Border and the WSC-HR.

The rating curve for the EMO-AF is shown in Figure 2.8. This rating curve was estimated by THR-EMO using the WSC-Border rating curve assuming zero travel time between the WSC-Border and the EMO-AF gauges.⁴ Effectively, this results in assuming a one day travel time between EMO-AF and WSC-HR, which is unreasonable giving the proximity of the stations. The EMO-AF rating curve was corrected by assuming no travel time between EMO-AF and WSC-HR. While this assumption is not perfectly correct either, it is more accurate than the previous assumption. It could not be improved at the time of this study because only mean daily discharges were available for the WSC-HR gauge. The revised EMO-AF rating curve is shown in Figure 2.9, along with the rating curve produced by THR-EMO.

2.4 Field Investigations and Progression of Breakup

The discussion of the field investigations that took place during breakup on the Hay River will be limited to the detection of ice jam release events. In order to model ice jam release events,

⁴ Personal communication, Floyd Hopkins, Town Flood Watch volunteer, 19-Apr-09.

several components of the event need to be identified: the location and length of the jam; observations of the released water wave, and observations of the resultant ice run. The hydrometric data discussed in section 2.3 was sufficient for the purposes of identifying the released water waves, and the methods for observing ice jams and ice runs on the study reach are discussed in this section. Observational flights were conducted to monitor ice conditions along the study reach and to identify any ice jams and ice runs and time-lapse cameras were installed at several gauged stations in order to observed local ice conditions.

2.4.1 Methods

In order to identify ice jams and ice runs within the study reach, observational flights were conducted by THR-EMO volunteers and UofA researchers. The limitation of observation flights is the short duration (usually about an hour) over which ice conditions can be documented. Time-lapse camera stations were installed at several of the gauged stations within the study reach so that near-continuous ice conditions could be obtained. The analysis of observational flights and time-lapse camera stations are discussed in this section.

2.4.1.1 Observational Flights

The length of the study reach makes ice conditions impossible to observe entirely from the ground and so aerial reconnaissance flights were conducted to circumvent this limitation. Typical observational flights were conducted from the Town of Hay River to the NWT/AB boundary at an altitude of ~3000 feet above ground level. During these flights, the ice conditions were extensively documented using photography (typically 200 to 300 photos per flight). Successive flights facilitated documentation of the progression of ice cover deterioration during breakup along the entire study reach, as well as the locations of any ice jams or ice runs.

The ice jams were documented by comparing the photographs to a digitized map of the study reach. This introduces uncertainty in the accuracy of the documented locations and lengths of the observed ice jams. It is estimated that the positioning along the river could only be determined within an accuracy of ± 100 m.

2.4.1.2 Time-Lapse Camera Stations

The first Time-Lapse Camera Stations (TLCS) were installed for breakup monitoring at EMO-AF, EMO-PG and EMO-PPB during the 2007 breakup season. Each of the TLCS contained primary and secondary cameras which were triggered at programmed intervals using a Campbell Scientific CR1000 datalogger. The cameras and datalogger were housed in a protective casing and mounted to a tree adjacent to the gauged stations. Campbell Scientific CC640 digital cameras were used as a primary camera for all TLCS. In 2010, TLCS at EMO-AF and EMO-PG used Canon EOS SD SLR digital cameras as the secondary camera and a Camtracker camera was used as a secondary camera at the EMO-PPB gauge.

During the 2007 breakup season the TLCS were triggered at 5 minute intervals during the early stages of breakup and data collection increased in frequency to 1 minute intervals as breakup progressed. The period of operation and frequency of data collection for the TLCS used during the 2007 breakup season is shown in Table 2.5. It is noted that no useful pictures were taken between the hours of 23:00 and 05:00 at any site due to an absence of light sources at TLCS.

Table 2.5, 2007 Period of record and frequency of data collection for the Time-Lapse Camera Stations.

Site	Start of Period	End of Period	Frequency of Data Measurement
EMO-AF	20-Apr, 12:30	26-Apr, 11:25	5 minutes
	26-Apr, 11:31	28-Apr, 14:11	1 minute
EMO-PG	19-Apr, 12:10	24-Apr, 19:35	5 minutes
	24-Apr, 19:35	26-Apr, 20:17	1 minute
	26-Apr, 20:17	27-Apr, 09:19	No Data
	27-Apr, 09:19	28-Apr, 11:26	1 minute
EMO-PPB	23-Apr, 17:15	24-Apr, 19:55	5 minutes
	24-Apr, 19:59	26-Apr, 19:58	1 minute
	26-Apr, 19:58	27-Apr, 08:29	No Data
	27-Apr, 08:29	28-Apr, 11:28	1 minute

For the 2008 breakup season, four remote camera stations were used to capture the events of breakup. Similar to the 2007 breakup season, TLCS were installed at the EMO-AF, EMO-PG and EMO-PPB gauges. The TLCS at EMO-PG was moved further upstream from its 2007 position to be near the EMO-PG gauge to river station 1066.8 km. This was done since snow levels made the original location inaccessible at the time the TLCS were installed. With this exception, the camera stations at the three EMO gauges were installed as described for the 2007 breakup season.

A fourth TLCS was installed next to the WSC-HR gauge in 2008. This TLCS used a Campbell Scientific CC640 digital camera as a primary camera triggered by a Campbell Scientific CR1000 datalogger and a Camtracker camera was used as a secondary camera. This TLCS was also mounted to a tree.

The TLCS at all four locations were triggered at a 5 minute frequency for the entire 2008 breakup season. No useful pictures were obtained from 22:00 to 06:00 due to low light conditions. The period of data collection of TLCS during the 2008 breakup season can be seen in Table 2.6.

Table 2.6, 2008 Period of record and frequency of data collection for the Time-Lapse Camera Stations.

Site	Start of Period	End of Period	Frequency of Data Measurement
EMO-AF	26-Apr, 10:55	29-Apr, 11:10	5 minutes
	29-Apr, 11:10	29-Apr, 11:40	No Data
	29-Apr, 11:40	06-May, 13:05	5 minutes
EMO-PG	26-Apr, 12:15	06-May, 15:30	5 minutes
WSC-HR	26-Apr, 13:35	06-May, 15:50	5 minutes
EMO-PPB	26-Apr, 14:25	06-May, 16:05	5 minutes

During the 2009 breakup season TLCS were installed at EMO-AF, EMO-PG, WSC-HR and EMO-PPB. The TLCS at the EMO-AF and EMO-PG were installed as described for the 2007 breakup season and the TLCS at WSC-HR was installed as described for the 2008 breakup season. The location of the TLCS at EMO-PPB was moved from the tree location adjacent to the river and was instead mounted directly to the Pine Point Bridge.

Spotlights were introduced to the installation of TLCS during the 2009 breakup season in order to document ice run events that occurred during the night. The spotlights were activated with the same dataloggers from the TLCS, so that the spotlight and cameras would be trigger simultaneously. The period of operation and frequency of data collection for the TLCS during the 2009 breakup season is summarized in Table 2.7.

Table 2.7, 2009 Period of record and frequency of data collection for the Time-Lapse Camera Stations.

Site	Start of Period	End of Period	Frequency of Data Measurement
EMO-AF	29-Apr, 22:28	02-May, 21:28	6 minutes
EMO-PG	30-Apr, 10:00	30-Apr, 18:24	6 minutes
	30-Apr, 18:24	01-May, 11:00	No Data
	01-May, 11:00	07-May, 12:18	6 minutes
WCS-HR	23-Apr, 16:45	30-Apr, 09:30	5 minutes
	30-Apr, 09:30	30-Apr, 11:30	No Data
	30-Apr, 11:30	07-May, 13:08	6 minutes
EMO-PPB	01-May, 09:48	07-May, 13:42	6 minutes

It is noted that the accuracy of the arrival times of the ice run features are limited to the frequency of TLCS data collection. For example, as shown in Table 2.7, photographs were taken every 6 minutes at the EMO-AF during the 2009 breakup season. This means that the arrival time of ice run features could only be estimated to within ± 3 minutes.

2.4.1.3 Identification of Ice Jam Release Events

Although many ice jams were identified during observational flights, only a few were suitable for analysis. These suitable ice jams had to be large enough (on the order of several kilometres) to store enough water than the release of the ice jam could be identified using downstream stage hydrographs. The receiving channel must also be free of ice between the initial jam and at least one downstream gauged station, so that the propagation of the released water and ice mass is not complicated by existing ice in the receiving channel. If a suitable ice jam was observed to have released in the time between successive observational flights, the data from the downstream hydrometric and TLCS used to look for evidence of the released water wave and ice mass.

If a wave was able to be seen at successive gauged stations, the travel time and speed between these stations can be determined, and if these travel times are consistent they may aid the field monitoring of breakup if accurate modeling is not available or practical. Similarly, the travel time of ice runs observed at multiple TLCS could also be determined. Since TLCS were installed at gauged stations, the interaction of water waves and transported ice masses were able to be observed, and lag-times (the amount of time that passes between an observed water wave feature and an ice run feature) were able to be calculated for related water wave and ice runs. The origin of the released ice mass was estimated from the observational of global ice conditions from the observation flights, and the lag-times were normalized so they were expressed as the period of time that an ice feature lags behind a wave feature per kilometre of propagation. This resulted in estimations of the rate at which ice features lag behind wave features.

2.4.2 2007 Breakup Observations and Analysis

Several water waves and ice runs were observed at multiple gauged stations during the 2007 breakup season. The speeds of these events and the normalized lag-times for related ice runs and water waves were determined and are presented in this section. The analysis of the 2007 breakup data lead to the documentation of two ice jam release events which are summarized in this chapter.

2.4.2.1 2007 General Progression of Breakup

Figure 2.10 illustrates the ice conditions observed during the 2007 breakup season during the observation flights that were conducted between 25-Apr and 27-Apr. The stationing of the observed ice conditions seen during the observation flights are summarized in Appendix D. Figure 2.10 shows that when ice conditions were first observed, the progression of breakup was

delayed in the extreme upstream and downstream portions of the study reach where large sections of deteriorated ice covers existed, when compared to the remainder of the study reach which exhibited sections of open water and small ice jams. The upstream and downstream ends of the study reach was observed to continue to degrade at a rate slower than observed elsewhere, and ice was observed to have collected behind these deteriorated ice covers and form ice jams as the river broke up. By 27-Apr, the deteriorated ice in the upstream end of the study reach broke and joined the ice jams in the downstream end of the study reach. During the analysis of the 2007 breakup season, two of the ice jams observed on the observational flights were found to be part of ice jam release events. The first ice release event was caused when the ice jam released that was first observed during the observational flight on 15-Apr at 19:00 just upstream of Alexandra Falls at station 1025.9 km, and is discussed in section 2.4.2.3. The second ice jam release events was caused due to the release of the ice jams observed near the NWT/AB boundary on the observational flight conducted at 11:00 on 26-Apr and is discussed in section 2.4.2.3.

2.4.2.2 2007 Observed Water Waves and Ice Runs

Figure 2.11 shows hydrographs for the EMO-AF, EMO-PG, WSC-HR and EMO-PPB gauge sites in conjunction with local ice conditions documented using the TLCS. The ice conditions at the gauged stations are represented by the multi-coloured line above the stage hydrograph. The speeds of the observed water waves and ice runs are discussed in this section, along with observed relationships between waves and ice runs.

In Figure 2.11, waves are denoted by letters so that each event can be tracked between stations. A red letter denotes that the wave was caused by the release of an observed ice jam. The fronts

and peaks of the waves are shown using a small red “x”. The peaks of the waves were taken to be the local stage maximums and are known within ± 1 minute at all EMO gauges and within ± 7 minutes at WSC gauges, as estimated from the frequency of data collection discussed in section 2.3. The front of the wave events were estimated by inspection of the hydrograph data and are estimated to be accurate within ± 10 minutes.

Numbers were used to denote individual ice runs, except for those ice runs that could be related to a particular wave, in which case the corresponding letter was used in lieu of a number. If the approximate river stationing from which the ice run originated could be estimated from the observation flights, it is displayed above the ice run. As discussed in section 2.4.2.1, the flightmap of observed ice conditions is shown in Figure 2.10.

To optimize accuracy in deducing travel times, the ice runs documented by the TLCS were analyzed for consistent features. Obvious features, such as the front and back of the ice run, were used in the analysis, as well as more subtle features such as the front and back of the maximum ice run concentration. These features are important, since the diffusion of the ice run makes the front and the back of the ice run difficult to distinguish from remnant ice floes that had been previously stranded are refloated and carried along on the front of the released water wave.

Figure 2.11 also shows annotations describing ice processes identified using data from the stage hydrographs, TLCS and flight observations. The ice jam processes identified were ice jam formation, ice jam shoving events, ice jam sliding events and the release of ice jams. The short distance (2.7 km) between the WSC-HR and EMO-PPB stations means that they are often affected by the same ice jam, which is also noted in the figure.

As seen in Figure 2.11, five waves were documented passing multiple gauged stations during the 2007 breakup season, and are labelled ‘A’ through ‘E’. Two of these waves, ‘A’ and ‘E’, were the result of ice jam release events. The time of arrival of the fronts and peaks of these waves, as well as their travel times and speeds between the EMO-AF and EMO-PG stations are summarized in Table 2.8.

Table 2.8, 2007 documented wave events and observed speeds.

Event	Description	EMO-AF		EMO-PG		Travel Time	Speed m/s
		Time of Event	Height, m	Time of Event	Height, m		
A	Front of Wave	25-Apr, 18:28	0.35	25-Apr, 20:28	0.93	02:00	6.8
	Wave Peak	25-Apr, 19:00		25-Apr, 21:35		02:35	5.3
B	Front of Wave	25-Apr, 21:46	1.13	26-Apr, 01:16	1.47	03:30	3.9
	Wave Peak	25-Apr, 23:12		26-Apr, 03:23		04:11	3.3
C	Front of Wave	26-Apr, 05:18	0.54	26-Apr, 08:34	0.53	03:16	4.2
	Wave Peak	26-Apr, 12:09		26-Apr, 15:13		03:04	4.5
D	Front of Wave	26-Apr, 17:25	0.12	26-Apr, 20:12	0.21	02:47	4.9
	Wave Peak	26-Apr, 20:00		26-Apr, 23:29		03:29	3.9
E	Front of Wave	26-Apr, 23:45	0.67	27-Apr, 02:00	0.91	02:15	6.1
	Wave Peak	27-Apr, 11:24		27-Apr, 13:22		01:58	6.9
Front of Wave Average:						02:45	5.2
Wave Peak Average:						03:03	4.8

As seen in Table 2.8, the front speeds between the EMO-AF and EMO-PG ranged between 3.9 m/s and 6.8 m/s, with an average of 5.2 m/s. Similarly, the speeds of the wave peaks between the EMO-AF and EMO-PG ranged between 3.3 m/s and 6.9 m/s with an average of 4.8 m/s. Interestingly, the waves did not attenuate between the EMO-AF and EMO-PG, in fact most waves grew in height. This must be due to the effects of ice on the flow, which may be momentarily stalling the wave and allowing for the build up of additional head. This additional

head would account for the increased stage at the EMO-PG as well as the high speeds seen between the stations.

The features of the ice runs that were able to be identified during the 2007 breakup season are shown in Table 2.9. The travel times and speeds of the identified ice runs between the EMO-AF and EMO-PG are also shown in Table 2.9. It is noted that for ice runs where the front of the maximum concentration coincided with the front or back of the ice run, only one time is reported in Table 2.9 Appendix E presents a detailed account of all ice conditions documented during the 2007 breakup season at all TLCS equipped stations.

Table 2.9, 2007 documented ice run events and observed speeds.

Event	Description	EMO-AF (1032.0 km) Event Arrival	EMO-PG (1067.5 km) Event Arrival	Travel Time	Speed, m/s
A	Front of Ice Run	Apr-25, 18:55	Apr-25, 21:00	02:05	4.7
	Front of Max Conc.		Apr-25, 21:40	02:45	3.6
	Back of Max Conc.	Apr-25, 19:25	Apr-25, 21:53	02:28	4.0
	Back of Ice Run		Apr-25, 22:22	02:57	3.3
E	Front of Ice Run	Apr-27, 05:00	< Apr-27, 09:20	< 04:20	> 2.3
	Front of Max Conc.	Apr-27, 06:00	Apr-27, 10:20	04:20	2.3
	Back of Max Conc.	Apr-27, 12:30	Apr-27, 15:50	03:20	3.0
	Back of Ice Run	Apr-27, 15:00	Apr-27, 16:20	01:20	7.4
Averages:				02:59	3.48

As seen in Table 2.9, the ice run features traveled between the EMO-AF and EMO-PG at an average speed of 3.5 m/s. It is noted that the front and back of event ‘E’ are included in Table 2.9 but were not considered when calculated the averages. This was done since the front of the ice run was not directly observed, and the speed of the back of the ice run was suspiciously high. Event ‘E’ came from the upstream end of the study reach (965 km) and the back of the ice run

may have been obscured at one or both of the EMO-AF and EMO-PG gauges, which in turn affected the reported speed of the event. Ice runs ‘A’ and ‘E’ are discussed in more detail in sections 2.4.2.1 and 2.3.2.2 respectively, as they are part of the documented ice jam release events.

Lag-times were established for ice runs that could be matched to waves. Lag-times are defined by the amount of time that passes between the arrival of a wave feature and the arrival of an ice feature. The wave features chosen for this analysis were the front and peak of the wave, and the ice features chosen were the front of the ice run and the front of the maximum concentration of the ice run. These lag-times are shown in Table 2.10.

Table 2.10, 2007 lag-times of ice run features to associated wave features.

Event	Feature of Ice Run	EMO-AF (1032.0 km)		EMO-PG (1067.5 km)	
		Front of Wave	Peak of Wave	Front of Wave	Peak of Wave
A	Front of Ice Run	+ 00:27	- 00:05	+ 00:32	- 00:35
	Front of Max Conc.			+ 01:12	+ 00:05
E	Front of Ice Run	+ 05:15	- 06:24	Not Observed	
	Front of Max Conc.	+ 06:15	- 05:24	+ 08:20	- 03:02
Note:		"-" indicates the ice feature was earlier than the wave feature "+" indicates the ice feature was later than the wave feature			

Table 2.10 shows that, in most cases the ice run features arrived before the peak of the water wave. Due to this fact, the front of the wave is the only useful predictor for the arrival of any ice runs. These lag-times of ice events behind the front of the wave were normalized using the approximate distance the ice run traveled so that the lag-times could be expressed in minutes per kilometre traveled, or the approximate rate at which the ice falls behind the water wave. The normalized lag-times for 2007 events are shown in Table 2.11. As the table shows, the

normalized lag-times are variable, and range from approximately 1 to 13 minutes per kilometre traveled.

Table 2.11, 2007 normalized lag-times of ice features to the associated front of wave, expressed in minutes-per-kilometre-travelled.

Event	Feature of Ice Run	EMO-AF (1032.0 km)	EMO-PG (1067.5 km)
A ~1030 km	Front of Ice Run	13.5	0.9
	Front of Max Conc.		1.9
E ~ 970	Front of Ice Run	5.1	Not Observed
	Front of Max Conc.	6.0	5.1

2.4.3 2008 Breakup Observations and Analysis

No waves were observed at multiple gauged stations, making wave speeds unattainable during the 2008 breakup season and similarly only a single ice run could be observed passing multiple TLCS. However at gauged stations that had both water wave and ice run data, ice runs were able to be matched to water waves and establish additional lag-times. The analysis of observed water waves and ice runs during the 2008 breakup season is discussed in this section.

2.4.3.1 2008 General Progression of Breakup

Figure 2.12 shows the flightmap for the ice conditions documented during the observational flights conducted from 1-May to 5-May during the 2008 breakup season, and the stationing of the ice conditions are summarized in Appendix D. When ice conditions along the study reach were first observed on 1-May at 14:00, it was observed that the ice conditions above Alexandra Falls, which exhibited mainly a deteriorated ice cover interspaced with small open water

sections, was deteriorating at a faster rate than the ice cover below Alexandra Falls, which was still largely intact. Over the next three days, the ice cover below Alexandra Falls degraded to a deteriorated ice cover that exhibited only small sections of open water, while the ice cover above Alexandra Falls had completely broke up in the same period. Some of released ice floes from the breakup of the upper reach had jammed at Grumbler Rapids, and the rest of the ice floes formed an ice jam downstream of Louise Falls when they were impeded by the deteriorated ice cover in the lower reach. The ice jam at Grumbler Rapids was observed to have released during the observation flight on 4-May at 14:35, and the subsequent released water and ice mass traveled downstream and triggered the release of the ice jam in the Gorge. These events are summarized in section 2.5.3 and 2.5.4 as Ice Jam Release Events 3 and 4, respectively.

2.4.3.2 2008 Observed Water Waves and Ice Runs

Figure 2.13 shows the stage data and observed ice conditions for the EMO-AF, EMO-PG, WSC-HR and EMO-PPB gauge sites. Waves and ice runs are identified in the figure as described for the 2007 breakup analysis. A complete summary of the ice conditions observed using the TLCS is available in Appendix E.

As mentioned, speeds of water waves could not be established during the 2008 breakup season, as no water waves were observed at more than one gauged station. However four waves observed at the EMO-AF station, labelled 'A' through 'D' were able to be paired with ice runs. The arrival time of the water waves are summarized in Table 2.12, and the arrival time of the ice events that were able to be paired with waves are summarized in Table 2.13. It is noted that for ice runs where the front of the maximum concentration coincided with the front or back of the

ice run, only one time is reported in Table 2.13. Finally, the lag-times of the ice run features are shown in Table 2.14.

Table 2.12, 2008 documented wave events.

Event	Description	EMO-AF (1032.0 km)		EMO-PG (1067.5 km)	
		Time of Event	Stage, m	Time of Event	Stage, m
A	Front of Wave Wave Peak	03-May, 16:44 03-May, 17:48	0.76		
B	Front of Wave Wave Peak	04-May, 04:28 04-May, 06:24	0.20		
C	Front of Wave Wave Peak	04-May, 08:20 04-May, 10:04	0.45		
D	Front of Wave Wave Peak	04-May, 17:37 04-May, 21:42	0.77		
E	Front of Wave Wave Peak			04-May, 21:55 04-May, 22:45	1.78

Table 2.13, 2008 Observed ice runs associated with water waves.

Event	Description	EMO-AF (1032.0 km) Event Arrival
A	Front of Ice Run	May-03, 17:05
	Front of Max Conc.	
	Back of Max Conc.	May-03, 19:00
	Back of Ice Run	
B	Front of Ice Run	May-04, 06:25
	Front of Max Conc.	May-04, 07:15
	Back of Max Conc.	
	Back of Ice Run	
C	Front of Ice Run	May-04, 09:35
	Front of Max Conc.	May-04, 13:05
	Back of Max Conc.	
	Back of Ice Run	
D	Front of Ice Run	May-04, 18:05
	Front of Max Conc.	May-04, 21:00
	Back of Max Conc.	After May-05, 22:00
	Back of Ice Run	After May-05, 22:00

Table 2.14, 2008 lag-times of ice run features to associated wave features and normalized lag-times for ice run features and the front of the associated wave.

Event	Feature of Ice Run	EMO-AF (1032.0 km)		Normalized Lag-Times for Ice Features and the Front of Wave.
		Front of Wave	Peak of Wave	
A	Front of Ice Run Front of Max Conc.	+ 00:21	- 00:43	3.0
B	Front of Ice Run Front of Max Conc.	+ 01:57	+ 00:01	6.9
C	Front of Ice Run Front of Max Conc.	+ 01:15	- 00:29	2.8
D	Front of Ice Run	+ 00:28	- 00:29	0.7
	Front of Max Conc.	+ 03:23	- 00:42	5.1
Note: "-" indicates the ice feature was earlier than the wave feature "+" indicates the ice feature was later than the wave feature Normalized lag-times are expressed in minutes-per-kilometre-traveled.				

As was seen in the 2007 analysis, Table 2.14 also shows that most ice run features arrived before the peak of the water waves. The normalized lag-times ranged from 0.7 to 6.9 minutes per kilometre traveled for events 'D' and 'B' respectively. It is noted that ice run 'D' is associated with an ice jam release event, which is discussed further in section 2.5.3, which could account for its comparatively low normalized lag-time.

2.4.4 2009 Breakup Observations and Analysis

Several water waves and ice runs were observed passing multiple gauged stations, allowing travel times and speed to be established. A total of seven ice runs were matched with water waves, which increased data available for lag-time analysis. This was the only breakup season

for which an ice run event was able to be observed passing all stations between and including the EMO-AF and EMO-PPB gauges.

2.4.4.1 2009 General Progression of Breakup

The general progression of breakup is illustrated in Figure 2.14, which shows the flightmap of observed ice conditions during flights conducted between 30-Apr and 5-May 2009. When first observed, the ice conditions over the majority of the reach was still intact due to a late snowfall, and only minor portions of the study reach had sections of deteriorated ice cover or sections of open water. In a similar manner to 2008, the ice cover upstream of Alexandra Falls deteriorated at a faster rate than the downstream portion of the study reach, and by 5-May, the upper portion was almost completely free of ice and a small ice jam was present near the NWT/AB boundary. During the same period, the deterioration of the ice cover below Alexandra Falls progressed from downstream to upstream which caused ice jams to form at both the THR (due to ice floes released from the breaking ice cover in the lower reach) and near Enterprise (due to ice floes released from the breaking ice cover in the upper reach). The small ice jam seen near the border on 5-May released, and the release water wave and ice mass traveled downstream and triggered the release of the ice jams near Enterprise. The release of these ice jams are discussed in detail in sections 2.5.4 and 2.5.5 as Ice Jam Release Events 4 and 5, respectively.

2.4.4.2 2009 Observed Water Waves and Ice Runs

Figure 2.15 shows the progression of breakup for the EMO-AF, WSC-HR and EMO-PPB during the 2009 breakup season. As mentioned in section 2.4.2, floodlights were installed at the remote camera stations for the 2009 breakup season, which allowed for 24 hour observation of ice

conditions at the TLCS. Figure 2.15 was constructed as discussed in the 2007 analysis, and a complete summary of the ice conditions observed by the TLCS can be found in Appendix E.

As shown in Figure 2.15, features of nearly all wave events could be seen at multiple gauged stations, with the exception of events ‘A’ and ‘F’. It is noted that the speeds of waves ‘B’ through ‘E’ are not representative of open water conditions due to the deteriorated ice cover that was present during these events between the EMO-AF and EMO-PG gauges, as seen on the flightmap shown in Figure 2.14. The observation times of the wave features are shown in Table 2.15, and the travel time and speeds of the wave events are shown in Table 2.16.

Table 2.15, 2009 observations of wave features.

Event	Description	EMO-AF		EMO-PG		WSC-HR	EMO-PPB
		Time of Event	Height, m	Time of Event	Height, m	Time of Event	Time of Event
A	Front of Wave Wave Peak	02-May, 13:17 02-May, 14:05	0.2				
B	Front of Wave Wave Peak	02-May, 14:29 02-May, 15:34	0.5	02-May, 18:40 02-May, 20:30	0.5		
C	Front of Wave Wave Peak	03-May, 05:28 03-May, 07:34	0.4	03-May, 09:28 03-May, 12:42	0.4		
D	Front of Wave Wave Peak	03-May, 13:28 03-May, 15:33	0.2	03-May, 19:27 03-May, 21:05	0.1		
E	Front of Wave Wave Peak	03-May, 21:35 03-May, 22:53	0.3	04-May, 03:00 04-May, 05:22	0.3		
F	Front of Wave Wave Peak	04-May, 16:44 04-May, 21:24	0.2				
G	Front of Wave Wave Peak	06-May, 00:24 06-May, 10:45	0.7	06-May, 14:59			
H	Front of Wave Wave Peak			May-06, 03:01 May-06, 04:58	2.5	May-06, 03:30	May-06, 04:31

Table 2.16, 2009 travel times and speeds of wave features.

Event	Description	EMO-AF to EMO-PG		EMO-PG to WSC-HR		WSC-HR to EMO-PPB	
		Travel Time	Speed, m/s	Travel Time	Speed	Travel Time	Speed, m/s
B	Front of Wave	04:11	2.4				
	Wave Peak	04:56	2.0				
C	Front of Wave	04:00	2.5				
	Wave Peak	05:08	1.9				
D	Front of Wave	05:59	1.6				
	Wave Peak	05:32	1.8				
E	Front of Wave	05:25	1.8				
	Wave Peak	06:29	1.5				
G	Front of Wave						
	Wave Peak	04:14	2.3				
H	Front of Wave			00:29	16.0	01:01	0.7
	Wave Peak						
Front of Wave Average:		04:53	2.1				
Wave Peak Average:		05:15	1.9				

Table 2.15 shows that the wave heights have not attenuated between the EMO-AF and EMO-PG stations. This suggests that the waves travel as kinematic waves due to the steepness of the channel between these stations, and the waves did not stall and rebuild as was seen during the 2007 breakup season.

As shown in Table 2.16, the front of wave speeds for events ‘B’, ‘C’, ‘D’ and ‘E’ averaged 2.1 m/s and ranged between 1.6 m/s and 2.5 m/s, while the wave peaks averaged 1.9 m/s and ranged between 1.5 m/s and 2.3 m/s between the EMO-AF and EMO-PG stations. The wave speeds observed between the EMO-AF and EMO-PG during the 2009 breakup season are significantly slower than the speeds of the waves observed between these stations during 2007. This could be due to the fact that the 2009 waves were smaller in magnitude, which would result in a slower

propagation speed. Also, the 2009 waves traveled beneath a deteriorated ice cover, as shown in Figures 2.14 and 2.15, which likely decreased the speeds of the events and did not allow for the stalling and building phenomena that was hypothesized for 2007.

As mentioned in section 2.5.5, wave ‘G’, which was the result of an ice jam release event, triggered the release of event ‘H’, which makes the front of wave ‘G’ impossible to distinguish from the front of wave ‘H’ on the downstream stage hydrographs. As such, the front of wave ‘H’ was also taken to be the front of wave ‘G’ when ice lag-times were established.

Several ice runs were observed during the 2009 breakup season that were observed at multiple TLCS, or paired with a water waver, or both. Only the ice runs matched with a water wave or were observed at multiple gauged stations are summarized in Table 2.17 and the observed speeds of the ice runs between stations are shown in Table 2.18. As mentioned above, the details of all annotated ice runs can be found in Appendix E.

Table 2.17, 2009 observations of ice run features.

Event	Description	EMO-AF (1032.0 km)	EMO-PG (1067.5 km)	WSC-HR (1095.4 km)	EMO-PPB (1098.0 km)
G1	Front of Ice Run	06-May, 03:04	06-May, 06:24	06-May, 10:38	06-May, 10:48
	Front of Max. Conc.		06-May, 07:00	06-May, 11:03	06-May, 11:30
	Back of Ice Run	06-May, 04:10	06-May, 08:00	06-May, 11:38	06-May, 11:54
G2	Front of Ice Run	06-May, 06:43	06-May, 09:00	06-May, 13:56	06-May, 14:02
	Max Conc.	06-May, 06:58	06-May, 10:12	06-May, 14:20	
	Back of Ice Run	06-May, 07:34	06-May, 11:18	06-May, 15:08	06-May, 15:24
G3	Front of Ice Run	06-May, 08:46	06-May, 11:54	06-May, 15:50	06-May, 16:12
	Front of Max. Conc.	06-May, 08:58	06-May, 12:42	06-May, 16:50	06-May, 17:18
	Back of Max Conc.	06-May, 10:48	06-May, 14:12		
	Back of Ice Run	06-May, 12:10	06-May, 16:00	06-May, 19:32	06-May, 20:06
H	Front of Ice Run		06-May, 03:24	06-May, 06:50	06-May, 07:12
	Max Conc.		06-May, 03:38	06-May, 07:26	06-May, 07:42
	Back of Ice Run		06-May, 05:12	06-May, 09:50	06-May, 10:12
13	Front of Ice Run			04-May, 08:02	04-May, 08:24
	Front of Max Conc.			04-May, 08:32	
	Back of Ice Run			04-May, 08:50	04-May, 09:46
14	Front of Ice Run			04-May, 23:44	05-May, 00:06
	Back of Ice Run			05-May, 01:26	05-May, 01:48
15	Front of Ice Run			05-May, 04:02	05-May, 04:18
	Front of Max Conc.				05-May, 04:48
	Back of Ice Run			05-May, 04:26	05-May, 05:06

Table 2.18, 2009 travel times and speeds of ice run features.

Event	Description	EMO-AF to EMO-PG		EMO-PG to WSC-HR		WSC-HR to EMO-PPB	
		Travel Time	Speed, m/s	Travel Time	Speed, m/s	Travel Time	Speed, m/s
G1	Front of Ice Run	03:20	3.0	04:14	1.8	00:10	6.2
	Front of Max. Conc.			04:03	1.9	00:27	2.3
	Back of Ice Run	03:50	2.6	03:38	2.1	00:16	3.9
G2	Front of Ice Run	02:17	4.3	04:56	1.6	00:06	10.4
	Max Conc.	03:14	3.0	04:08	1.9		
	Back of Ice Run	03:44	2.6	03:50	2.0	00:16	3.9
G3	Front of Ice Run	03:08	3.1	03:56	2.0	00:22	2.8
	Front of Max. Conc.	03:44	2.6	04:08	1.9	00:28	2.2
	Back of Max Conc.	03:24	2.9				
	Back of Ice Run	03:50	2.6	03:32	2.2	00:34	1.8
H	Front of Ice Run			03:26	2.2	00:22	2.8
	Max Conc.			03:48	2.0	00:16	3.9
	Back of Ice Run			04:38	1.7	00:22	2.8
13	Front of Ice Run					00:22	2.8
	Front of Max Conc.						
	Back of Ice Run					00:56	1.1
14	Front of Ice Run					00:22	2.8
	Back of Ice Run					00:22	2.8
15	Front of Ice Run					00:16	3.9
	Front of Max Conc.						
	Back of Ice Run					00:40	1.6
		Average:	3.0	Average:	1.9	Average:	3.4

Table 2.18 shows that between the EMO-AF and EMO-PG stations, the speeds of ice features ranged between 2.6 m/s and 4.3 m/s, averaging 3.0 m/s. In the reach between the EMO-PG and WSC-HR stations, the ice runs moved at an average speed of 1.9 m/s, and ranged between 1.7 m/s and 2.2 m/s. Similarly, between the WSC-HR and EMO-PPB stations, the ice runs ranged between 1.1 m/s and 6.2, and averaged 3.4 m/s. The speed of 10.4 m/s was not included in the average, since it appears to be an outlier. The lag-times of ice runs with associated water waves

are shown in Table 2.19 and normalized lag-times of all ice runs that could be matched to a water wave are shown in Table 2.20.

Table 2.19, 2009 lag-times of ice run features to associated wave features.

Events	Feature of Ice Run	EMO-AF (1032.0 km)		EMO-PG (1067.5 km)		WSC-HR (1067.5 km)		EMO-PPB (1098.0 km)	
		Front of Wave	Peak of Wave	Front of Wave	Peak of Wave	Front of Wave	Peak of Wave	Front of Wave	Peak of Wave
A	Front of Ice Run	+ 00:29	- 00:19						
	Fron of Max Conc.	+ 00:41	- 00:07						
B	Front of Ice Run	+ 00:11	- 00:54						
	Fron of Max Conc.	+ 00:59	- 00:06						
C	Front of Ice Run	+ 01:30	- 00:36						
	Fron of Max Conc.	+ 01:48	- 00:18						
D	Front of Ice Run	+ 03:18	+ 01:13						
E	Front of Ice Run	+ 03:35	+ 02:17						
F	Front of Ice Run	+ 04:26	- 00:14						
G1	Front of Ice Run	+ 02:40	- 07:41	+ 03:23	- 08:35	+ 07:08		+ 06:17	
	Fron of Max Conc.			+ 03:59	- 07:59	+ 07:33		+ 06:59	
G2	Front of Ice Run	+ 06:19	- 04:02	+ 05:59	- 05:59	+ 10:26		+ 09:31	
	Fron of Max Conc.	+ 06:34	- 03:47	+ 07:11	- 04:47	+ 10:50			
G3	Front of Ice Run	+ 08:22	- 01:59	+ 08:53	- 03:05	+ 12:20		+ 11:41	
	Fron of Max Conc.	+ 08:34	- 01:47	+ 09:41	- 02:17	+ 13:20		+12:47	
H	Front of Ice Run			+ 00:23		+ 03:20		+ 02:41	
	Fron of Max Conc.			+ 00:37		+ 03:56		+ 03:11	
Note: "-" indicates the ice feature was earlier than the wave feature "+" indicates the ice feature was later than the wave feature									

Table 2.20, 2009 normalized lag-times of ice features to the front of associated wave features, expressed in minutes-per-kilometre-traveled.

Event	Feature of Ice Run	EMO-AF (1032.0 km)	EMO-PG (1067.5 km)	WSC-HR (1067.5 km)	EMO-PPB (1098.0 km)
A ~ 1025 km	Front of Ice Run	4.14			
	Front of Max Conc.	5.86			
B ~ 1025 km	Front of Ice Run	1.57			
	Front of Max Conc.	8.43			
C ~ 1015 km	Front of Ice Run	5.29			
	Front of Max Conc.	6.35			
D ~1005	Front of Ice Run	7.33			
E ~1000	Front of Ice Run	6.72			
F ~ 990 km	Front of Ice Run	6.33			
G1 ~ 965	Front of Ice Run	2.39	1.98	3.28	2.83
	Front of Max Conc.		2.33	3.47	3.15
G2 ~965	Front of Ice Run	5.66	3.50	4.80	4.29
	Front of Max Conc.	5.88	4.20	4.98	
G3 ~965	Front of Ice Run	7.49	5.20	5.67	5.27
	Front of Max Conc.	7.67	5.67	6.13	5.77
H ~ 1049	Front of Ice Run		1.24	4.31	3.29
	Front of Max Conc.		2.00	5.09	3.90

As seen in Table 2.20, lag-times for events ‘A’ through ‘E’ were only available for the EMO-AF stations, while lag-times for events ‘G1’, ‘G2’, ‘G3’ and ‘H’ could be established at successive stations. Consistent with the analysis of the 2007 and 2008 breakup seasons, the majority of the features of the ice run were observed to arrive before the peak of the water wave. It is interesting

to note that when events were tracked through multiple stations, the lag-time of the ice increased as the event traveled downstream as expected, but the normalized lag-times remained relatively constant over successive stations, suggesting that the ice runs fall behind the water wave at a consistent rate.

2.4.5 Summary of Breakup Analysis 2007-2009

The speeds of wave events were able to be ascertained for the 2007 and 2009 breakup seasons were presented in section 2.4.2 to 2.4.4. As discussed, the WSC-HR and WSC-PPB gauges were often ice affected during breakup, and only a single wave event (the front of wave 'H', discussed in section 2.4.4.1) was able to be tracked between these stations. Several waves were able to be tracked between the EMO-AF and EMO-PG stations; however the speeds of the waves between the stations were not consistent between breakup seasons. For example, the speeds of all wave features (front and peak) ranged between 3.3 m/s and 6.9 m/s during the 2007 breakup season and the speeds of all wave features for the 2009 breakup season were much lower, ranging between 1.5 m/s and 2.5 m/s. The average front of wave speed was 3.8 m/s and the average wave peak speed was 3.3 m/s for over all breakup seasons, but these speeds may not be a reliable forecasting tool.

Over the successive breakup seasons, multiple ice runs were able to be seen traveling between the TLCS. The majority of the ice run data is from the 2009 and 2007 breakup seasons, both of which contained ice runs between the EMO-AF and EMO-PG stations. Unlike the water wave speeds, the speeds of these events between these common stations seemed to be similar, ranging between 2.3 m/s and 4.7 m/s for the 2007 breakup season and 2.6 m/s and 4.3 m/s for the 2009 breakup season. A big disparity between the differing features of the ice runs (front/back of ice

run and maximum concentration) was not observed, and so an average speed of 2.7 m/s was calculated using the speeds of all observed ice features for the 2007, 2008 and 2009 breakup seasons.

The ice normalized lag-times for related water and ice events were plotted against the estimated station of origin of the ice masses and are shown in Figure 2.16. The Figure shows that normalized lag-times were highly variable, ranging between 0.7 and 8.4 minutes-per-kilometre-traveled (ignoring the value of 13.5 as an outlier). The normalized lag-times did not seem to be dependent on the initial location of the ice mass. An average value of 4.4 minutes-per-kilometre-traveled was calculated using all the events for the 2007 to 2009 breakup seasons for which lag-times could be determined. It is interesting to note that nearly all of the lag-times for ice runs had to be determined using the front of the wave, as most ice runs were observed to arrive before the peak of the wave.

2.5 Observed Ice Jam Release Events

The above analysis for the 2007, 2008, and 2009 breakup seasons include the speeds and relationships between all observed water waves and ice runs, including events associated with ice jam release events. During this analysis, two ice jam release events were identified in each of the breakup seasons. All observations related to the six observed ice jam release events are summarized in this section.

2.5.1 Ice Jam Release Event 1 - 2007

The intact ice jam associated with Ice Jam Release Event 1 was observed during the 25-Apr observation flight conducted at 19:00 during the 2007 breakup season. As shown in Figure 2.17,

this ice jam was toed just behind an in-channel island at station 1025.9 km, and was 4.8 km long. The released wave was observed during the 2007 analysis and was labelled 'B' on Figure 2.11 as discussed in section 2.4.2.2, and can be found in Table 2.8. No ice run data was able to be observed.

The time of the ice jam release was estimated by extrapolating the observations of the released wave 'B' at the downstream gauged station back to the observed toe of the ice jam, and was further refined by modeling. The estimated time of release is 22:00 on 25-Apr. The discharge on the study reach at the approximate time of release is also shown in Figure 2.17 and was estimated to be 290 m³/s, which was estimated using the rating curve for the EMO-AF gauge as introduced in section 2.3.3. It is noted that the discharges are difficult to estimate during breakup events due to the highly dynamic processes, and the best estimate of the discharge must be used.

2.5.2 Ice Jam Release Event 2 - 2007

Ice Jam Release Event 2 was the second observed release event of 2007, and the initial ice jams associated with the release was observed during the observation flight conducted at 11:00 on 26-Apr as shown in Figure 2.18. When initially observed during the observation flight two ice jams were present: the first ice jam was toed at station 958.2 km behind a deteriorated ice cover and was 6.7 km long; the second ice jam was toed 2 km upstream of the head of the first ice jam at station 949.5 and was 9.5 km long. At 11:51, the second ice jam was observed sliding downstream which caused the first ice jam to shove downstream and consolidate. The final ice jam that resulted from the second ice jam joining the first ice jam was not directly observed and the WSC-Border gauge was used to interpret the events.

Figure 2.19 shows the stage hydrograph for the WSC-Border gauge and the estimated discharge hydrograph for the EMO-AF, which were used to interpret Ice Jam Release Event 2. A drop in stage was seen at the WSC-Border gauge on 26-Apr from 10:30 to 12:00, corresponding with the observed movement of the ice jams. The water level rose after this period, which suggests that the first ice jam did not release as it was joined by the ice mass from the second jam, and a new ice jam was formed at the location of the first ice jam. The stage begins to drop at 16:30 before rapidly dropping at 18:00, indicating that the ice jam may have slid or shoved briefly before it released at 18:00. The estimated discharge at the time of release on the study reach was determined to be 450 m³/s using the calculated discharge at the EMO-AF.

The released wave from this ice jam release event was identified during the 2007 breakup analysis, discussed in section 2.4.2.2 and shown in Figure 2.11 labelled ‘E’. Water wave ‘E’ was observed at both the EMO-AF and EMO-PG stations. The resultant ice run was observed prior to its arrival at the EMO-AF, during an observation flight conducted on 27-Apr at 19:00, as shown on Figure 2.20. The features of the ice run as observed during the observation flight and the TLCS are summarized below in Table 2.21.

Table 2.21, Observed ice run features and speeds for Ice Jam Release Event 2.

Ice Run Feature	Observed at		Speed, m/s
	Station	Date/Time	
Back of 100% Concentration	951.0	26-Apr, 20:05	--
	1032.0	27-Apr, 12:30	1.4
Front of 100% concentration	969.5	26-Apr, 19:55	--
	970.0	26-Apr, 20:09	0.6
	1032.0	27-Apr, 06:00	1.7
Front of ice run	973.3	26-Apr, 19:54	1.6
	974.5	26-Apr, 20:11	1.2
	1032.0	27-Apr, 05:00	1.8

2.5.3 Ice Jam Release Event 3 - 2008

The release of the ice jam comprising Ice Jam Release Event 3 was observed during the observation flight conducted on 4-May at 14:35. The initial ice jam was toed at station 992.5 km and was 6.2 km long as illustrated in Figure 2.21. The observations of the released ice mass are shown in Figure 2.22.

Figure 2.22 shows a diagram illustrating the flight path and ice movements observed during the 4-May observation flight. The solid, multi-coloured line depicts the flight path and is colour coded according to the ice conditions observed along the river. Solid (filled) symbols denote individual, distinguishable ice floes that were photographed multiple times to give an estimation of the surface water velocity. Open symbols represent identifiable parts of an ice jam and/or ice run that were tracked photographically as well.

Figure 2.22 illustrates the 6.2 km long ice jam was observed at 15:03, during the flight up-river. It had toed out on some juxtaposed, broken ice sheets just downstream of Grumbler Rapids, as previously shown in Figure 2.21. The jam had released by the time the return flight was made, and the plane circled the site so that the release could be documented as thoroughly as possible. Within the ice jam, and the subsequent ice run, the following features were identified: the front of the 100% ice concentration, the back of the 100% ice concentration, and two identifiable ice floes within the jam, denoted 'A' and 'B' in Figures 2.21 and 2.22. The toe of the jam was originally at station 992.5 km at 15:03, Particle A was at 989.4 km (roughly the middle of the jam), Particle B was at station 986.8 km (near the head of the jam), and the upstream end of the 100% ice concentration point was at station 986.3 km. The locations of these features were each documented four times after the release occurred, as seen in Figures 2.23 through 2.26, and summarized in Table 2.22.

Table 2.22, Features and speeds of observed ice run from Ice Jam Release Event 3, as observed from during the observation flight of 4-May at 14:35.

Feature of Ice Run	Observed:		
	Station	Date/Time	Speed, m/s
Front of 100% Concentration	992.5	04-May, 15:03	Jammed
	999.1	04-May, 15:52	2.3
	999.5	04-May, 15:56	1.8
	1000.6	04-May, 16:07	1.6
	1001.4	04-May, 16:09	5.0
Observed Particle 'A'	989.4	04-May, 15:02	Jammed
	993	04-May, 15:51	1.2
	993.9	04-May, 15:57	2.4
	994.5	04-May, 16:05	1.2
Observed Particle 'B'	986.8	04-May, 15:03	Jammed
	989.6	04-May, 15:50	1.0
	990.4	04-May, 15:58	1.7
	991	04-May, 16:04	1.6
Back of 100% Concentration	986.3	04-May, 15:03	Jammed
	988.5	04-May, 15:50	0.8
	989.1	04-May, 15:58	1.2
	989.5	04-May, 16:03	1.3

Figure 2.22 summarizes this data, from which the following speeds were deduced: 2.19 m/s for the front of the 100% concentration; 1.74 m/s for Particle ‘A’; 1.66 m/s for Particle ‘B’; and 1.23 m/s for the back of the 100% concentration. Projecting the last four points back in each case also facilitates the estimation of the time of release from each segment of the jam, as summarized in Table 2.23 (and shown as blue Xs in Figure 2.22).

Table 2.23, Estimated time release for Ice Jam Release 3, and average observed propagation speed.

Feature	Estimated Time of Release	Average Propagation Speed, m/s
Front of 100% concentration	15:02	2.19
Particle 'A' (near mid-jam)	15:16	1.74
Particle 'B' (near head of jam)	15:22	1.66
Back of 100% concentration	15:20	1.23

Table 2.23 and Figure 2.22 both suggest that the front of the ice run moved quicker than indicated by these last four points, since the jam was known to still be in place at 15:03. This means that earlier during the release event, the 100% concentration front would have had to move faster than 2.19 m/s. Interestingly, Figure 2.22 also illustrates that the other features appear to have moved at relatively constant speeds from the time of release, at least up to the point of the last measurement, approximately 1 hour later.

The released water wave and ice run were observed at the EMO-AF station. The stage hydrograph and ice conditions at the EMO-AF station was discussed in section 2.4.3.2, and the release event was labelled 'D' in Figure 2.12. The ice run arrived at the EMO-AF TLCS at 18:05 and increased to a maximum concentration of 90% at 21:00. This results in a speed of 1.74 m/s for the front of the maximum concentration of the ice run from the time it was observed during the observation flight to when observed at the EMO-AF TLCS, which is slightly lower than the speed of 2.19 m/s as previously observed. Although the front of the ice run was not tracked for the analysis, it is noted that if the time of release is taken to be 15:03, the front of the ice run traveled at an average speed of 3.62 m/s, timed from the toe of the ice run at release to when first observed at the EMO-AF TLCS.

Figure 2.22 also illustrates the velocities of four individually identifiable discrete floes that were each observed twice during the 4-May flight. The first solitary ice floe (shown as the solid diamond in Figure 2.22) was first seen at station 979.5 km (approximately 7 km upstream of the head of the jam at Grumbler Rapids) at 15:04. Based on a second observation 6 minutes later, this ice floe was moving at an estimated velocity of 0.77 m/s. This is a useful value, since it may be representative of the velocity of the river before the jam released. Two other discrete ice floes, located ~700 m apart, were tracked starting from river station 953 km at 15:16; these are shown as the solid triangles and circles in Figure 2.22. Based on a second observation 20 minutes later, these two ice floes were moving at 0.97 m/s and 1/13 m/s, respectively. A fourth discrete ice flow was first seen at station 985.3 km (~2 km upstream of the back of the 100% concentration point in the running ice) at 16:00. This particle moved 300 m in the ensuing 2 minutes, which suggests a local velocity of 2.56 m/s. Given that this speed is well in excess of the propagation velocities in the ice run itself, it is likely that this velocity is overestimated. This is probably due to the short distance and time between observations.

Ice Jam Release Event 4 triggered the release of the ice jam that was present in the Gorge, as discussed in section 2.4.4. and shown on the flightmap in Figure 2.12. This was deduced through field investigations, as well as the timing of the propagation of the wave from Ice Jam Release Event 3 with the estimated release of Ice Jam Release Event 4. Ice Jam Release Event 4 is discussed next.

2.5.4 Ice Jam Release Event 4 – 2008

Ice Jam Release Event 4 was comprised of the release of an ice jam seen during the 4-May observation flight at 20:00. As shown in Figure 2.27, this 6.0 km ice jam was toed at station

1051.0 km in the Gorge near Enterprise. The ice run from this event was not observed, and the released wave was only seen at the EMO-PG station, and is labelled 'E' on Figure 2.13, as discussed in section 2.4.3.2, and the features of the observed wave at the EMO-PG station is summarized in Table 2.12.

The time of release was estimated to be 21:00 on 4-May, which was interpolated using approximated arrival of the released wave from Ice Jam Release Event 3 and the arrival of the newly released wave observed at the EMO-PG, and was further refined with modeling attempts. This discharge on the study reach was estimated using the rating curve developed for the EMO-AF as discussed in section 2.3.3. At the estimated time of release, the carrier discharge on the Hay River was estimated to be 650 m³/s.

2.5.5 Ice Jam Release Event 5 - 2009

Ice Jam Release Event 5 was the result of the release of an ice jam that was originally observed near the NWT/AB Boundary during an observation flight conducted on 5-May at 14:00, as described in section 2.4.4.1 and shown in Figure 2.15. Figure 2.28 shows that the ice jam was 2.6 km long and was toed at station.948.6 km and there was a small 500 m sheet accumulation located approximately 500 m upstream of the head of the ice jam.

The stage hydrograph for the WSC-Border and estimated discharge hydrograph for the EMO-AF for this period are shown in Figure 2.29. The stage hydrograph at the WSC-Border suggests that this ice jam could have shoved or slid downstream but re-stabilized before it released. This could mean that the ice jam could have slid downstream and re-jammed behind the deteriorated ice cover seen at station 965 km (refer to the flightmap in Figure 2.14, as discussed in section 2.4.4.1), or the ice jam consolidated and lengthened due to an ice floe which joined the jam after

it was observed. The approximate time of release was estimated at 19:15 from the stage drop on the hydrograph at the WSC-Border, and the corresponding discharge on the study reach was estimated to be 550 m³/s from the EMO-AF discharge hydrograph.

The resulting water wave from this Ice Jam Release Event was introduced in section 2.4.4.2 and is labelled 'G' in Figure 2.15. The ice run could not be identified with confidence from three possible 'G1', 'G2' and 'G3' in Figure 2.15, so all three ice runs were analysed. The features of the water wave can be found in Table 2.15 and ice runs associated with Ice Jam Release Event 4 can be found in Table 2.16.

Similar to the 2008 breakup season, the released water wave and ice mass was responsible for triggering the release of a downstream ice jam, which caused Ice Jam Release Event 6. This was introduced earlier in section 2.4.4. Ice Jam Release Event 6 is discussed next.

2.5.6 Ice Jam Release Event 6 – 2009

Ice Jam Release Event 6 was comprised of the release of three ice jams in the gorge near Enterprise, due to the arrival of the released wave from Ice Jam Release Event 6. The location of these ice jams were last observed by the 5-May observation flight, as shown in Figure 2.15. As seen in Figure 2.30, the first ice jam was 1.4 km long and was toed against an in-channel island and deteriorated ice cover; the second jam was toed ~500 m upstream of the first ice jam at station 1047.1 km and was 1.1 km long; the third ice jam was ~1 km upstream of the second ice jam at station 1045.0 km, and was 4.3 km long. The release of this ice jam was observed by THR-EMO volunteers at 02:00 on 6-May.

The release water wave was observed at the downstream gauged stations as discussed in section 2.4.4.2, and were labelled ‘H’ in Figure 2.15. In addition to the ice run from this release event being identified through the analysis of TLCS data, the ice run was also observed from the several ground locations by THR-EMO volunteers and UofA researchers. All the observations of the released water wave can be found in Table 2.15 and ice run data is summarized below in Table 2.24.

Table 2.24, Front and back of the 100% concentration from the observed ice run resulting from
Ice Jam Release Event 6.

Feature	Location of Observation	River Stationing, km	Time of Observation	Observed Speed, m/s
Front of 100% Concentration	Toe of Initial Jam	1049.0	2:00	Time of Release
	EMO-PG	1067.5	3:24	3.7
	Ground obs from River Bank	1076.5	4:25	2.5
	Golf Course	1089.5	6:11	2.0
	WSC Gauge 07OB001	1095.3	7:07	1.7
	EMO-PPB	1098.0	7:32	1.8
	Chamber of Commerce Park	1103.5	9:30	0.8
Back of 100% Concentration	Head of Initial Jam	1039.5	2:00	Time of Release
	EMO-PG	1067.5	5:12	2.4
	Golf Course	1089.5	8:50	1.7
	WSC-HR	1095.3	9:50	1.6
	EMO-PPB	1098.0	10:12	2.0
	Chamber of Commerce Park	1103.5	11:28	1.2

Figures 2.30 also illustrates the discharge on the study reach at the time of release, which was determined to be 550 m³/s from the calculated EMO-AF discharge hydrograph.

2.5.7 Summary of Ice Jam Release Events

For quick reference, a table of was created to summarize all of the ice jam release events. In this table, the observations of the original ice jam are summarized along with the estimated discharge and time of release. The table also lists where the information regarding the released water wave and ice mass can be found. Table 2.25 contains a brief summary of all Ice Jam Release Events.

Table 2.25, Summary of all documented Ice Jam Release Events between 2007 and 2009.

Event	Observation of Ice Jam				Estimated Date/Time of Release	Estimated Discharge at Release, m ³ /s	Observation of Released	
	Description	Jam Toe, km	Jam Length, km	Observed Jam			Water Wave	Ice Mass
1 (2007)	U/S of EMO-AF	1025.9	4.8	Fig. 2.11	25-Apr, 22:00	290	'B' - Fig. 2.11 Table 2.8	Not Observed
2 (2007)	Near NWT/AB Boundary	958.2 949.5	6.7 9.5	Fig. 2.18	26-Apr, 18:00	480	'E' - Fig 2.11 Table 2.8	'E' - Fig 2.11 Table 2.9
3 (2008)	Near Grumbler Rapids	992.5	5.7	Fig 2.21	4-May, 15:00	450	'D' - Fig 2.13 Table 2.12	'D' - Fig 2.13 Table 2.12 Table 2.22
4 (2008)	Gorge, Near Enterprise	992.0	6.0	Fig. 2.27	04-May, 21:00	450	'E' - Fig 2.12 Table 2.12	Not Observed
5 (2009)	Near NWT/AB Boundary	948.6	2.6	Fig 2.29	05-May, 19:15	550	'G' - Fig 2.12 Table 2.15	'G' - Fig 2.15 Table 2.17
6 (2009)	Gorge, Near Enterprise	1049.0 1047.1 1045.0	1.4 1.1 4.3	Fig 2.30	6-May, 02:00	550	'H' - Fig 2.15 Table 2.15	'H' - Fig 2.15 Table 2.17

It should be noted that of the six observed ice jam release events, only the time of release for events 3 and 6 were observed, as discussed in sections 2.5.3 and 2.5.6 respectively. The release times for all other events were interpolated using hydrograph data and refined using modeling techniques which are discussed in chapter 3. As such, the accuracies of the estimated times of release are unknown.

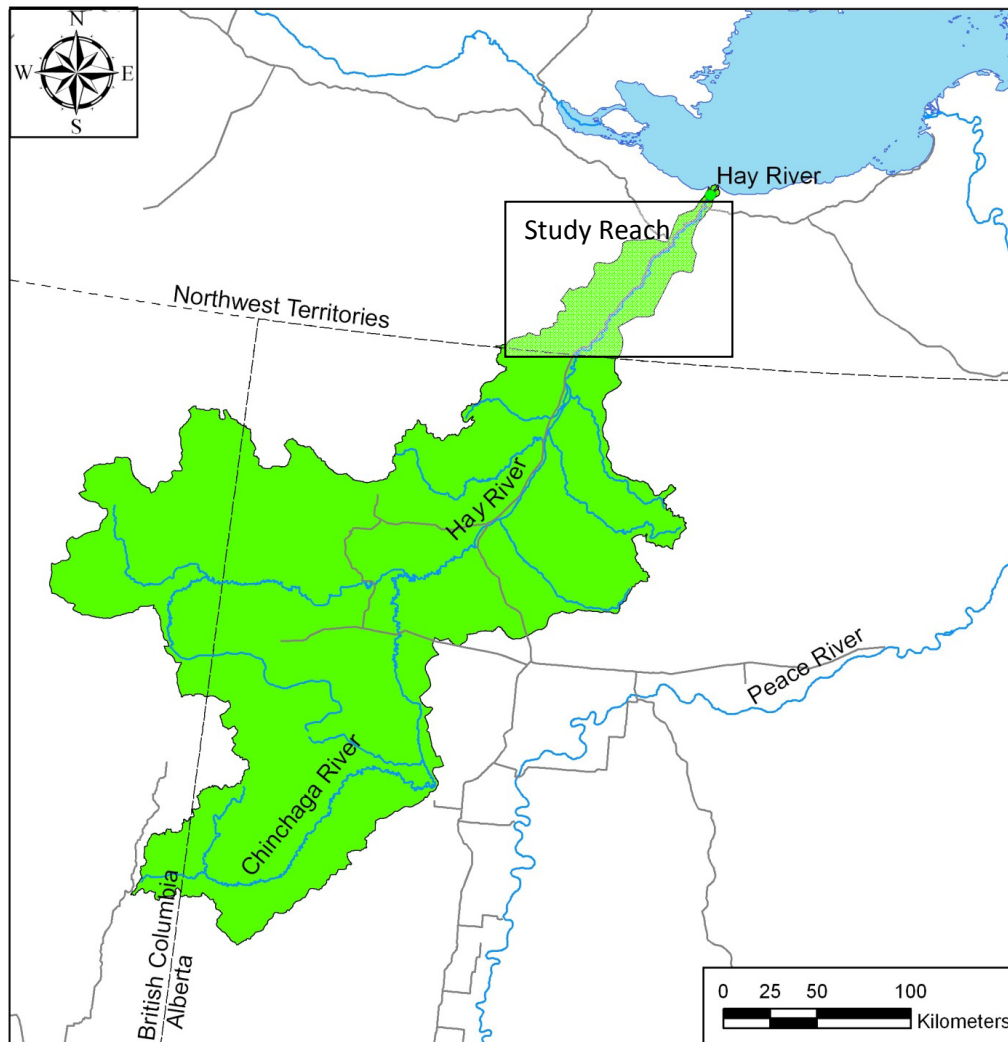


Figure 2.1, Hay River basin showing study reach.

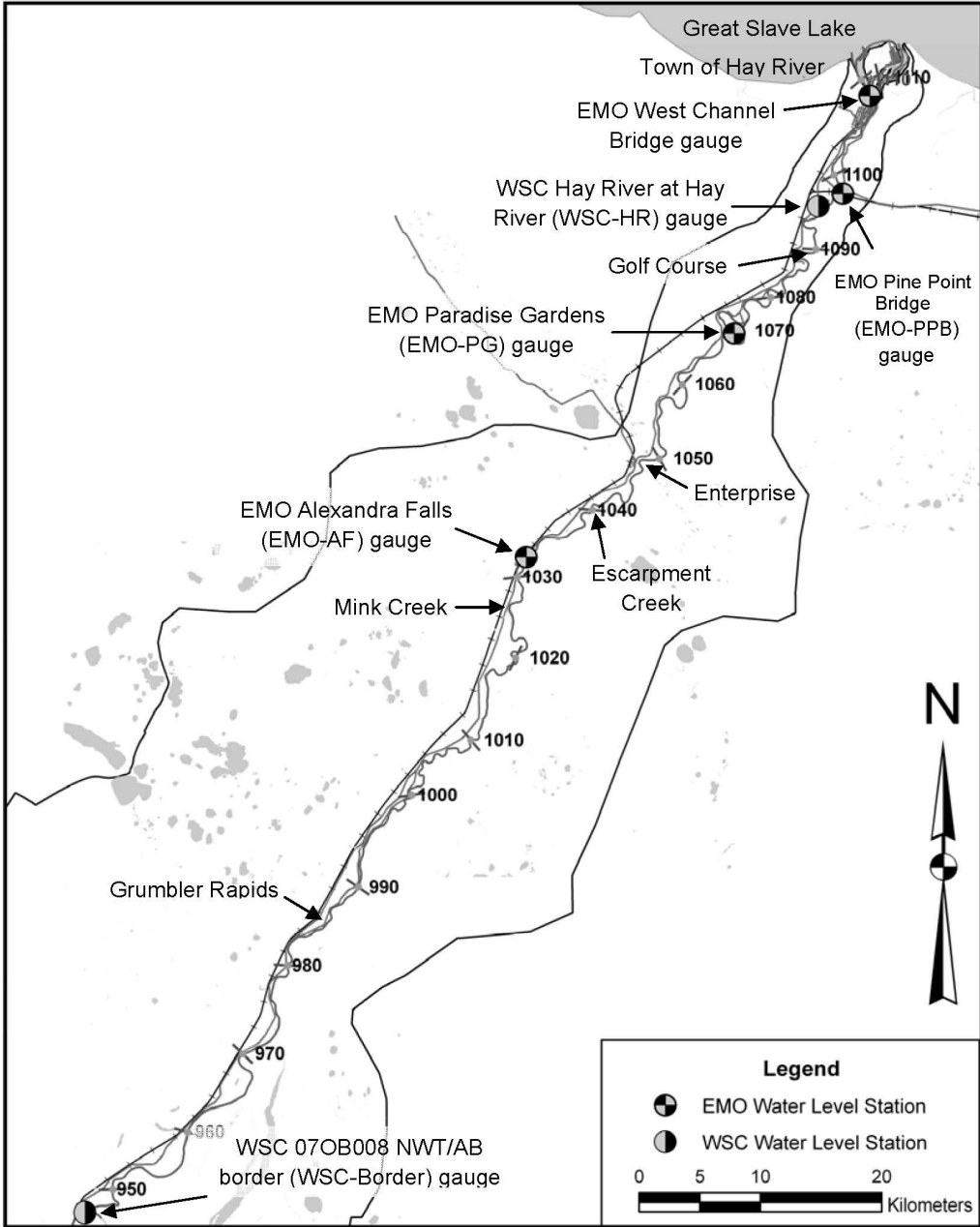


Figure 2.2, Study reach and locations of interest.

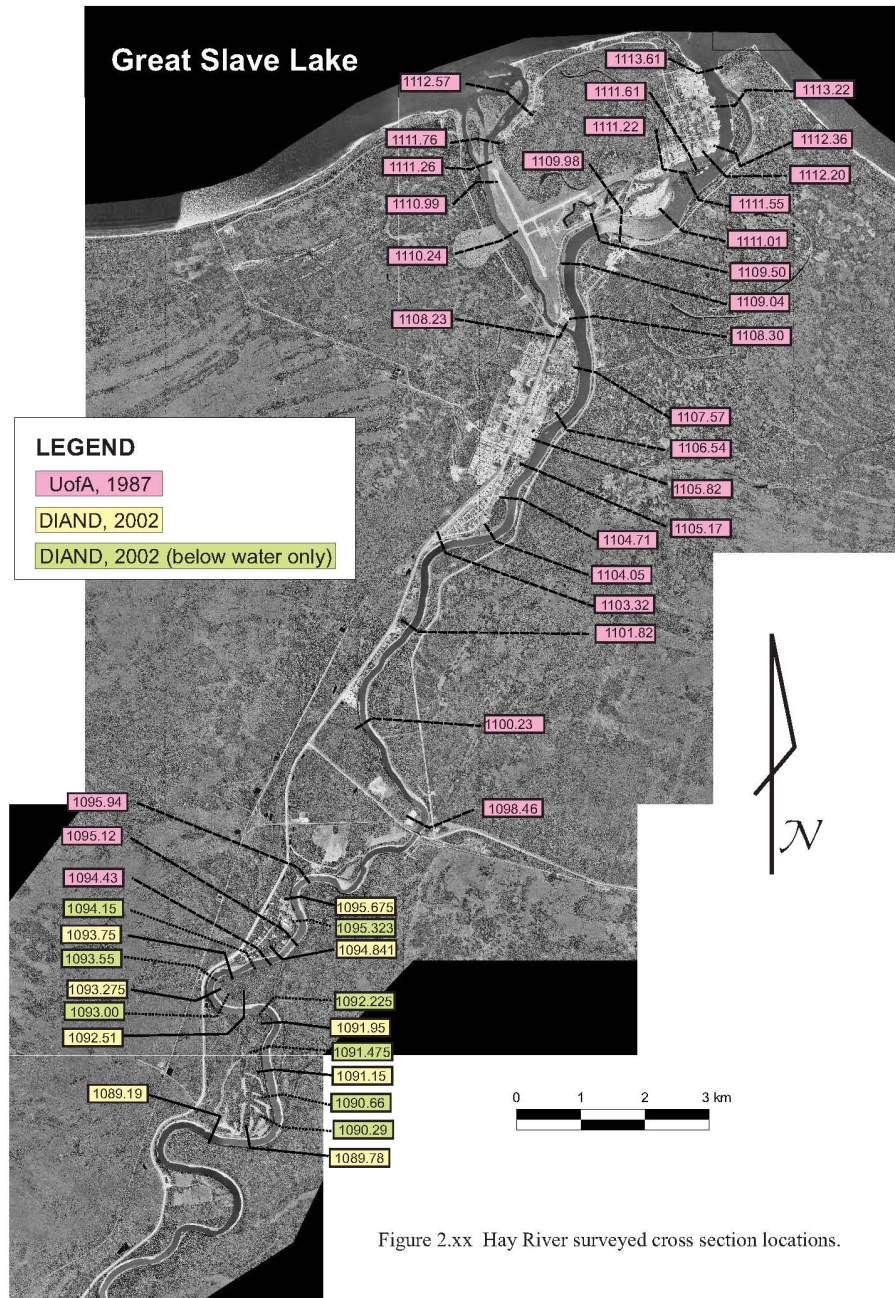


Figure 2.3, Available surveyed data within the study reach.

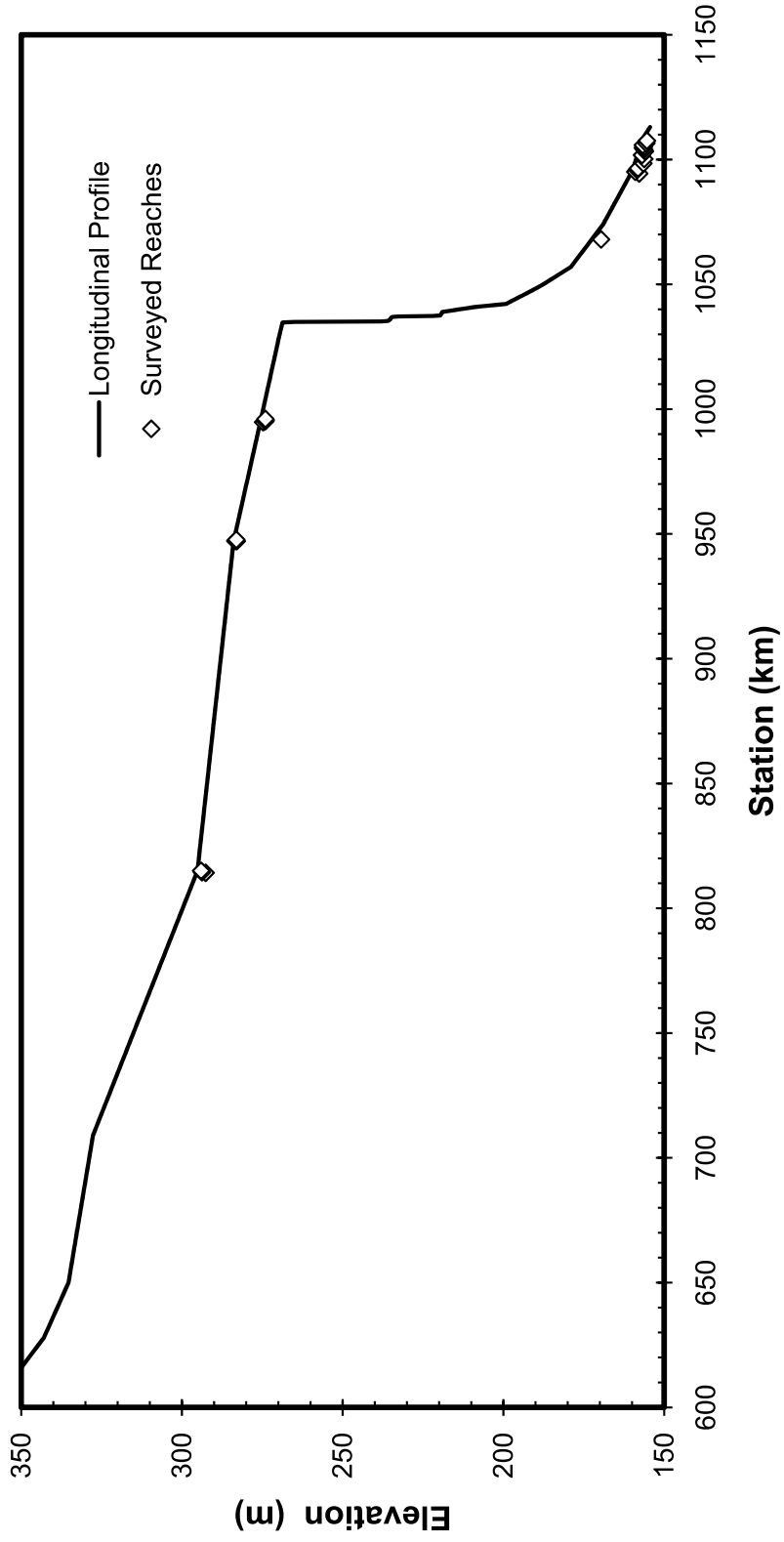


Figure 2.4, Bed profile of equivalent rectangular channel for the Hay River (adapted from Hicks *et al.*, 1992).

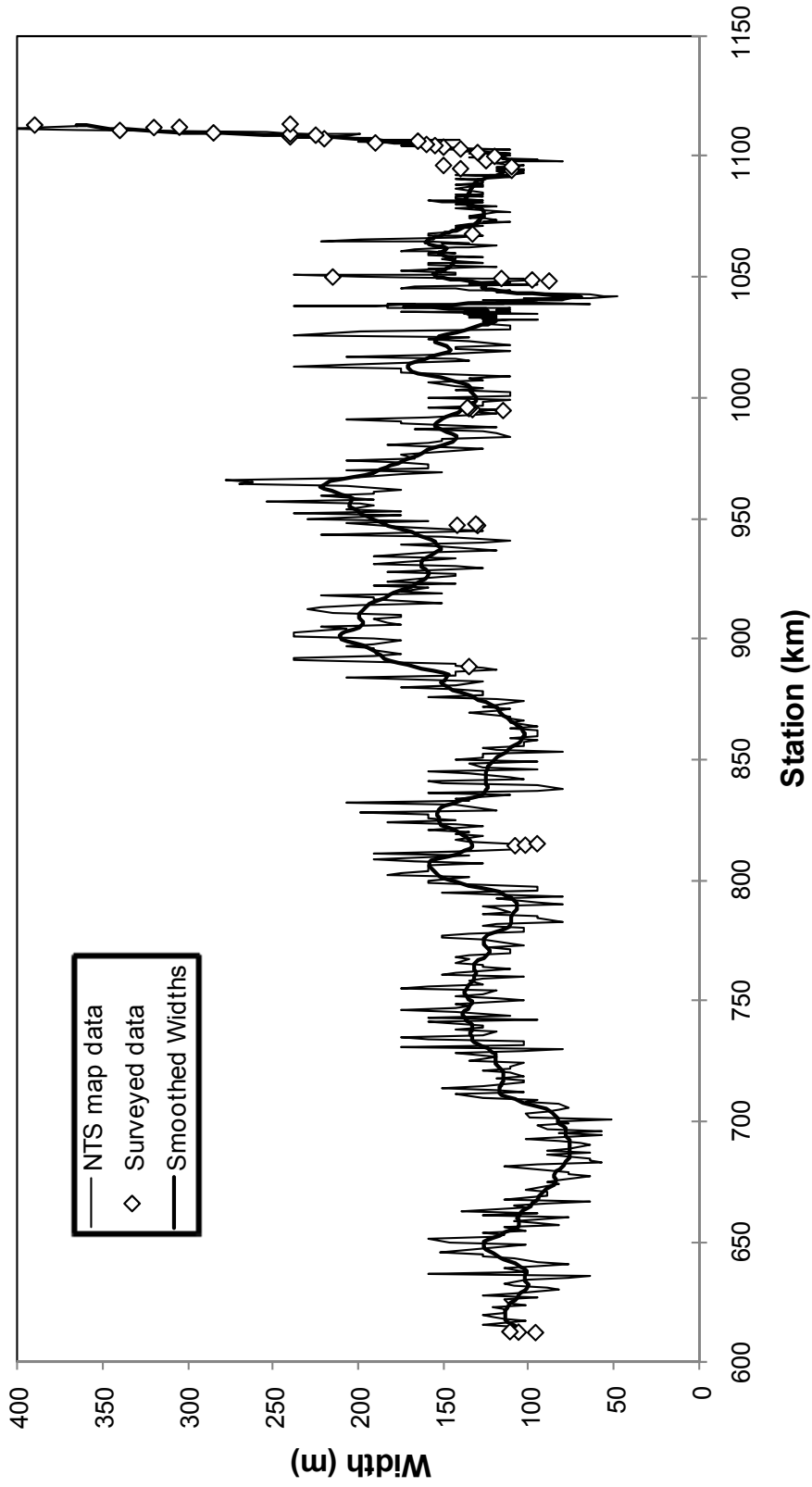


Figure 2.5, Top widths (smoothed and un-smoothed) of the Hay River (adapted from Hicks *et al.* 1992).

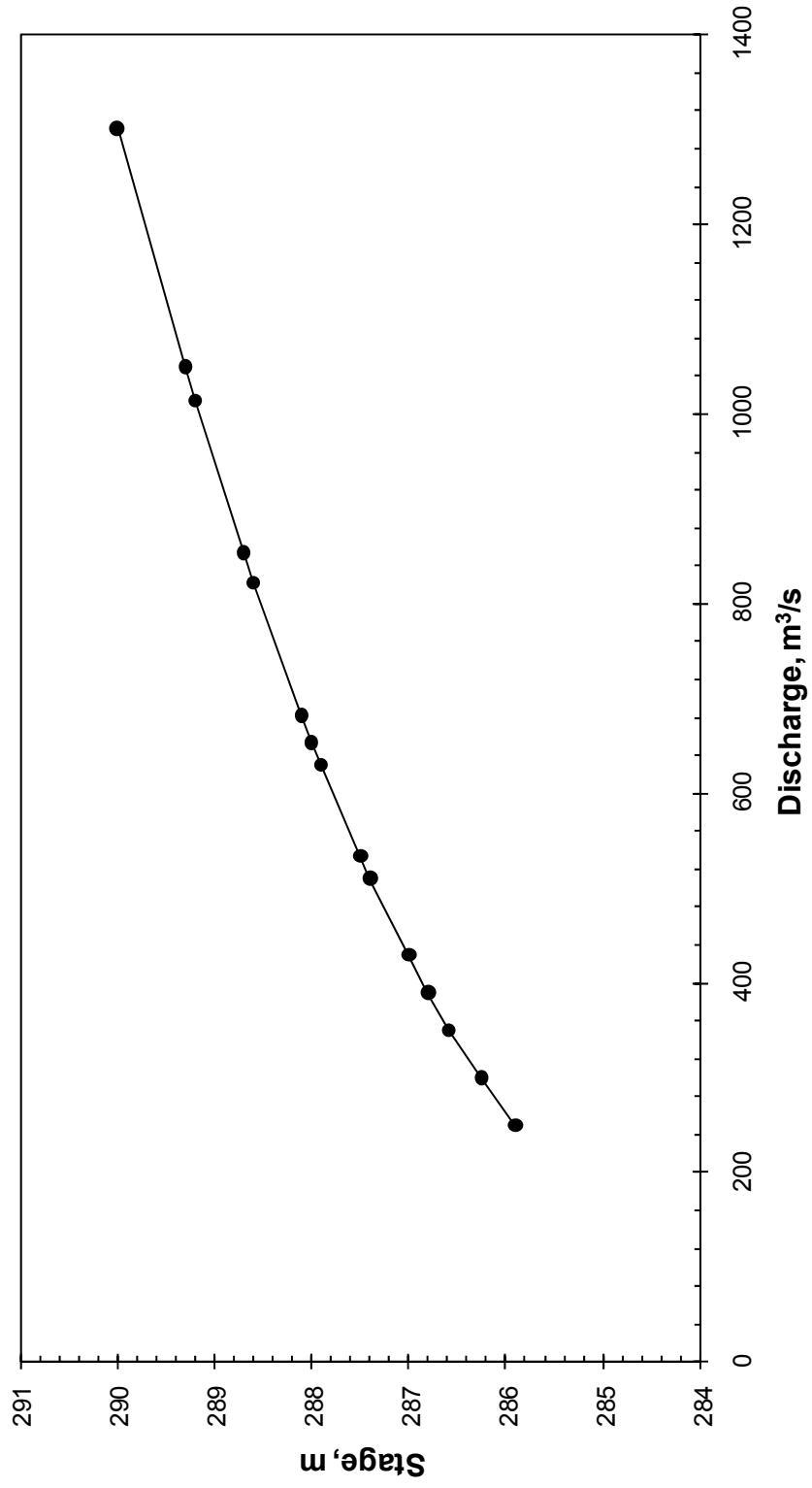


Figure 2.6, WSC provided rating curved for WSC gauge (07OB008) Hay River near ALTA/NWT Boundary.

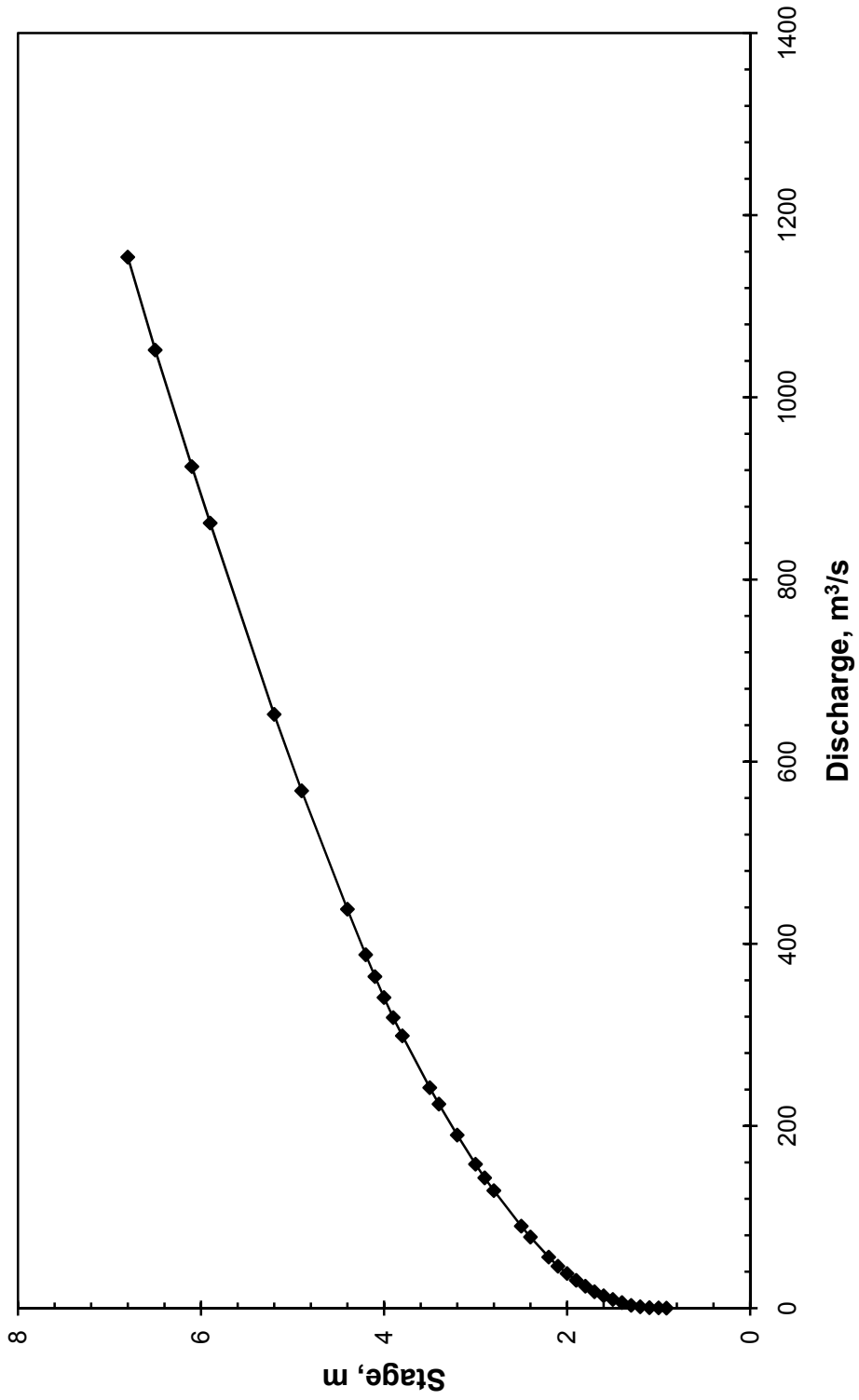


Figure 2.7, WSC provided rating curved for WSC gauge (07OB001) Hay River near Hay River.

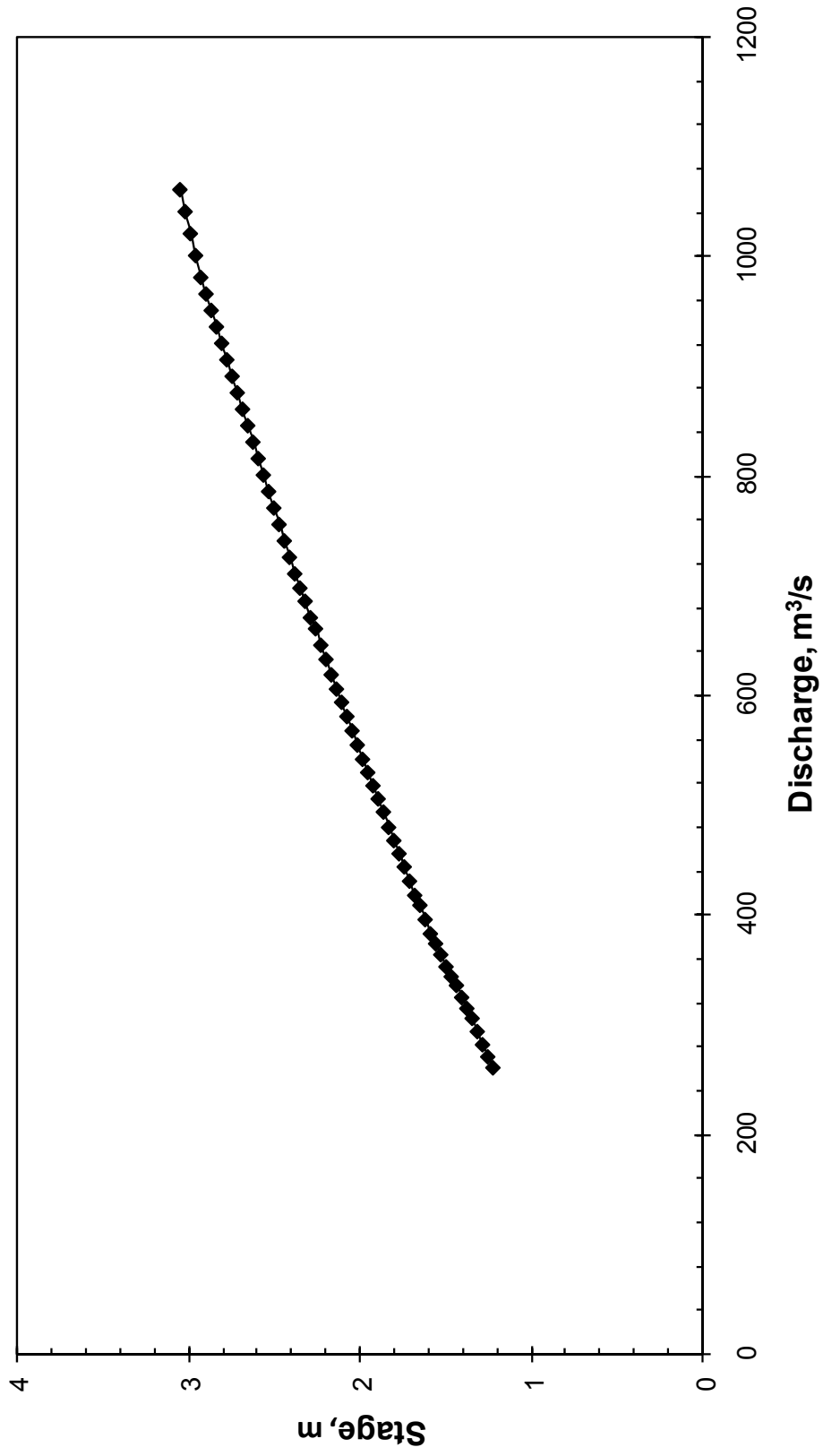


Figure 2.8, Rating curve for the EMO Alexandra Falls gauge as provided by THE-EMO.

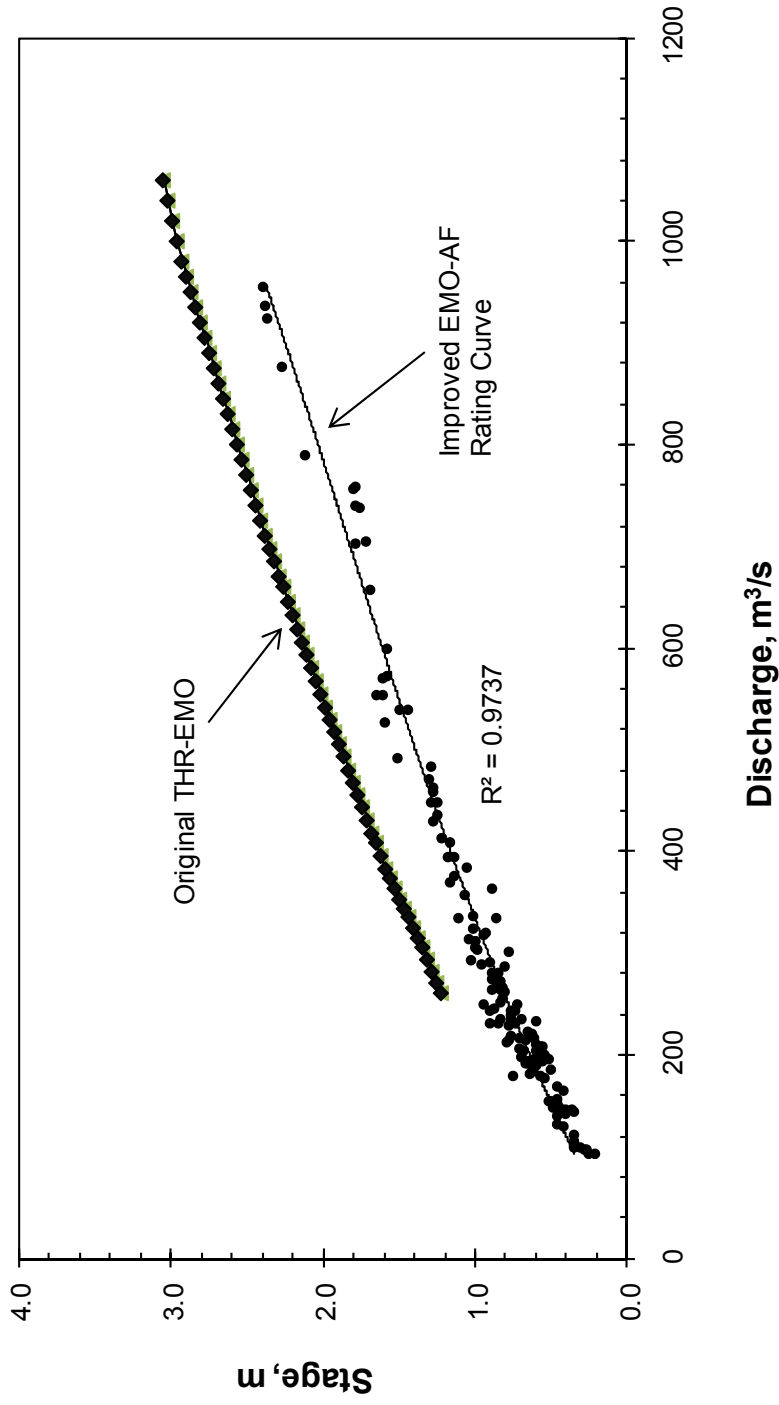


Figure 2.9, Improved EMO-Alexandra Falls gauge rating curve, with original rating curve from THR-EMO.

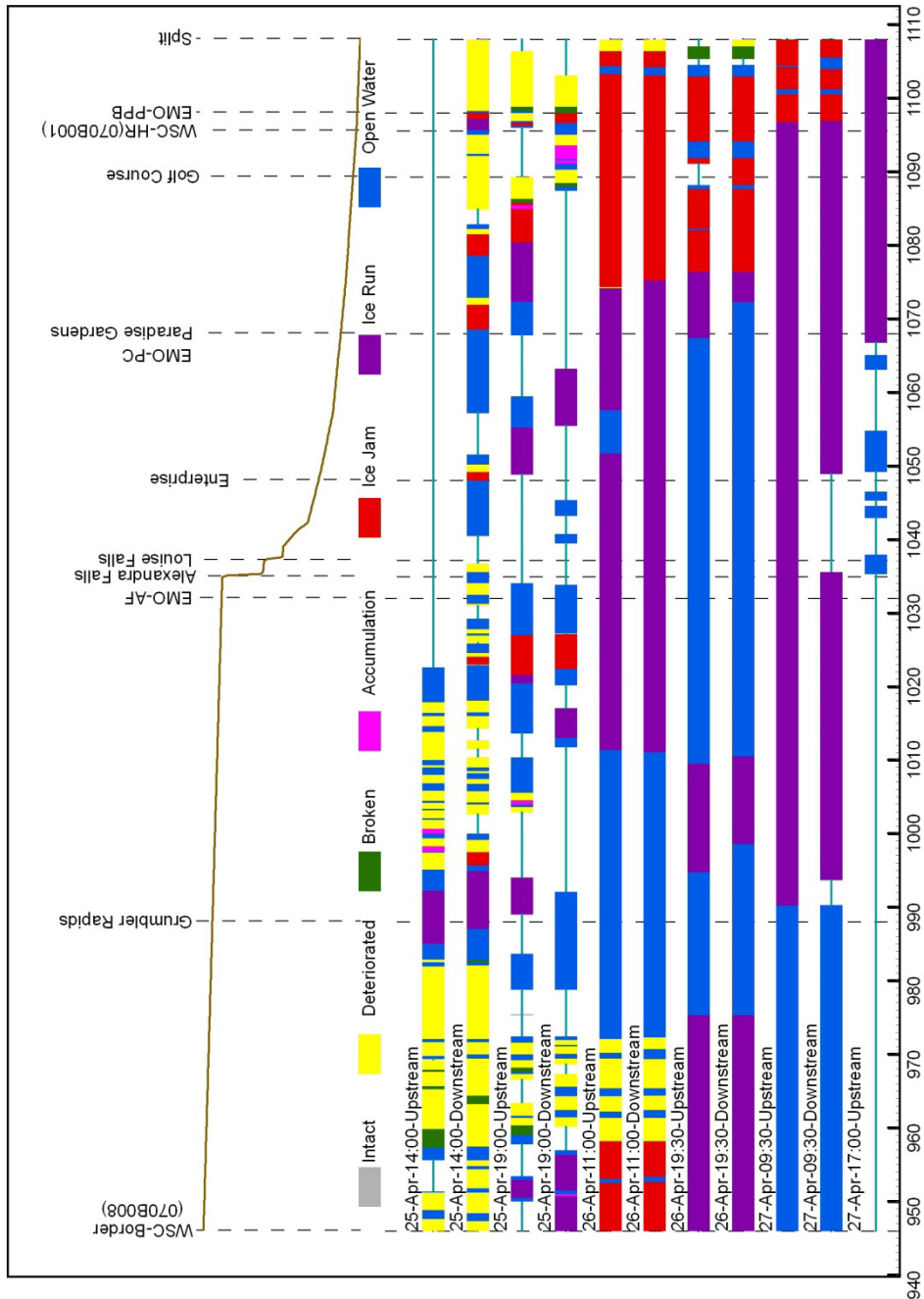


Figure 2.10, Flightmap showing the observed ice conditions during the 2007 breakup season.

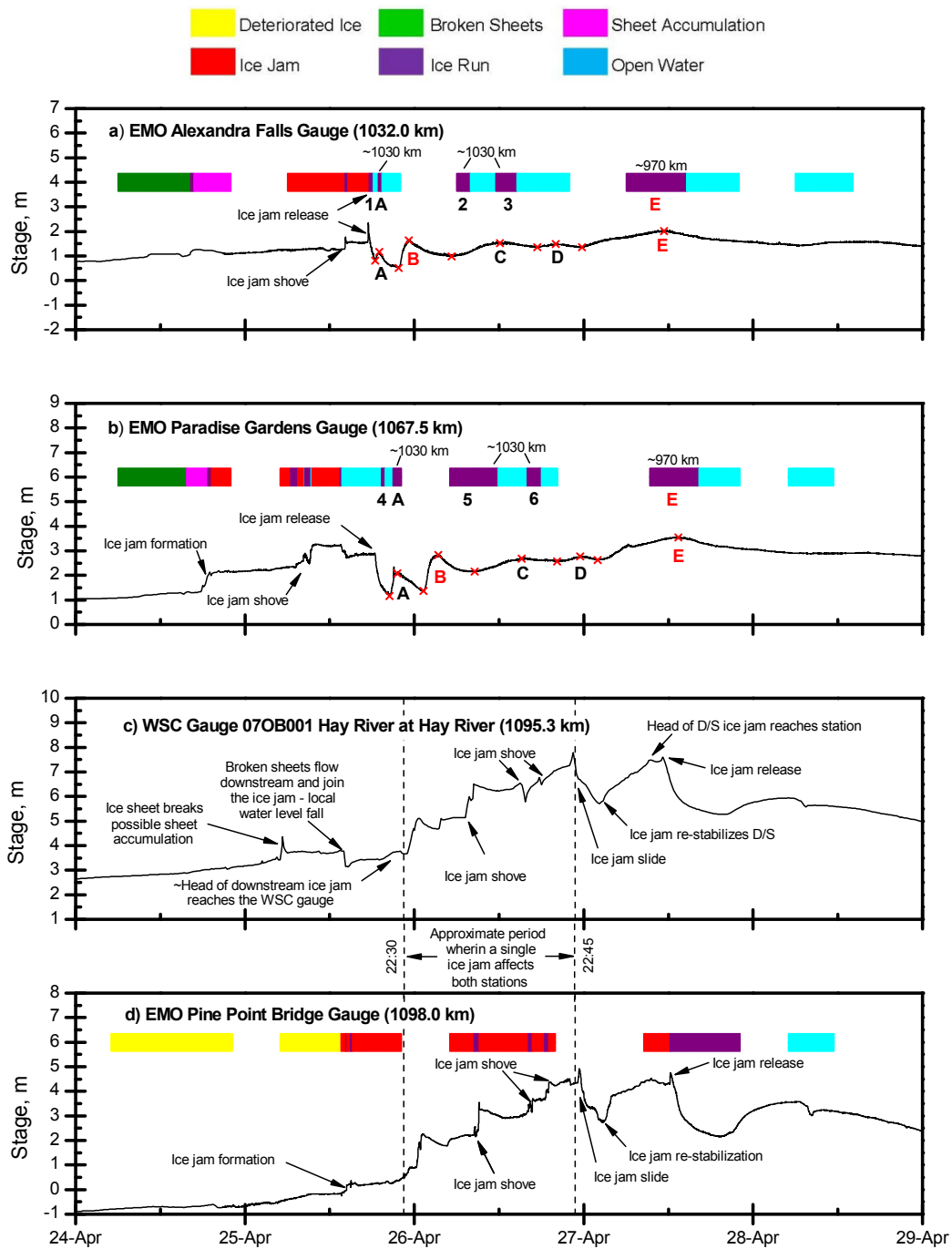


Figure 2.11, 2007 hydrographs showing progression of wave events and ice conditions.

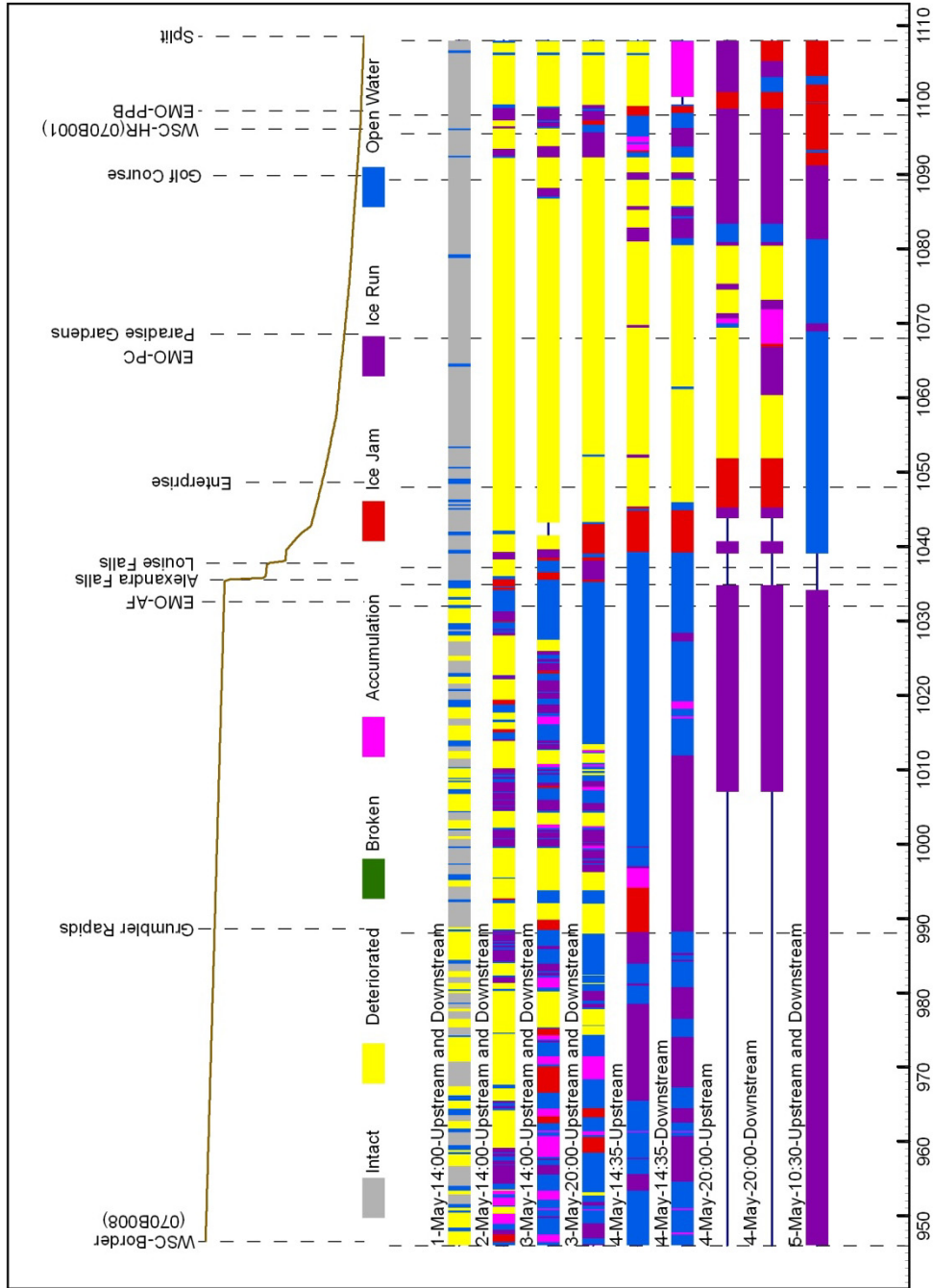


Figure 2.12, Flightmap showing the observed ice conditions during the 2008 breakup season.

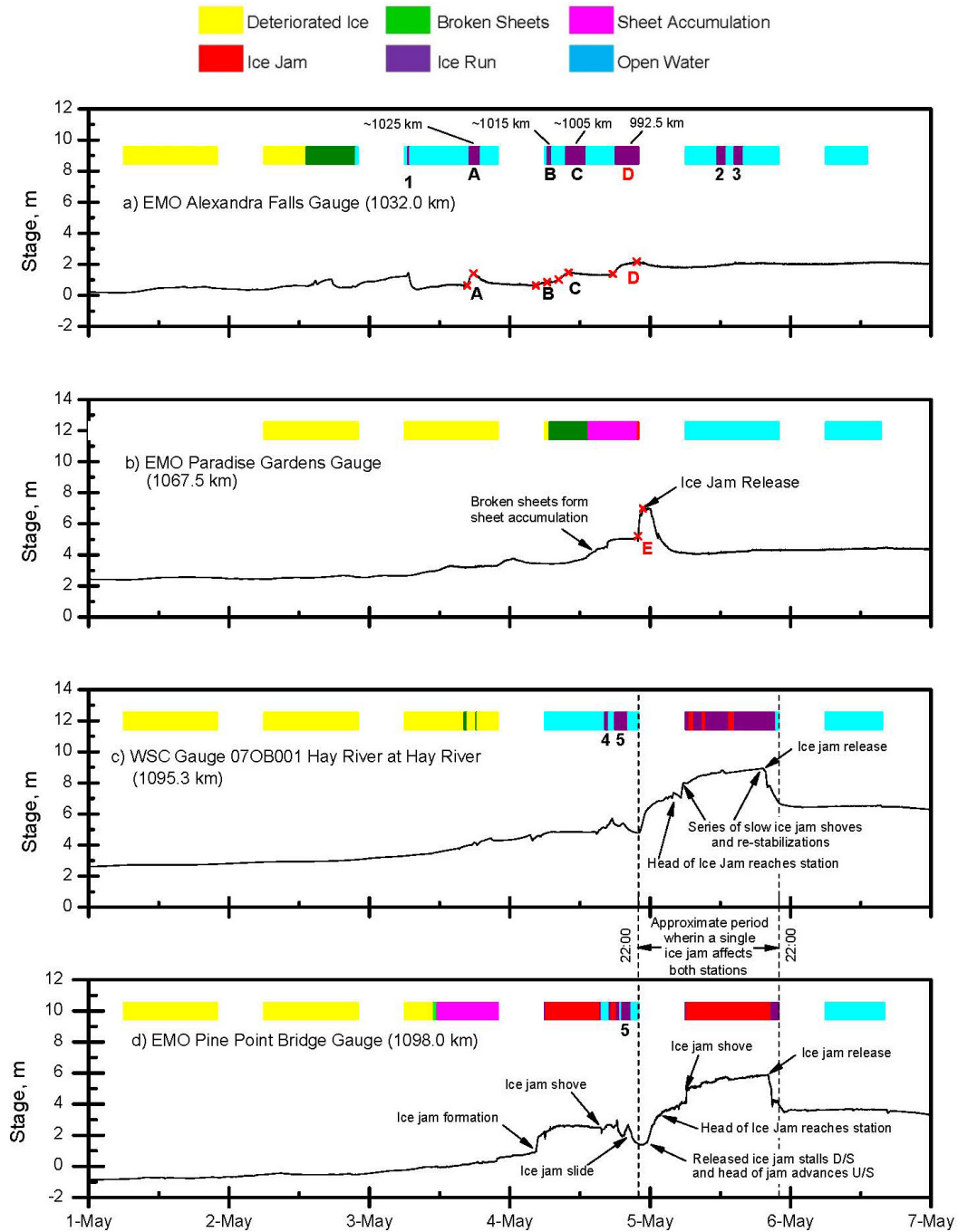


Figure 2.13, 2008 hydrographs showing progression of wave events and ice conditions.

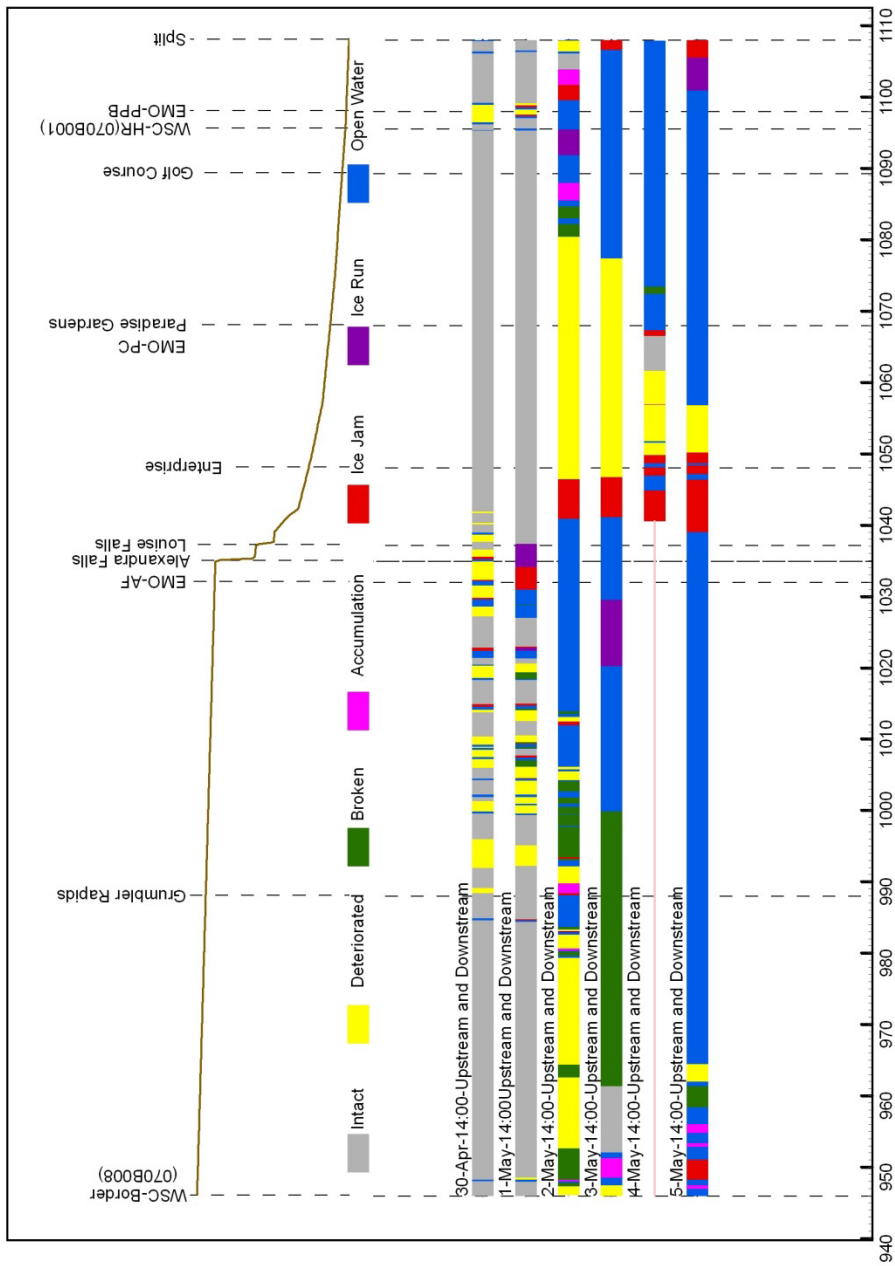


Figure 2.14, Flightmap showing the observed ice conditions during the 2009 breakup season.

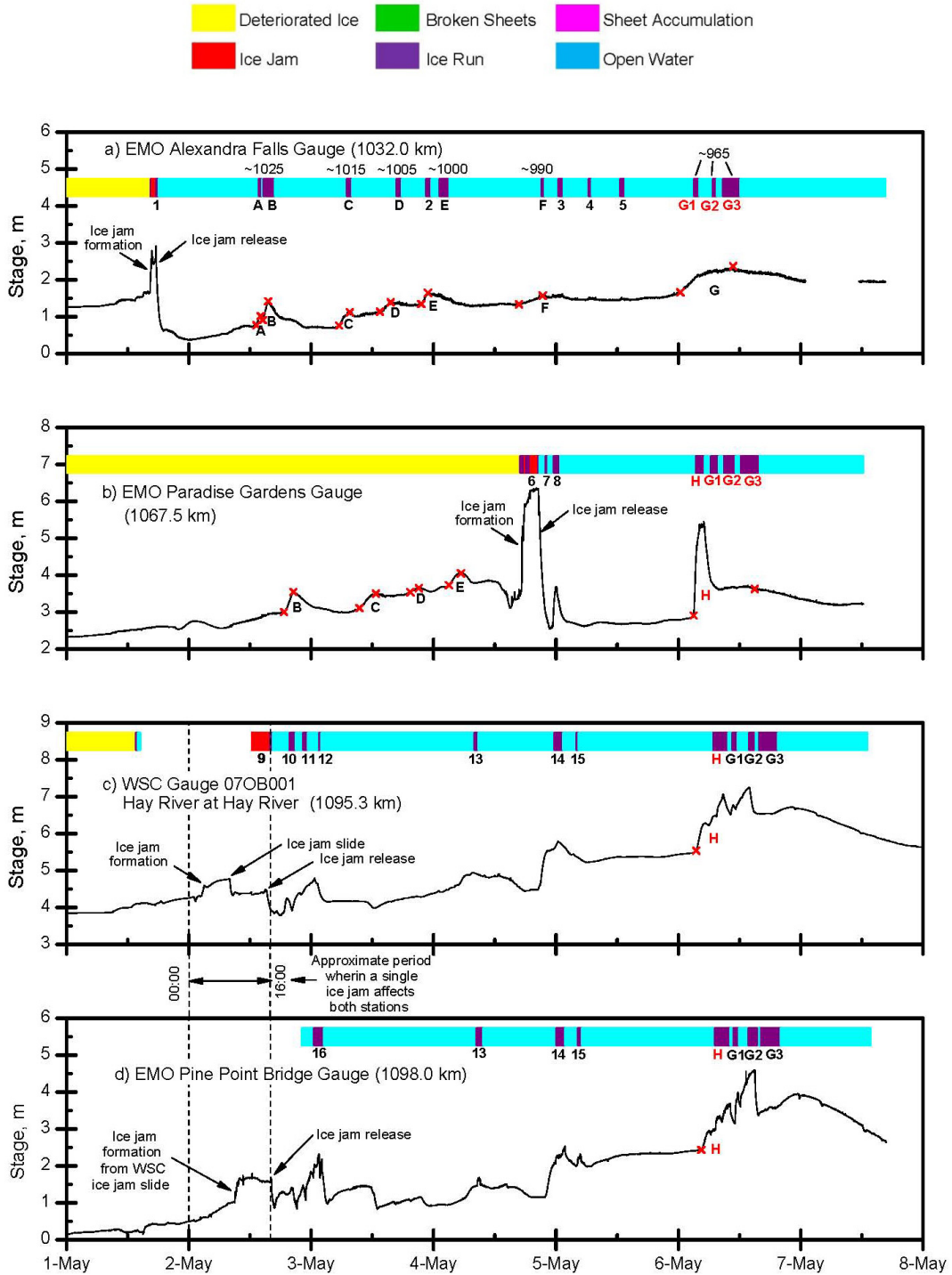


Figure 2.15, 2009 hydrographs showing progression of wave events and ice conditions.

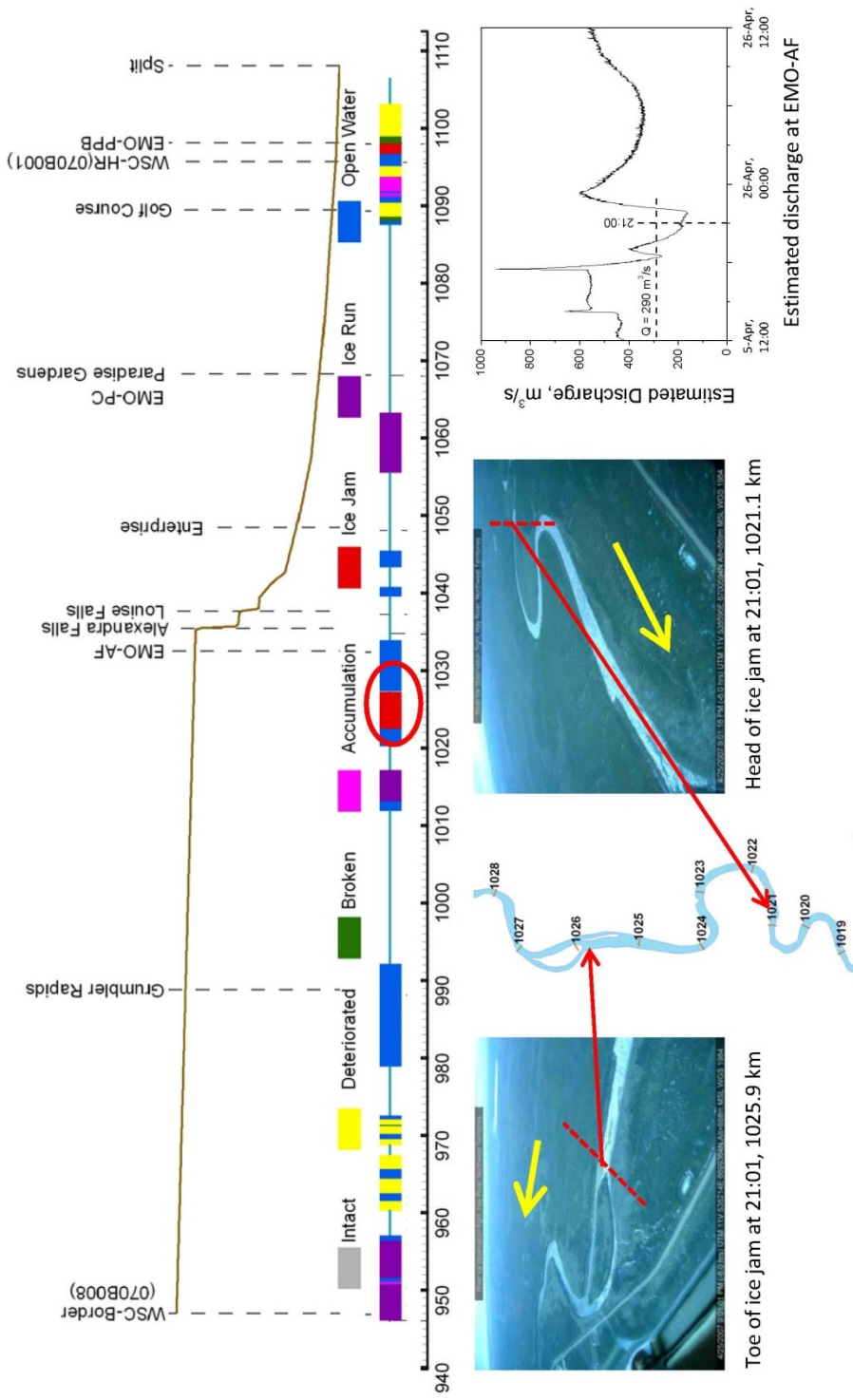


Figure 2.17, Observation of the ice jam corresponding to Ice Jam Release Event 1 during the 25-Apr-07 observation flight at 19:00.

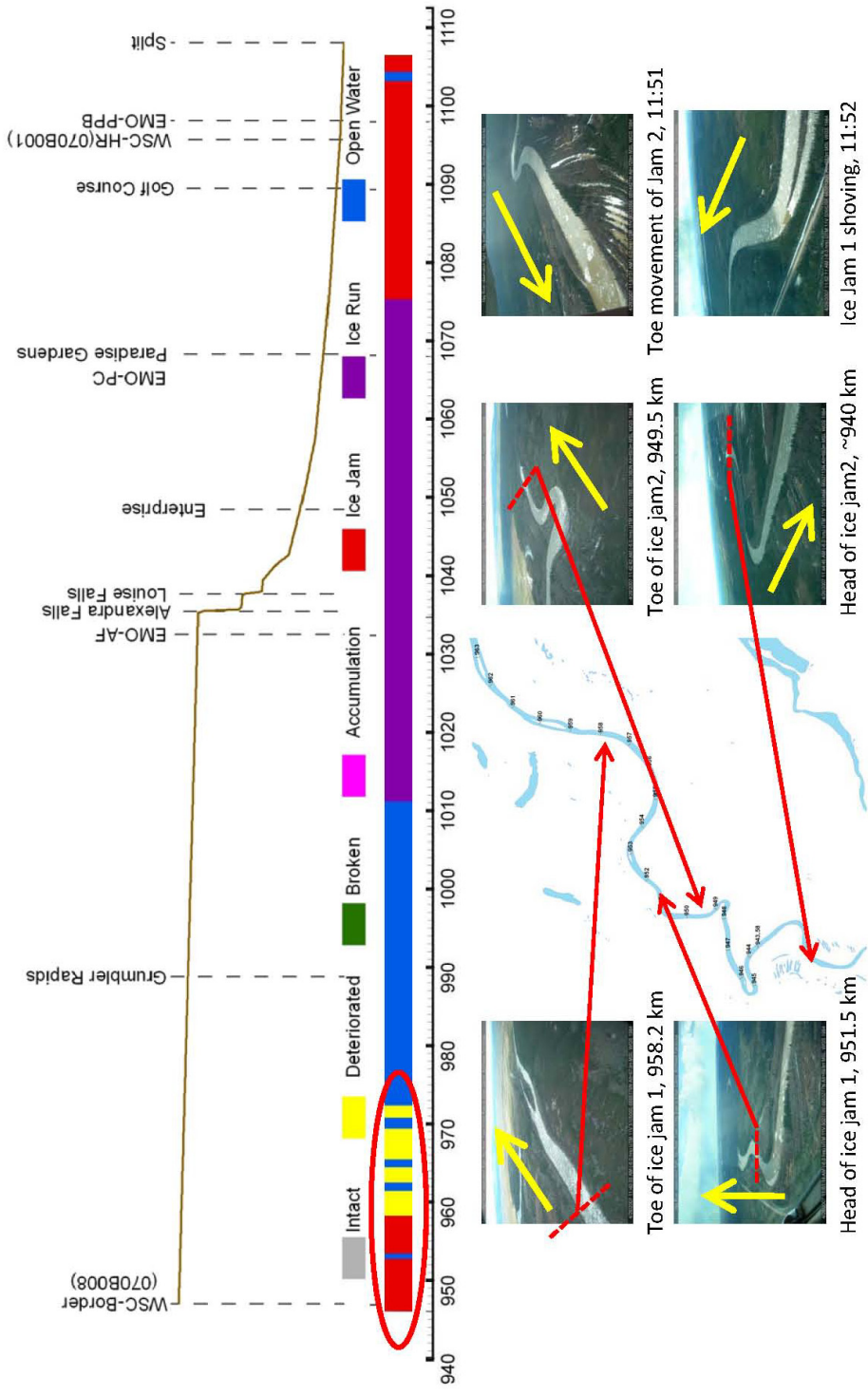


Figure 2.18, Observations of the ice jams corresponding to Ice Jam Release Event 2 during the 26-Apr-07 at 11:00.

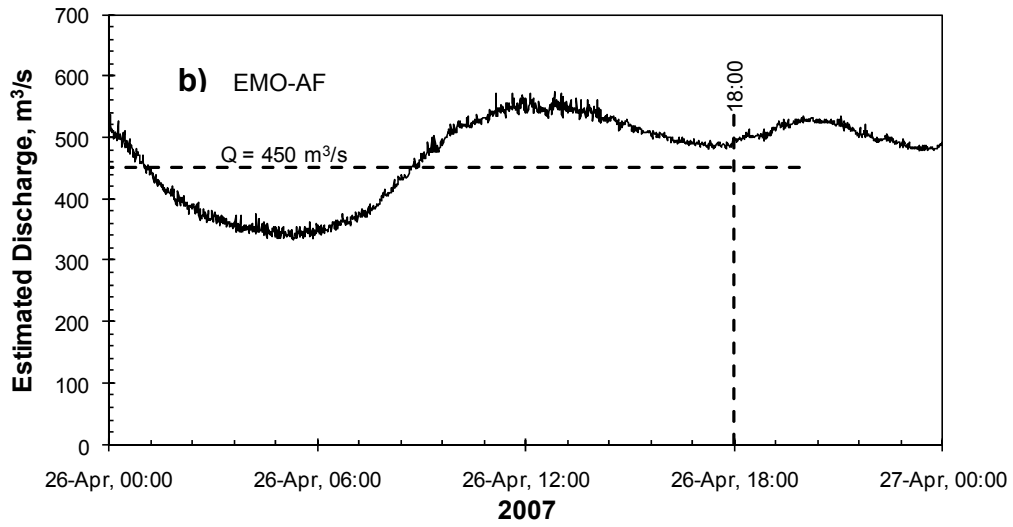
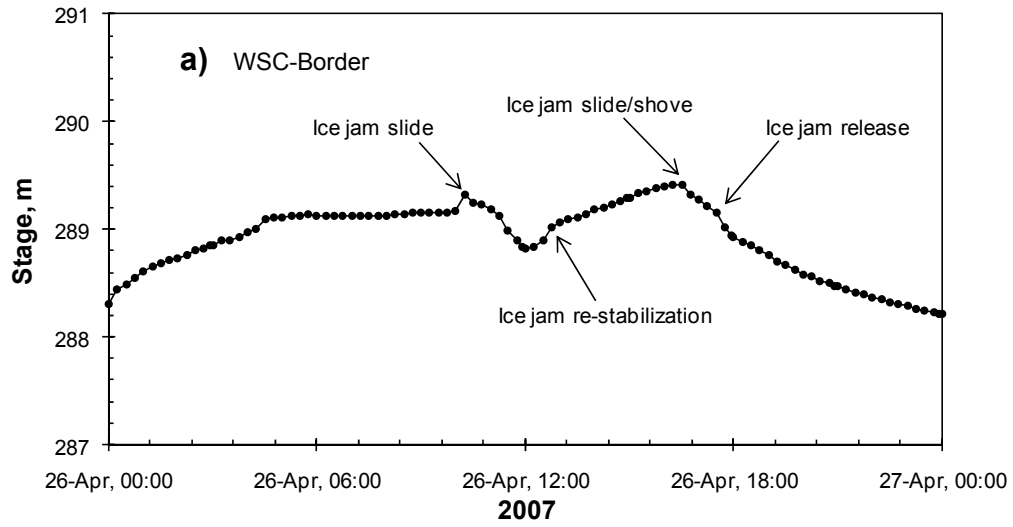


Figure 2.19, Estimated time of release and discharge of Ice Jam Release Event 2 using the WSC-Border and EMO-AF gauges.

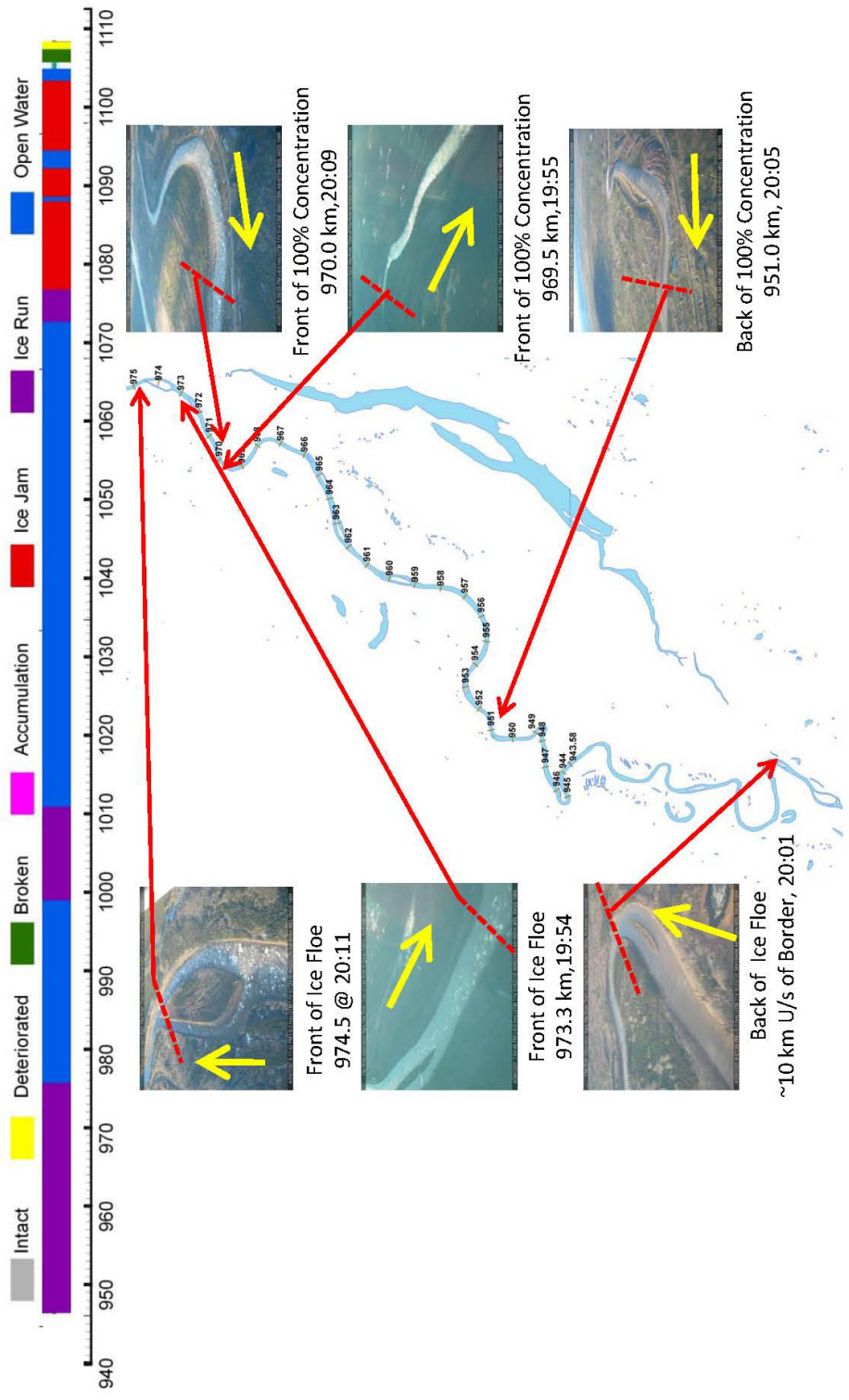


Figure 2.20, Observation of the ice run from Ice Jam Release Event 2 during the 27-Apr-07 observation flight at 19:00.

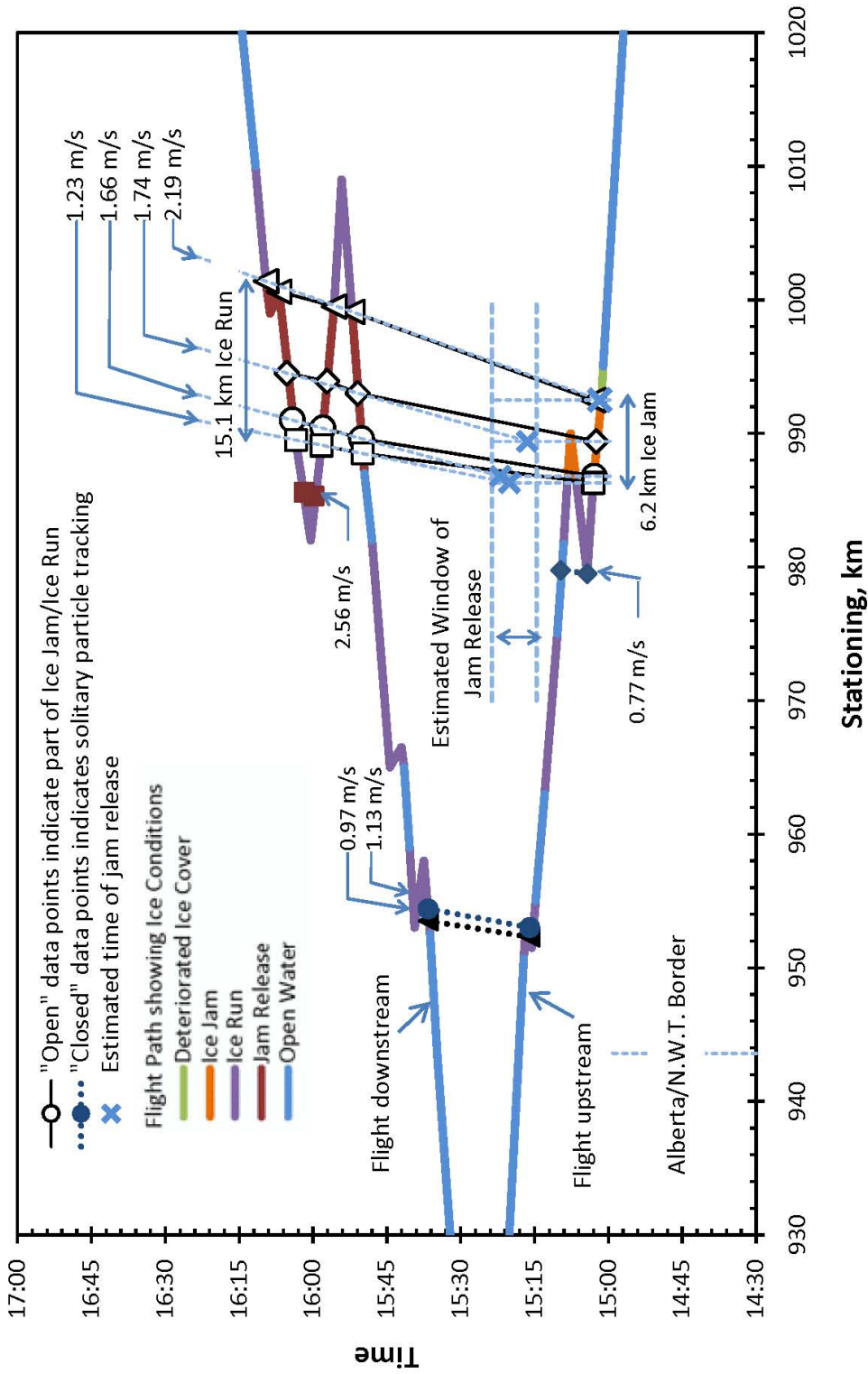


Figure 2.22, Flightmap for 2-May-08 at 14:35 tracking individual ice pieces and the release of Ice Jam Release Event 3.

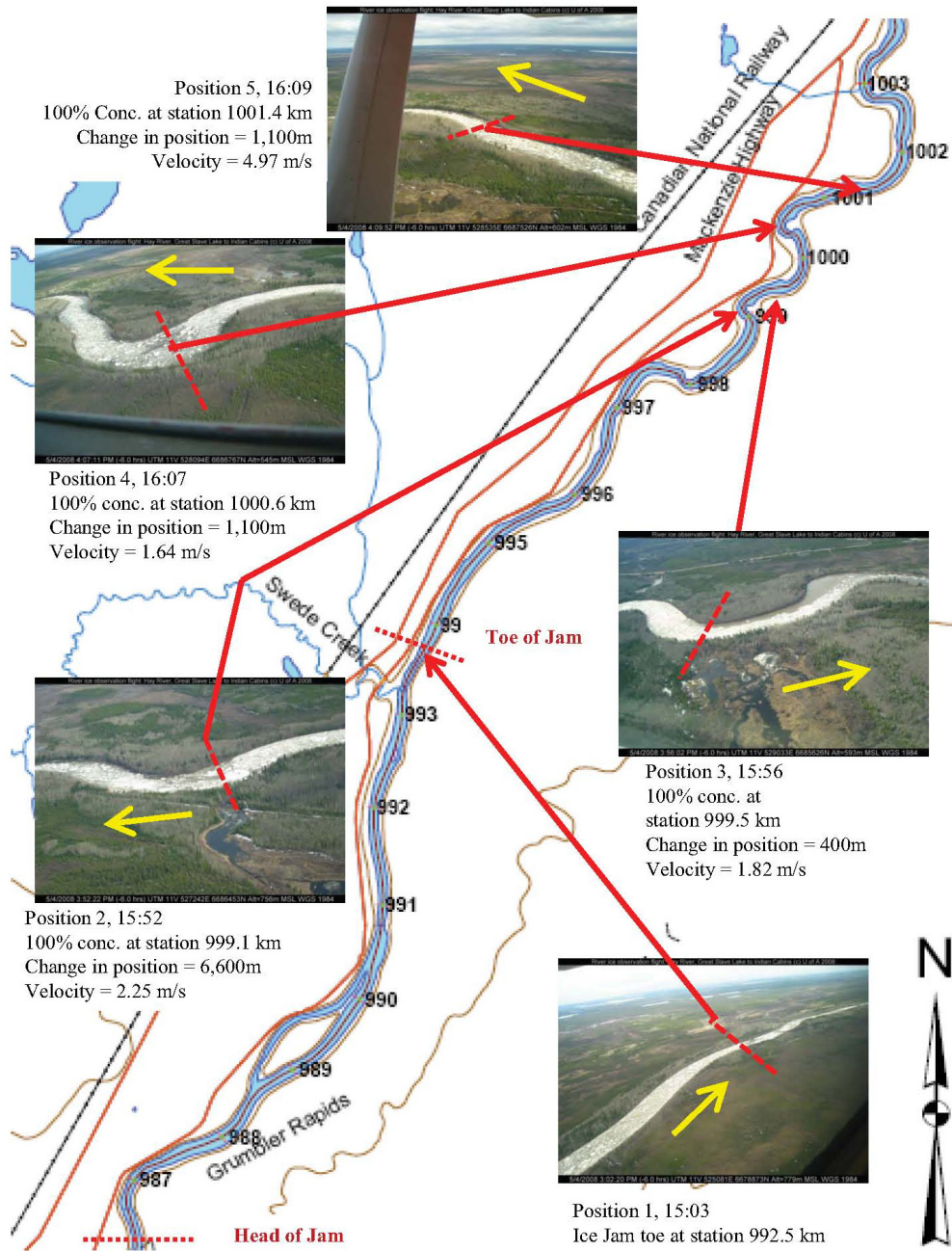


Figure 2.23, Tracking the front of the 100% concentration point in the ice run resulting from Ice Jam Release Event 3.

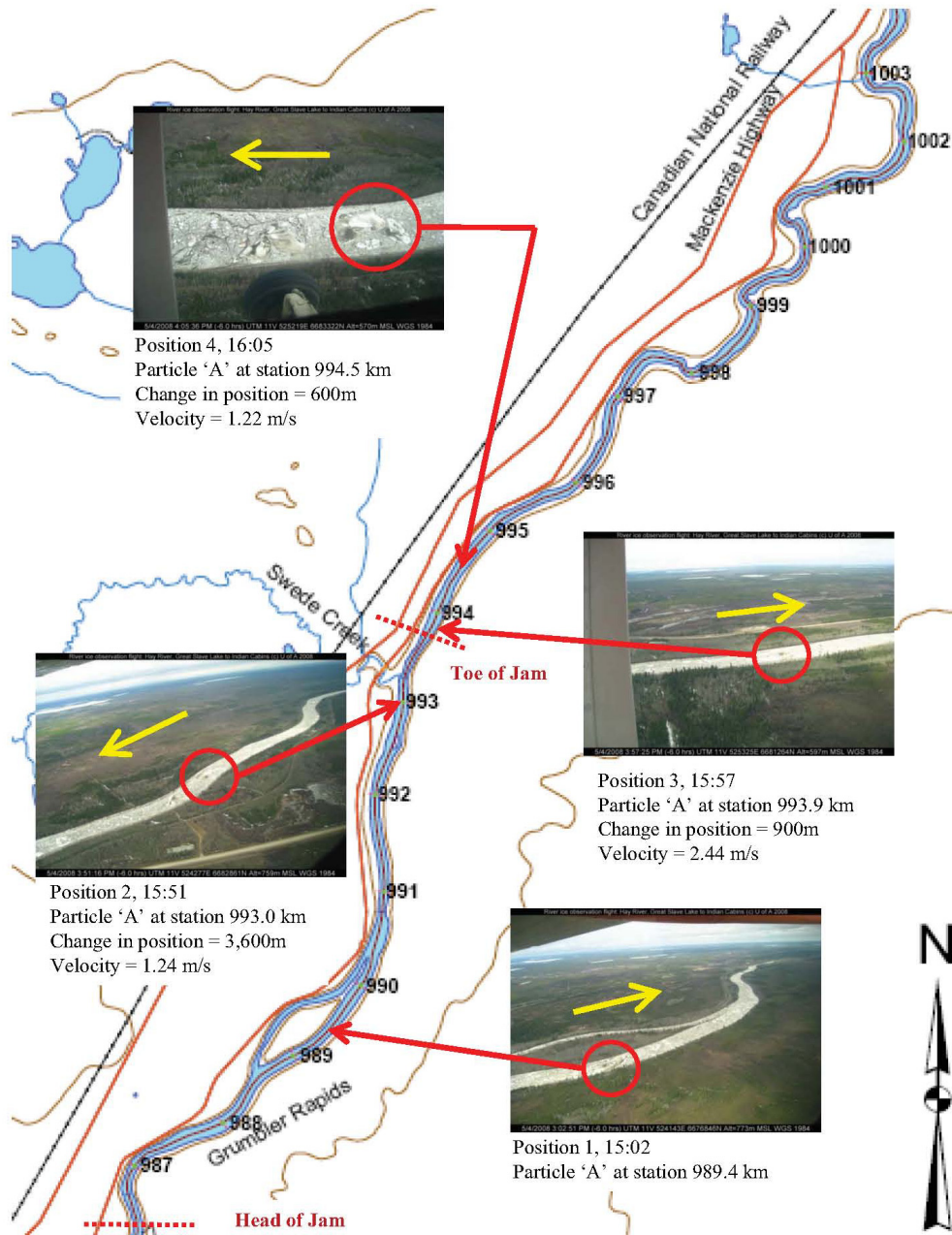


Figure 2.24, Tracking particle 'A' in the ice run resulting from Ice Jam Release Event 3.

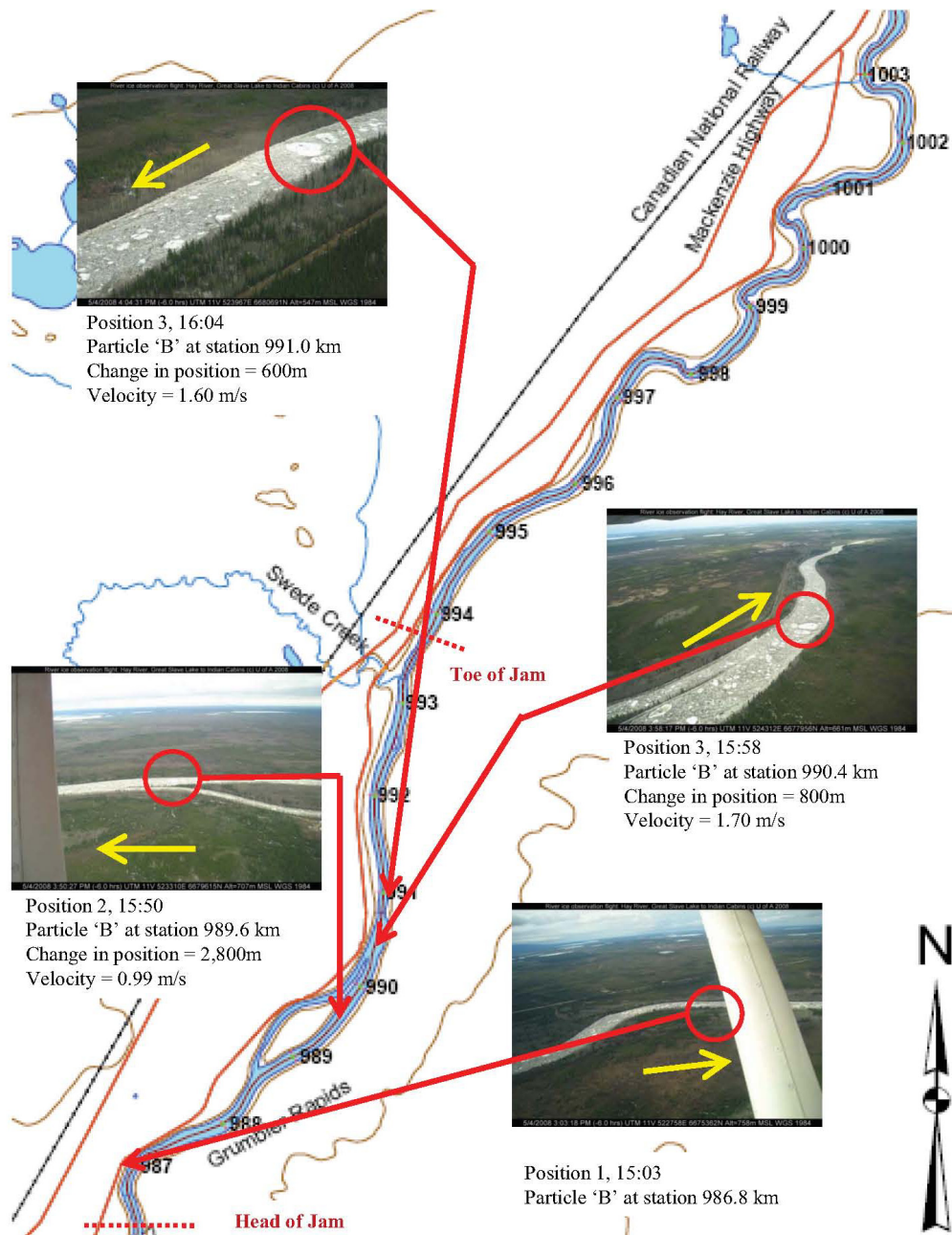


Figure 2.25, Tracking particle 'B' in the ice run resulting from the Ice Jam Release Event 3.

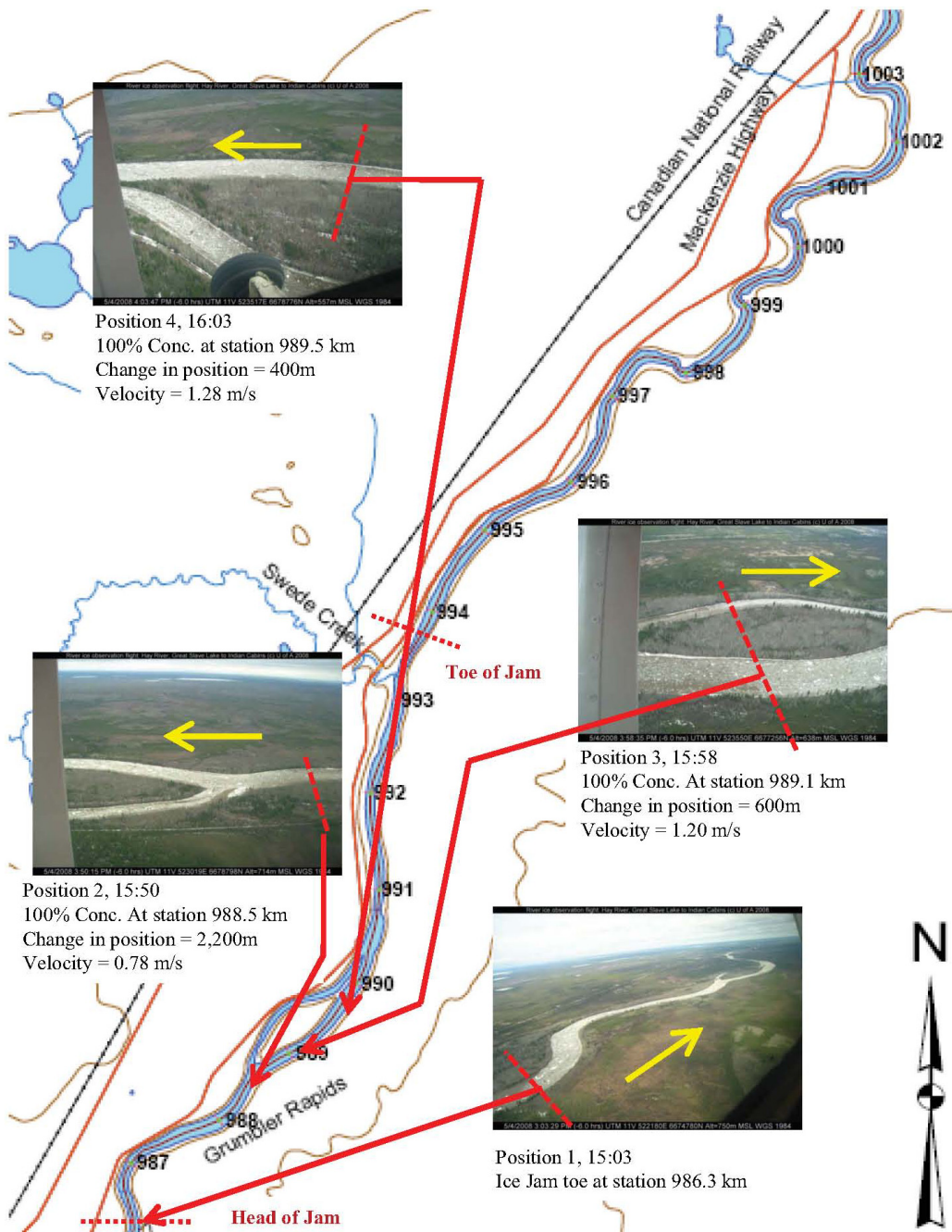
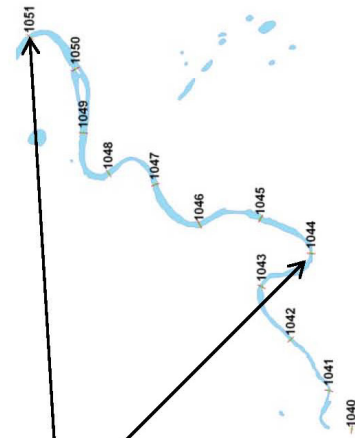
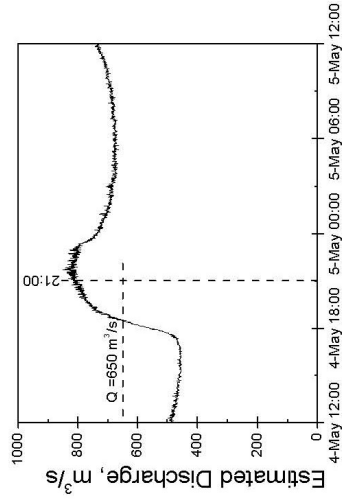
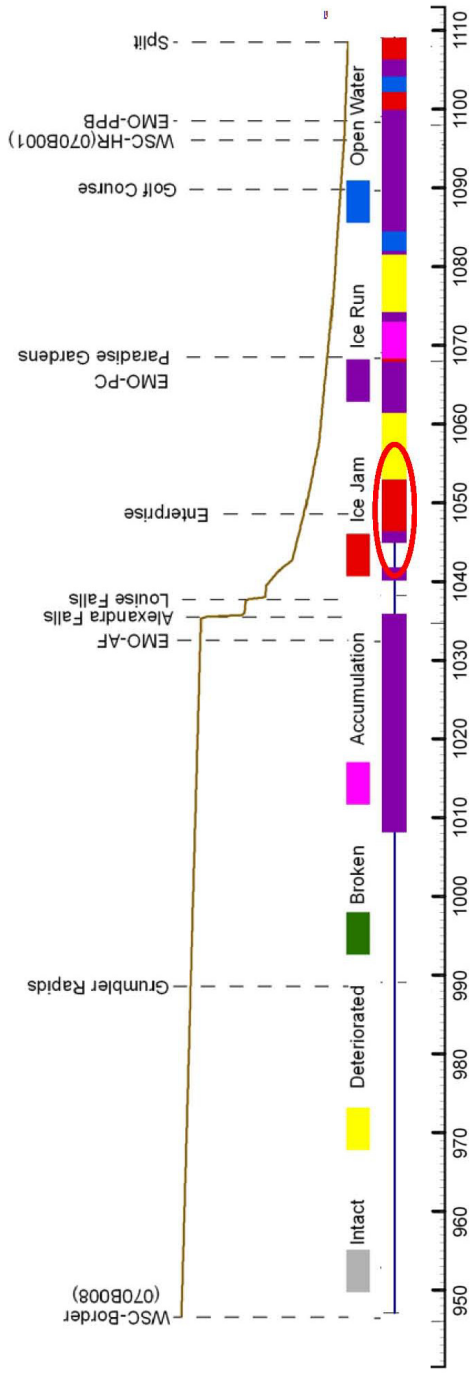


Figure 2.26, Tracking the back of the 100% concentration point in the ice run resulting from Ice Jam Release Event 3.



Toe of Jam, 1051.0 km.

Head of Jam, 1044.0 km.

Note:
Clear photos of this ice jam were not available. Ice jam location determined by UofA researchers.

Estimated EMO-AF discharge hydrograph

Figure 2.27, Observation of the ice jam corresponding to Ice Jam Release Event 4 during the 4-May-08 observation flight at 20:00.

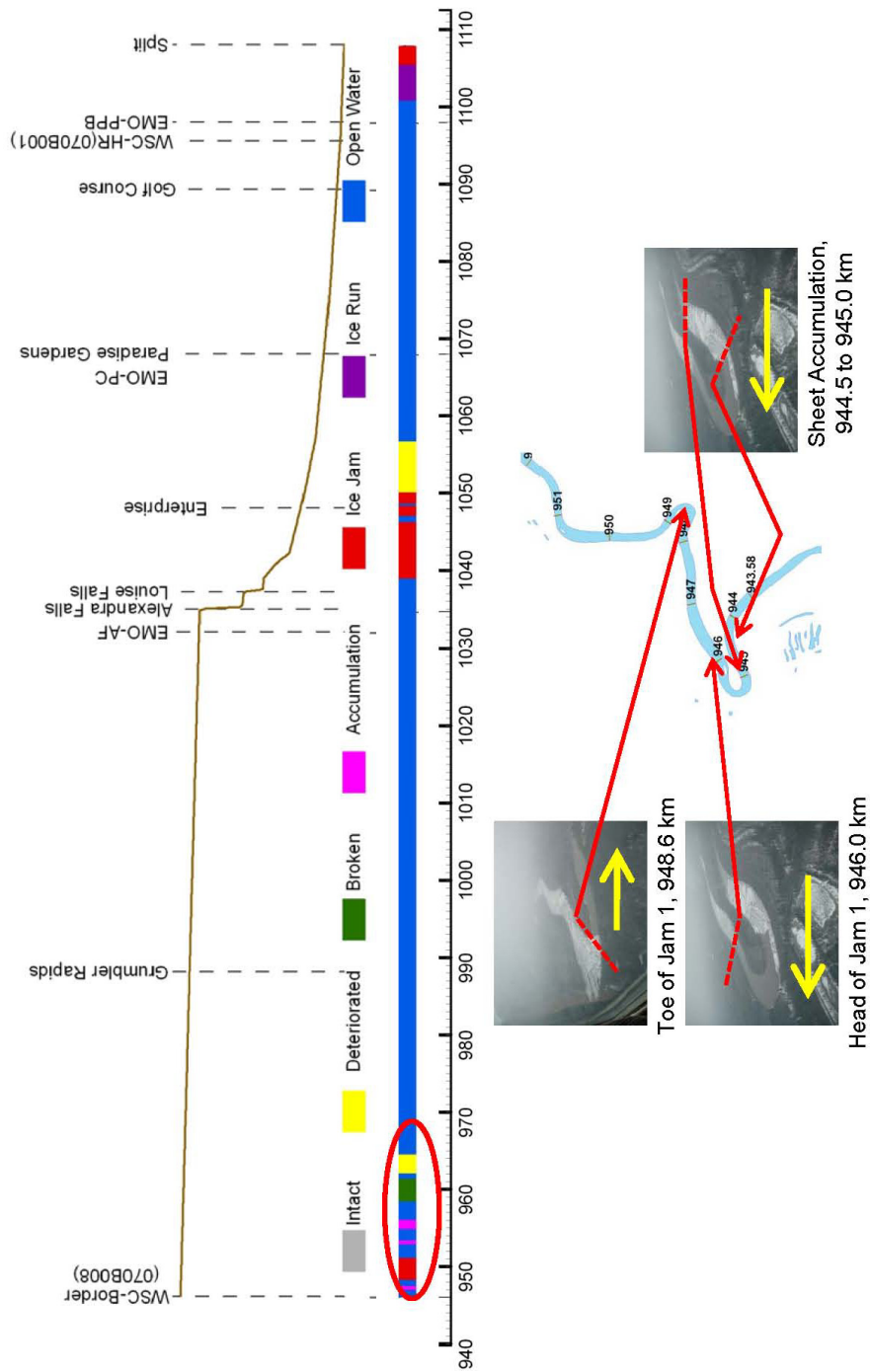


Figure 2.28, Observation of the ice jam corresponding to Ice Jam Release Event 5 during the 5-May-09 observation flight at 14:00.

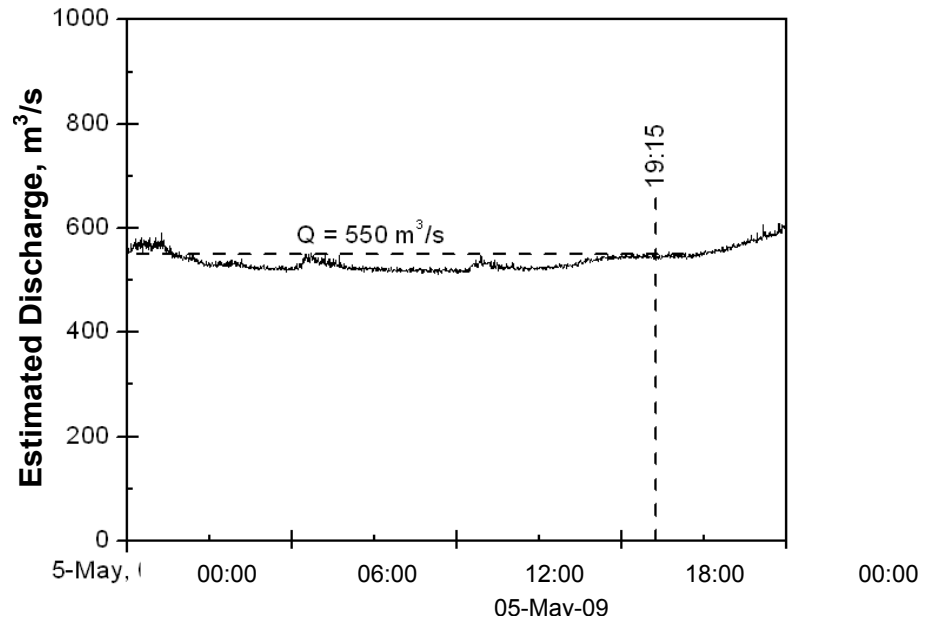
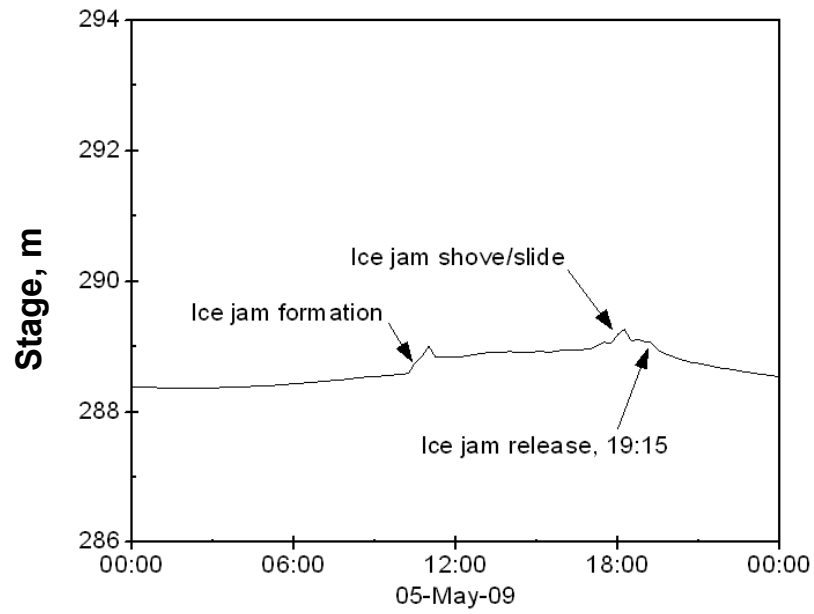


Figure 2.29, Estimation of time of release and discharge for Ice Release Event 5 using WSC-Border and EMO-AF.

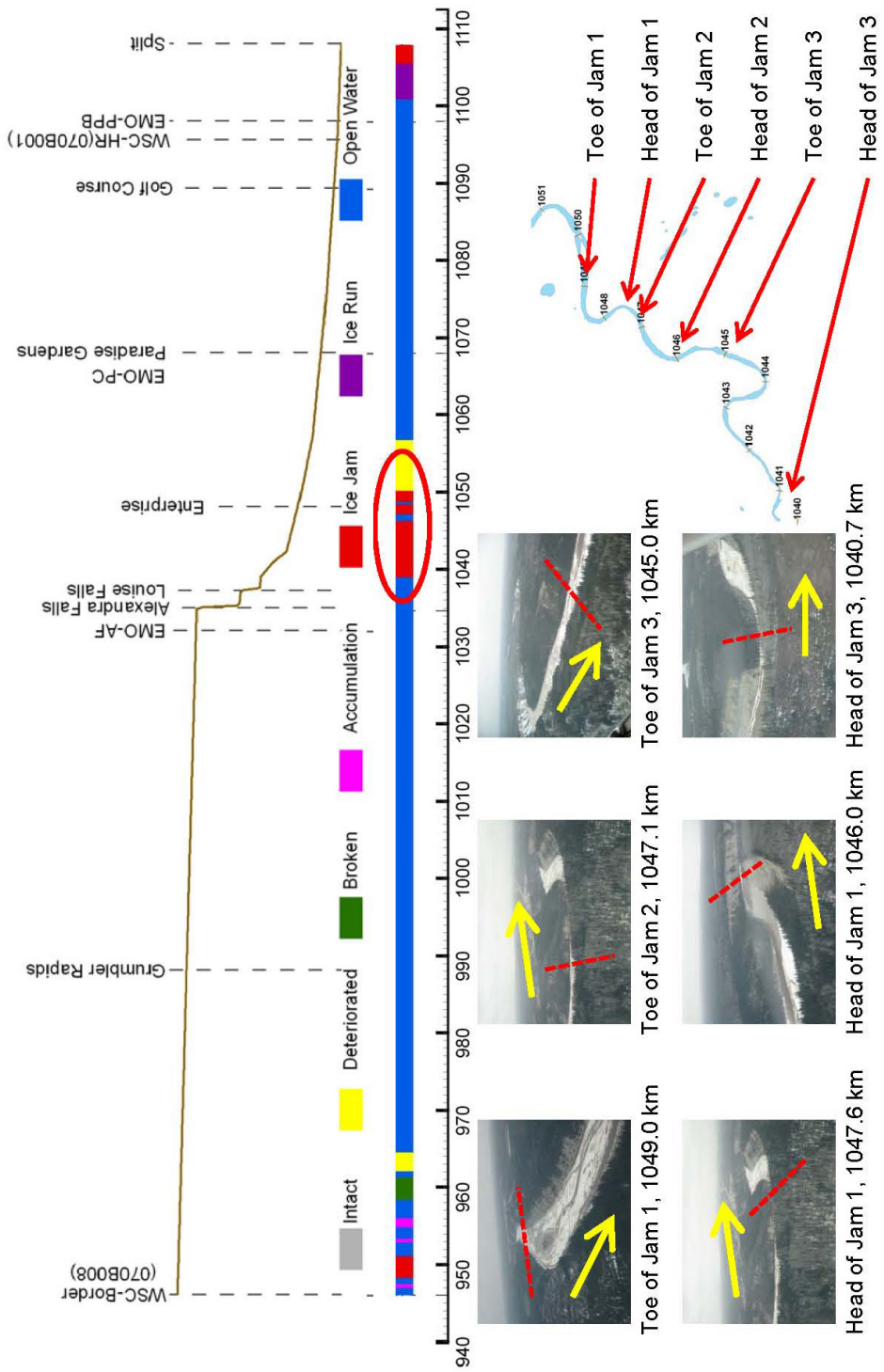


Figure 2.30, Observations of the ice jams corresponding to Ice Jam Release Event 6 during the 5-May-09 observation flight at 14:00.

3.0 *River1D* Modeling of Ice Jam Release Events

Previous investigations into modeling ice jam release events indicated that the effects of ice on the propagation of a released water wave could not be neglected. This led to the development of more robust models which included formulations considering ice effects on the ice jam release wave. Since data were not yet available describing the transport of the released ice mass, this previous modelling research focused mainly on the speed of propagation and magnitude of the released wave. With the ice run data for ice jam release events collected in this study, the current version of *River1D*, an open-source hydrodynamic program developed by Hicks and Steffler (1990) at the University of Alberta and modified by She and Hicks (2006) to include formulations for ice dynamics, was tested for its ability to reproduce observations of the water wave and released ice mass for ice jam release events on the Hay River.

3.1 Previous Ice Jam Release Event Modeling

Henderson and Gerard (1981) used a classic dam break solution to propose an analytical solution for an ice jam release event. In this solution, an idealized rectangular channel was used and the effects of channel slope and friction were neglected. This solution was tested against ice jam release event data from the Athabasca River, where an initial ice jam profile was measured and a downstream stage hydrograph was available. The modeled wave was faster than the observed wave, and the authors hypothesized that ice floes slowed the wave and increased its height.

Beltaos and Krishnappen (1992) modeled ice jam release events using a finite difference scheme, developed by Krishnappen and Snider (1977) to solve the St. Venant Equations. This model used rectangular geometry and included effects of channel slope and roughness, but ice effects on the flow were neglected. A global friction factor was used in this model which accounted for

both the bed and ice roughness. The model was tested using data from an ice jam release event on the Athabasca River, AB, documented by Doyle and Andres (1979), and it was found that the peak height of the predicted wave was in good agreement with observations, but the authors had difficulty matching the shape of the downstream hydrograph.

Hicks et al. (1992) applied a newly developed one-dimensional (1-D) finite element model to modeling ice jam release waves on the Hay River. The model employed the characteristic-dissipative-Galerkin (CDG) finite element scheme to solve the St. Venant equations (Hicks and Steffler 1990) and was shown to be able to handle kinematic, diffusive and dynamic waves (and the transition between these extremes) and the extreme ranges of slopes through the Alexandra and Louise Falls that cause transcritical flow situations. However, there was no ice jam release data for the Hay River at that time with which to assess the model accuracy.

Hicks et al. (1997) further tested this 1-D hydrodynamic model for a 1993 ice jam release event on the Saint John River documented by Beltaos et al. (1994). For that case, a longitudinal profile had been measured along the length of the intact jam prior to release, and a stage hydrograph was measured approximately 5 km downstream of the jam after the release. Hicks et al. (1997) approximated the geometry of the Saint John River using a rectangular channel of varying width and slope and neglected ice effects on wave propagation. The model results showed good wave speed accuracy, but the peak magnitude of the wave was over-predicted by approximately 1 m. They hypothesized that this poor stage accuracy might be attributed to rectangular channel geometry approximation.

Blackburn and Hicks (2003) developed a version of the 1-D CDG model capable of handling natural channel geometries and applied it to the 1993 ice jam release event that was observed on

the Saint John River by Beltaos et al. (1994). It was found that modelling natural channel geometry did improve the stage accuracy, but did not significantly affect the wave speed. Their results suggested that the effects of an instantaneous versus a non-instantaneous ice jam release were negligible for the timing and magnitude of the events downstream of the initial jam position, but that local conditions in the proximity of the releasing ice jam may be more drastically affected by this assumption.

Liu and Shen (2004) used a two-dimensional (2-D) coupled flow and ice dynamic model, DynaRICE, developed by Shen et al. (2000) to evaluate the effects of ice on an ice jam release wave. This model included both the internal ice resistance and boundary friction resistance effects. They too attempted to model the 1993 Saint John River ice jam release event documented by Beltaos et al. (1994) but had to employ a highly idealized geometry (rectangular cross section of constant width and constant bed slope) because the actual channel geometry was not available to them. Their model results showed that ice resistance effects slowed down the release of the ice in the jam and, as a result, they concluded that ice dynamic effects cannot be neglected when modeling ice jam release events. They also concluded that the actual peak discharges at downstream locations might be much lower than calculated with models that neglect these ice. However, there was no actual data with which to confirm either of these model findings.

She and Hicks (2006) developed a 1-D ice jam release model based on the CDG finite element scheme as developed by Hicks and Steffler (1990) in which the St. Venant equations were adapted to include ice effects. This model (called '*RiverID*') used empirical parameters to account for the resistance effects of the ice on the flow as well for the dispersion of ice runs (as had been qualitatively observed in field accounts). The physics within this model were

intentionally simplified compared to those employed by Liu and Shen (2004), as the 2-D model is extremely computationally and data intensive and thus not yet practical for short term flood forecasting purposes involving 10s or 100s of km of river. She and Hicks (2006) tested their model for the idealized 1993 Saint John River ice jam release scenario developed by Liu and Shen (2004), obtaining comparable results for the shape of the diffused ice mass. Also, wave peak arrival times were within about 2 to 10% of Liu and Shen's (2004) 2-D model results.

She and Hicks (2006) also tested their 1-D model for the 2002 Saint John River ice jam release event documented by Beltaos and Burrell (2005a,b). Unlike the 1993 event (which had only one documented stage hydrograph 5 km downstream of to the ice jam release site), the data for the 2002 ice jam release event included additional stage hydrographs at ~10 and ~40 km downstream of the release site. They also tested the model for a large ice jam release event on the Athabasca River, AB, documented by Kowalczyk and Hicks (2003), for which stage hydrographs were documented downstream of the ice jam at 11 sites over 80 km. Both simulations employed a rectangular channel approximation. She and Hicks (2006) found that the empirically modeled ice effects only affected the shape of the stage hydrograph for the first few jam lengths of propagation. Calibration of the empirical ice parameters for these two events improved the wave speed accuracy substantially, but only improved water level accuracy slightly. Both parameters were found to be very site specific.

In all of these modelling efforts, a key limiting factor was the lack of complete data. Most particularly, none of the earlier field studies provided any information on the ice run travelling with the water wave to enable an assessment of the models' abilities to reproduce that, despite its importance to ice jam flood forecasting. Thus the data collected in this study provides a unique opportunity to test the practical ice jam release event model of She and Hicks (2006): *River1D*.

3.2 Model Description and Setup

3.2.1 Model Formulation

To model ice jam release events, steady and unsteady modeling practices must be implemented. Steady flow modeling is necessary to create an ice jam profile and backwater curve, which is then used for an initial condition for modeling the unsteady flow involved in an ice jam release event. The *RiverID* model uses the steady flow ice jam stability equation as formulated by Flato and Gerard (1986) and as implemented in the U.S. Army Corps of Engineering HEC-RAS model to establish the initial conditions for the ice jam release model. The unsteady ice jam release event is then modelled using CDG finite element scheme developed by Hicks and Steffler (1990), to solve the equations for total (ice and water) mass and momentum and ice mass continuity as formulated by She and Hicks (2006). The formulation and discretization of the model are discussed in this section, along with boundary and initial conditions.

3.2.1.1 Ice Jam Formation: Steady Flow Analysis Modelling

In *RiverID* the initial ice jam thickness profile is calculated using the jam stability equation, based on water depths and velocities solved by steady gradually varied flow (GVF). Since the ice thickness is affected by the flow, and the flow is affected by the ice jam thickness, the jam stability and GVF equations are solved iteratively in an uncoupled sequence following the approach originally devised by Flato and Gerard (1986).

Flato and Gerard (1986) proposed the following formulation of the ice jam stability equation:

$$t_i \frac{\partial t_i}{\partial x} = a + bt_i + ct_i^2 \quad (1)$$

in which:

$$a = \frac{\tau}{2K_x \gamma_e} \quad (2)$$

$$b = \frac{g \rho_i S_o - \left(\frac{2C_f}{B} \right)}{2K_x \gamma_e} \quad (3)$$

$$c = \frac{-C_o}{K_x B}$$

$$\gamma_e = \frac{g \rho_i}{2} (1-e) \left(1 - \frac{\rho_i}{\rho} \right) \quad (4)$$

and

t_i = thickness of the ice jam accumulation

x = longitudinal co-ordinate

τ = shear stress of flow on underside of accumulation

K_x = a passive pressure coefficient

g = acceleration due to gravity

ρ_i = density of ice

S_o = river bed slope

C_f = cohesion

B = width of the accumulation

ϕ = angle of internal friction of the ice accumulation

$C_o = \tan \phi$

e = porosity of the ice accumulation

ρ = density of water

C_f is generally used to incorporate the effects of freezing cohesion between ice particles, and is generally considered to be zero in breakup ice jams. Since it is not practical to measure either the angle of internal friction of the ice accumulation, ϕ , or its porosity, e , these two variables are generally combined into a “jam strength parameter, μ , as follows (Ashton, 1986):

$$\mu = C_o (1-e) \quad (5)$$

The energy equation is used to solve the gradually varied flow using the standard step method (Chow, 1959):

$$y_1 + z_1 + \frac{V_1^2}{2g} = y_2 + z_2 + \frac{V_2^2}{2g} + S_f \Delta x \quad (6)$$

where,

y = flow depth

z = bed elevation

V = average flow velocity

Subscripts $_1$ and $_2$ refer to the downstream and upstream cross sections in the step solution, respectively. The GVF solution steps between adjacent cross sections, starting with a known downstream boundary condition. This assumes a subcritical profile which is invariably the case for ice jam situations.

Chezy's equation is:

$$V = C_* \sqrt{gRS_f} \quad (7)$$

Where R is the hydraulic radius (= flow area/wetted perimeter), S_f is the friction slope and C_* is Chezy's resistance factor, calculated using:

$$C_* = 2.5 \ln \left(\frac{R}{k} \right) + 6.2 \quad (8)$$

For the ice covered flow, a composite roughness must be calculated – to combine the effects of the ice underside and river bed. *RiverID* uses Sabaneev's equation to compute this composite roughness.

$$k = \left(\frac{k_i^{1/4} + k_b^{1/4}}{2} \right)^4 \quad (9)$$

where k is the effective roughness height in metres.⁵

In *RiverID* the calculation of the ice jam profile proceeds as follows:

1. The initial ice jam thickness is assumed to be 1m along its entire length
2. The GVF solution proceeds from downstream to upstream
3. Based on the GVF solution in step 2, a new ice thickness profile is calculated using the jam stability equation, stepping downstream from a specified upstream ice thickness at the head of the jam.⁶
4. A new GVF profile is calculated based on the new ice jam profile determined in step 3.
5. Steps 3 and 4 are repeated until there is not change in the compute ice jam thickness and GVF profiles.

At present, there is no model to describe the configuration of the toe of an ice jam. The main problem being that there is no practical or safe way to measure this in the field so little is actually known about it. To circumvent this, *RiverID* adopts the approach used by Flato and Gerard (1986) in which the user specifies a maximum erosion velocity (V_{max}) under the ice at the jam toe, and the flow depth is simply calculated as the discharge divided by this velocity in this region. If the depth calculated by this method is less than that obtained with the jam stability equation, then the V_{max} criteria is taken to govern. This can tend to produce some unrealistic looking ice jam toe shapes, although it cannot be said to be entirely unrealistic, given that an ice

⁵ Note – this equations is incorrect in Hicks and Steffler, 1990 and Hicks et al. 1992. The corrected version is shown here.

⁶ Note –some models step in the other direction – but this has been found to be less stable (Healy and Hicks, 1999).

jam toe has never yet been measured. However, it is true that it can sometimes require unrealistically high values of V_{max} to produce a stable ice jam profile computation, since V_{max} would be limited by the erosive resistance of the bed. Current practice is to accept this limitation with the understanding that the computed profile at the jam toe is an estimate (Healy and Hicks, 1999).

3.2.1.2 Ice Jam Release: Unsteady Flow Modelling

Hydrodynamic equations that include the effects of both ice and water on mass and momentum conservation were developed by She and Hicks (2006). The equations assume the mobilized ice moves at the mean flow velocity from the moment of ice jam release, and neglect the acceleration phase of the ice jam release. The equations of total (ice plus water) mass and momentum for rectangular channels can be written as (She and Hicks, 2006):

$$\frac{\partial A}{\partial t} + \frac{\partial Q}{\partial x} = 0 \quad (10)$$

$$\frac{\partial Q}{\partial t} + \frac{\partial(VQ)}{\partial x} + gA \frac{\partial H}{\partial x} = -gAS_f + gAS_o - 2\lambda_1 g B t_i S_f \quad (11)$$

where,

Q is the total discharge, including both water and ice flow;

H is the depth of flow under the water surface;

A is the total area of the cross-section under the water surface, measured perpendicular to the flow;

λ_1 is an empirically determined coefficient approximating the effects of bank resistance on the ice run;

and the other variables are as defined earlier. The ice mass continuity equation can be written as (She and Hicks, 2006):

$$\frac{\partial t_i}{\partial t} + \frac{\partial(Vt_i)}{\partial x} + \frac{Vt_i}{B} \frac{dB}{dx} = \lambda_2 \frac{\partial^2 t_i}{\partial x^2} \quad (12)$$

where λ_2 is an empirically determined coefficient approximating the observed diffusion of ice runs.

λ_1 and λ_2 are the only user defined parameters for this unsteady flow analysis. These parameters can be varied by the user to affect the propagation of the water wave and ice mass to better match observed phenomenon.

3.2.2 Model Geometry and Discretization

The rectangular channel geometry data used in this investigation was developed by Hicks et al. (1992), using the bed profile as described in section 2.2.2.1, the smoothed top widths as described in section 2.2.2.2 and using a channel roughness of $k = 0.2$ m as described in section 2.2.3. In the upstream portion of the reach, a spacing of 1 km was used, which was decreased in 15% steps to 200 m between stations 1027 and 1032.5 to provide increased discretization for resolving the transcritical flows over Alexandra and Louise Falls, as well as the steep slopes in the gorge (Hicks et al. 1992). The 200 m discretization was increased to 500 m in 15% steps between stations 1041.945 and 1045, from which point on the spacing remained constant at

500 m for the remainder of the reach. The discontinuities at Alexandra Falls (33 m) and Louise Falls (15 m) were each approximated as a steep chute over a single 200 m element.

It is noted that increasing the discretization may increase the model's accuracy in two ways. First, the calculated ice jam profile could be improved by increasing the discretization used in the *RiverID* model; however, no measured ice jam profiles exist for comparison and the model's discretization was assumed to be sufficient for this study. Secondly, the accuracy of wave propagation speed and magnitude are directly related to the discretization chosen. The effects of differing spatial discretization was beyond the scope of this study and were not included in the analysis.

3.2.3 Boundary Conditions

The flows at the extreme upstream and downstream ends of the study reach are subcritical, even though subcritical and critical flow regimes exist within the reach. This means that a boundary condition is required at both the upstream and downstream locations. The upstream boundary condition was taken to be a constant carrier discharge, which was estimated from the EMO-AF, using the rating curve developed as discussed in section 2.3.3. The downstream boundary condition was a constant water level which was estimated from the WSC-GSL gauge.

3.2.4 Initial Conditions

The ice jam profile that is created as a result of the steady state modeling is used as the initial condition for the unsteady flow modeling of ice jam release events. To model an ice jam, a gradually varied flow profile is established for the entire study reach at a chosen constant carrier discharge. In *RiverID*, the ice jam profile is created using the calculated gradually varied flow

profile with the ice jam stability equation as described in section 3.2.1.1, and the M1 backwater curve behind the ice jam is approximated using a horizontal water surface that extends from the calculated stage at the head of the ice jam to an intersection with the upstream water level.

3.3 Selection of Model Parameters

Both the steady state modeling (ice jam formation) and the unsteady state modeling (ice jam release) require input parameters. The parameters required for modeling ice jam formation and release events are introduced in sections 3.2.1.1 and 3.2.1.2, respectively. The selection of these parameters is discussed in this section.

3.3.1 Ice Jam Formation Parameters

The head thickness parameter requires the user to input an estimate of the ice thickness at the head of the jam. Since no direct measurements of ice jam thicknesses are available on the Hay River, this thickness was estimated to be 0.5 m in mild reaches of the river, which corresponds to an estimated thickness of a single incoming ice floe. In steeper reaches of the river, this value could reasonably be increased to 1 to 2 m, where incoming ice floes may get entrained in the floe and thicken the jam.

A value of 2.0 m was used for k_i , the ice jam underside roughness height. This value was suggested for ice jams on the Hay River by Hicks et al. (1992), as it represented a conservative value for newly formed ice jams. This parameter is site specific, and cannot be practically measured along the entirety of the study reach.

The jam strength parameter μ , is site specific and has been found to vary greatly between locations, however a range of 0.8 to 1.2 is considered most realistic (Beltaos 1983; Ashton

1986). Healy and Hicks (1999) noted that computed ice jam profiles are not very sensitive to changes in this parameter with this range, and the same tendency was observed in this study.

The erosion velocity, V_{max} , represents the maximum allowable flow velocity under at the toe of the ice jam. The practical range of values for this parameter was estimated by Healy and Hicks (1999) to be between 1.0 to 2.0 m/s. A value of 1.2 m/s was used for jams modeled in mild slopes of the study reach, and this value was increased to 1.7 m/s for modeled jams in steeper sections of the river, such as the gorge.

The last required user input for modeling ice jam formation is K_x , the passive pressure coefficient. There is no way to actually measure this parameter in the field; however, it has been deduced indirectly using the ice jam stability equation for a number of ice jam cases (e.g. Healy and Hicks 1999). They did not find the computed ice jam thickness profiles to be particularly sensitive to this parameter and suggested a value of 10 to be a reasonable value to adopt for practical applications. That value was adopted for this study.

3.3.2 Ice Jam Release Parameters

The λ_1 parameter is used to empirically account for the ice-to bank resistance effect in slowing the ice run. This parameter is used in the total (ice plus water) momentum equations and slows the progression of the released water and ice mass. Values ranging from 0 to 3.5 were found to be appropriate for accurate modeling of the propagation of the released wave, as documented by She and Hicks (2006) but, as noted earlier, ice run data was not available to them for validation.

The λ_2 parameter is used to empirically account for the field observations of the dispersion of ice runs from jam release events. This parameter is included in the ice mass continuity equation.

She and Hicks (2006) used values ranging from 0 to 100; however, they had no ice run dispersal data to evaluate this with.

3.4 Model Validation for Hay River Data

No additional data is available for the study reach than was available for the original determination of channel roughness to be $k = 0.2$ m, as discussed in section 2.2.3. Since breakup is a highly dynamic process, waves of varying speeds and magnitudes can be observed which is excellent validation data, if the flow is not affected by an ice cover. Since discharges can be estimated for the EMO-AF gauge, periods during which open water conditions were likely between EMO-AF and EMO-PG were identified during past breakup seasons. The discharges for these periods at the EMO-AF gauge were determined using the rating curve developed and discussed in section 2.3.3. The model was used to route these discharges from the EMO-AF to the EMO-PG, where the predicted change in stage was compared to the observed stage change at the EMO-PG. Open water periods were identified for the 2004 to 2007 and can be found in Table 3.1.

Table 3.1, Estimated periods of open water between the EMO-AF and EMO-PG used for River1D validation.

Year	Period Start	Period End
2004	01-May, 12:00	04-May, 12:00
2005	22-Apr, 18:00	25-Apr, 12:00
2006	25-Apr, 00:00	28-Apr, 12:00
2007	25-Apr, 18:00	28-Apr, 00:00

The predicted stage change compared to the observed stage change at the EMO-PG for the “open water” periods for 2004 to 2007 are shown in Figures 3.1 to 3.4. These figures show generally good phase accuracy and stage accuracy of the predicted wave, with reaffirms the decision to use a roughness parameter of $k = 0.2$ m.

3.5 Model Application

The model's ability to analyse ice jam release events was tested using these new observations of ice jam release events, which includes ice run data not available to previous researchers.

Specifically the assumptions that the released ice mass moves at the average speed of the water, and that the ice effects can be approximated using the empirical parameters λ_1 and λ_2 were tested. The six ice jam release events that were suitable for modeling were discussed in detail in section 2.5 and can be found summarized in Table 2.24. In the *RiverID* model, only one jam can be created per run and the toe of the ice jam must also be located at a node. Also, for the Hay River model application, ice jams could only be created in lengths of 1 km increments, since that was the model discretization in the areas where ice jams formed. This could be increased for more detailed analysis, but was not found to be a major constraint for the purposes of this study.

The *RiverID* input parameters used to approximate the initial ice jam profile for all ice jam release events were as follows: head thickness = 0.5m, ice roughness height, $k_i = 2.00$, jam strength parameter, $\mu = 1.2$, passive pressure coefficient, $K_x = 10.0$, erosion velocity, $V_{max} = 1.2$ m/s, jam porosity, $e = 0.4$; with the exception of the gorge jams (associated with ice jam release events 4 and 6) which were modeled with the erosion velocity, V_{max} , increased to 1.7 m/s. The results of the modeled ice jam release events will be discussed in this section.

3.5.1 *River1D* Modeling of Ice Jam Release Events

Recall that the release of Ice Jam Release Event 3 was observed during an observation flight, as discussed in section 2.5.3, and more ice run data is available for this event than the others, which makes it an ideal event for which to test *River1D*'s ice transport capabilities. During the modeling of the event, the λ_1 and λ_2 parameters were varied as follows: $\lambda_1 = 0, \lambda_2 = 0$; $\lambda_1 = 0, \lambda_2 = 100$; $\lambda_1 = 3, \lambda_2 = 0$; $\lambda_1 = 3, \lambda_2 = 100$. The simulated ice runs were plotted against the ice run observed during the flight, and Figure 3.5 illustrates the effects of the λ_1 and λ_2 parameters on the simulated ice runs.

As shown in Figure 3.5, the model results agree best when the bank friction parameter is set to zero. From this, it appears that the diffusion parameter has a minimal effect on the propagation speed of the ice run; the model appears more sensitive to the bank friction for this case. Overall, the model reproduced the observed behaviour remarkably well for this case, although it is noted that the ice run was only simulated over a short distance. Since the simulated ice run matched the observed ice run best when using zero for both λ_1 and λ_2 , these parameters were set to zero and the model was tested against all ice jam release event observations at the gauged stations. The modeling results are shown below in Table 3.2, and the predicted stage hydrographs are shown plotted against the observed hydrographs for Ice Jam Release Events 1 through 6 in Figures 3.6 through 3.11, respectively.

Table 3.2, Comparison of River1D simulations to observed wave/ice run features of documented ice jam release events.

Event	Observation of Wave/Ice Feature	Modeled Wave Feature			Modeled Ice Run	
		Front	Peak	Height	Front	Back
1	EMO-AF	+ 00:28	- 00:02	15%	--	--
	EMO-PG	- 00:26	- 00:42	-32%	--	--
2	EMO-AF	- 01:31	- 06:28	64%	+ 02:47	+ 06:49
	EMO-PG	- 00:50	- 05:40	19%	+ 03:11	+ 08:39
3	EMO-AF	- 00:39	- 00:44	-27%	+ 02:27	--
4	EMO-PG	- 00:15	- 00:22	-8%	--	--
5	EMO-AF	- 01:43	- 06:18	31%	- 00:27	+ 01:33
	EMO-PG	- 01:25	- 07:34	31%	+ 00:30	+ 02:54
	WSC-HR	--	--	--	+ 01:18	--
	EMO-PPB	--	--	--	+ 01:20	--
6	EMO-PG	- 00:12	- 01:24	-44%	+ 00:21	+ 07:09
	WSC-HR	+ 00:50	--	--	+ 01:38	+ 02:01
	EMO-PPB	- 00:02	--	--	+ 01:54	+ 02:12

Note: '-' indicates that the modeled event arrived earlier than the observed event
 '+' indicates that the modeled event arrived later than the observed event

Table 3.2 shows that most of the simulated ice runs were found to be slower than the observed ice runs (ranging from 00:30 to 03:11). Although the simulation of the initial propagation of ice jam release event 3 (as documented from the observation flight) seemed reasonable, the modeled ice run was found to be 2.5 hours behind the documented ice arrival at the EMO-AF. This suggests that the assumption that the ice travels at the mean flow velocity is incorrect.

As discussed, the *River1D* model assumes that the ice mass is transported at the surface velocity of the water. The modeled results are inconsistent with the field observations which show that, as discussed in section 2.4, the majority of ice runs arrived before the peak of its associated wave, and suggests that the ice mass propagates at a speed greater than the surface velocity of the

water. It is clear that a more physically based formulation which includes ice hydraulics is needed for more accurate predictions.

The modeled wave results were variable for the different events, as seen in Table 3.2. The simulated released waves were generally shown to propagate faster than the observed waves, and increasing the bank resistance parameter, λ_b , was not found to increase the accuracy of the simulated waves. Also seen in Table 3.2, the front of the simulated waves were generally closer to the observed front of wave (time difference ranged from +00:28 to -01:43), than the simulated wave peak was to the observed wave peak (time difference ranged from -00:02 to -07:34). It is noted that the differences between the simulated and observed arrival times could be due to the difficulty in ascertaining a release time for many of the events. Of all the events, only the releases of Ice Jam Release Event 3 and 6 were directly observed, and all other release times were estimated.

Table 3.2 and Figures 3.6 through 3.11 also show that modeled stage changes was highly variable, and were not found to be consistently higher or lower than the observed stage change. Also, the shape of the observed hydrographs could not be accurately reproduced using the *RiverID* model. The inability of the model to reproduce the observed hydrographs could be due to many factors, such as the approximated geometry used or the assumption that the ice jam released simultaneously along its length, or due to the lack of ice hydraulics in the model formulation.

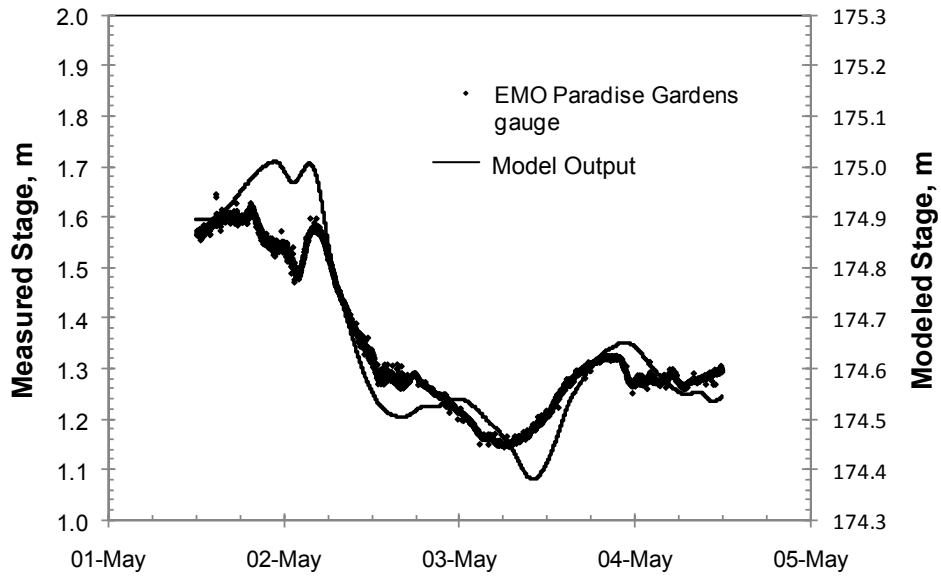


Figure 3.1, *River1D* validation using estimated 2004 open water periods, $k = 0.2$ m.

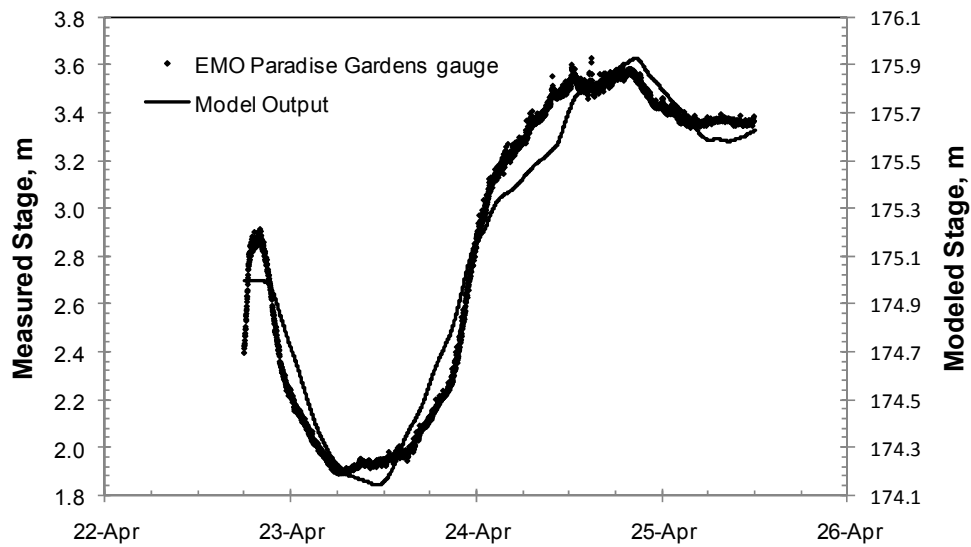


Figure 3.2, *River1D* validation using estimated 2005 open water periods, $k = 0.2$ m.

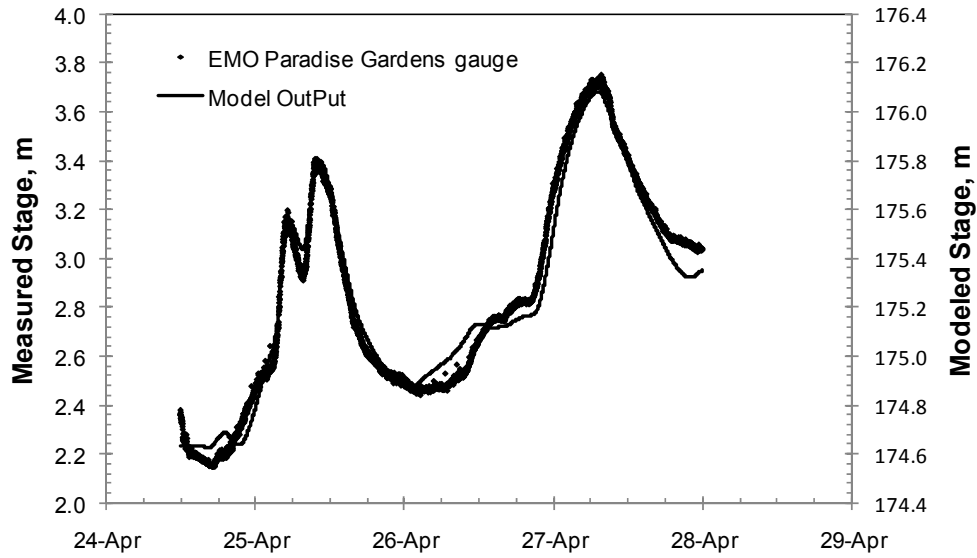


Figure 3.3, *River1D* validation using estimated 2006 open water periods, $k = 0.2$ m.

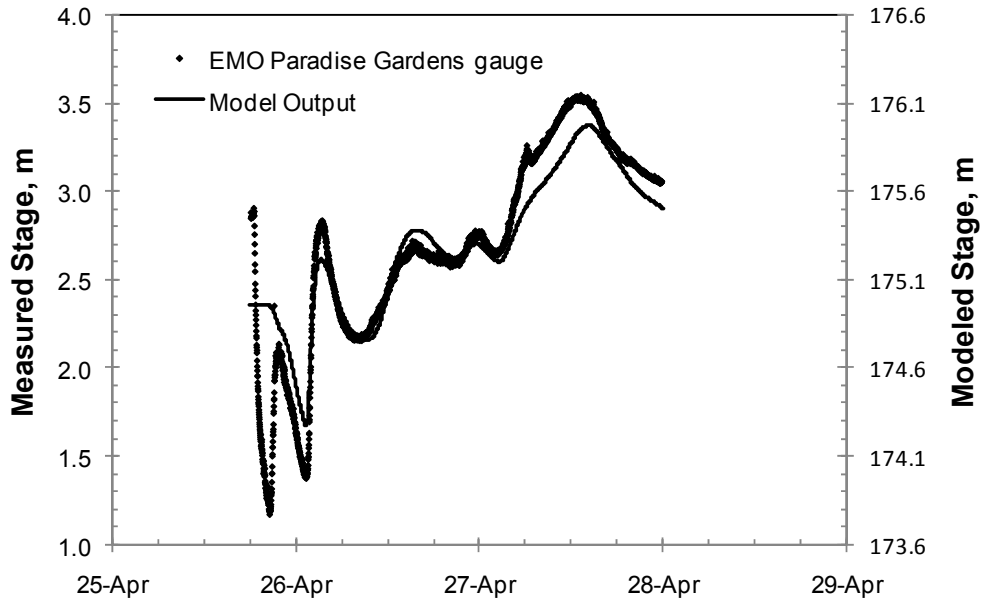


Figure 3.4, *River1D* validation using estimated 2007 open water periods, $k = 0.2$ m.

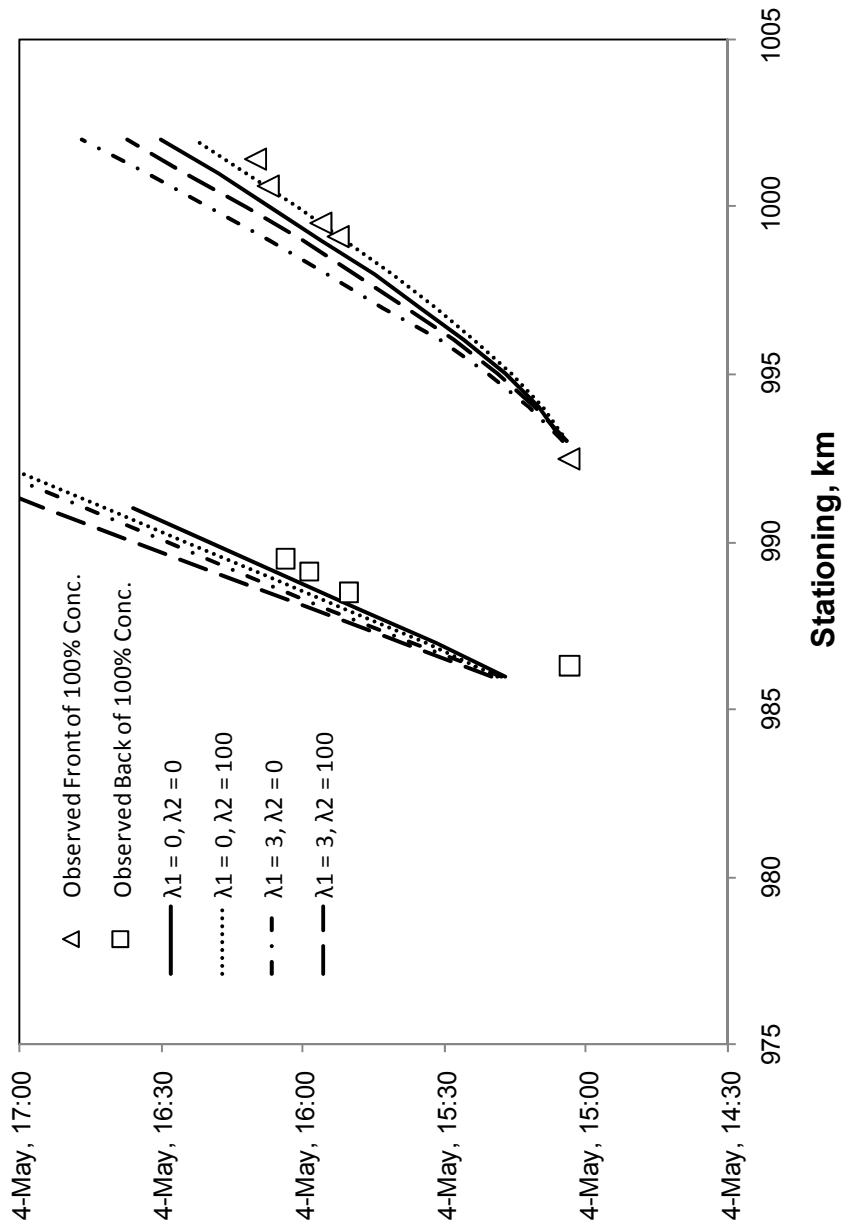


Figure 3.5, Observed and simulated *River/D* ice runs from Ice Jam Release Event 3, with varying parameters of λ_1 and λ_2 .

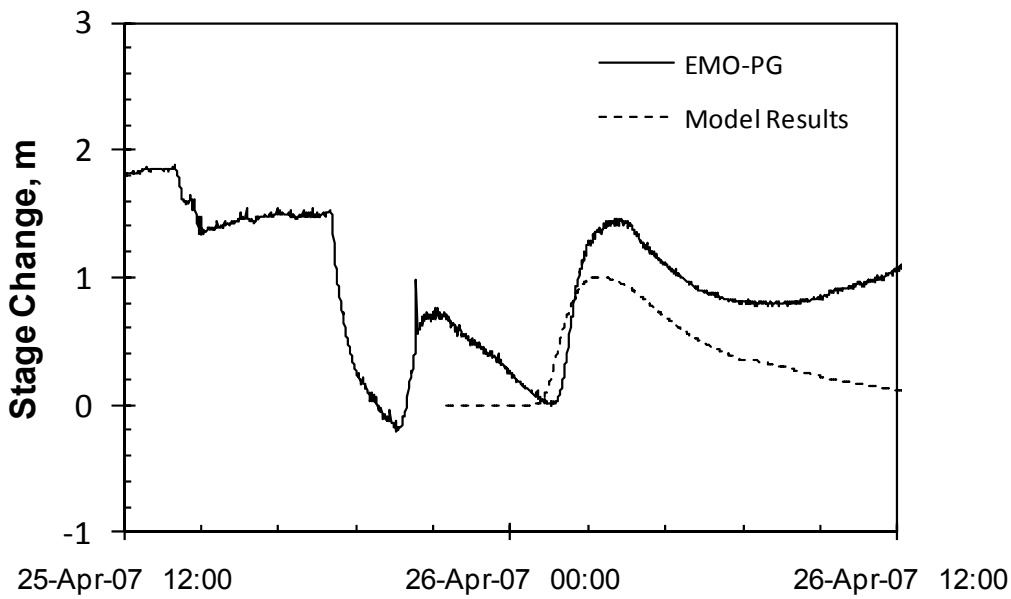
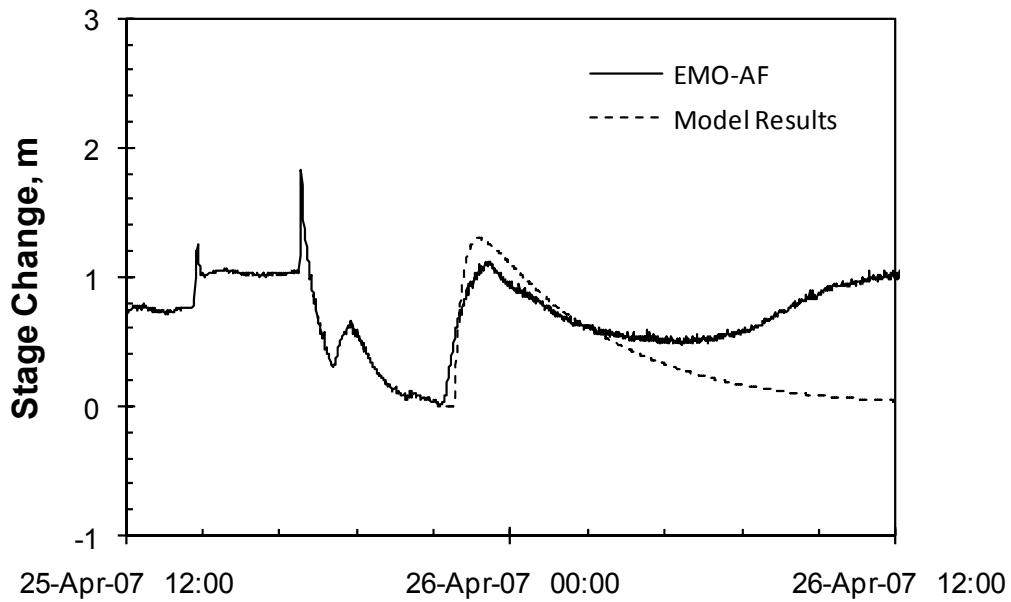


Figure 3.6, *River1D* simulation of released wave 'B' from Ice Jam Release Event 1.

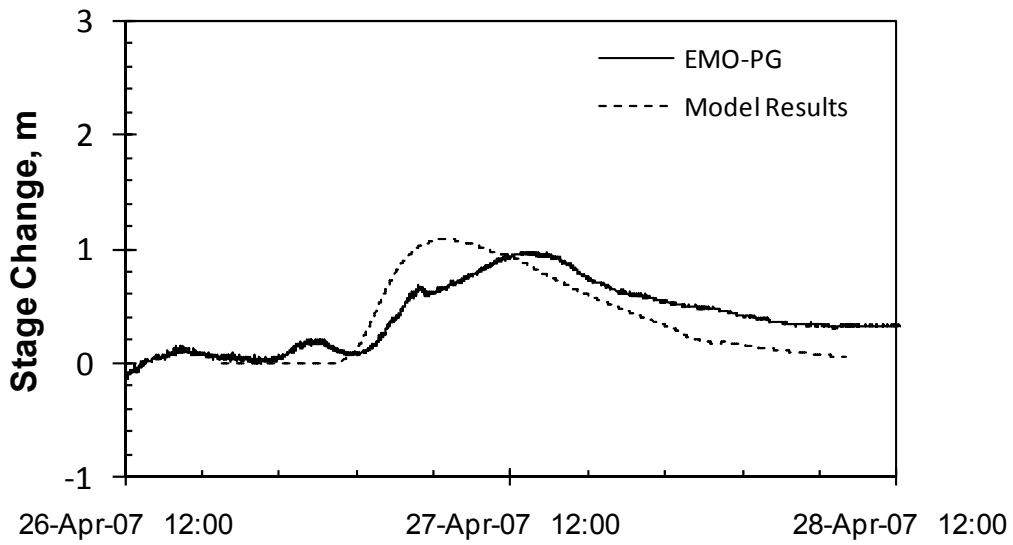
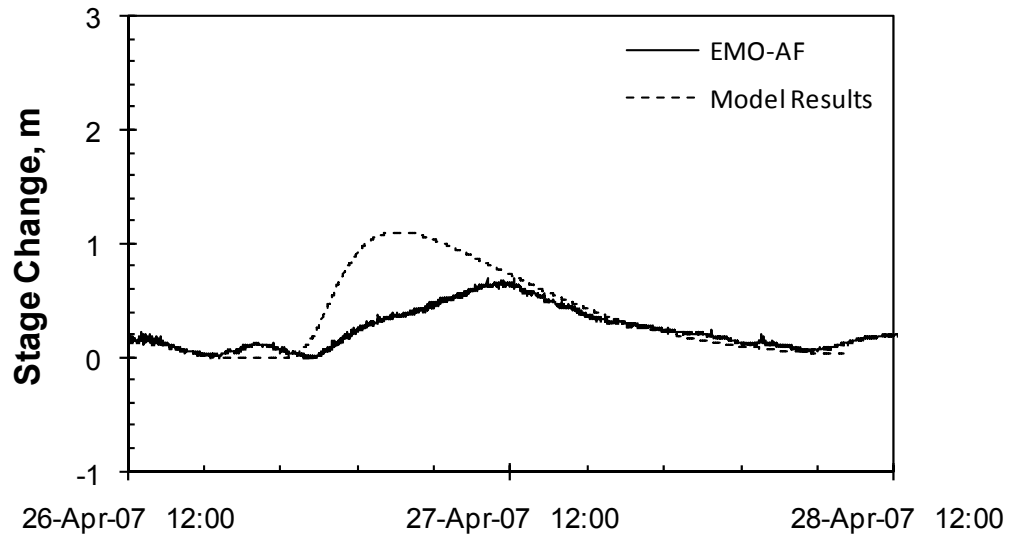


Figure 3.7, *RiverID* simulation of released wave 'E' from Ice Jam Release Event 2.

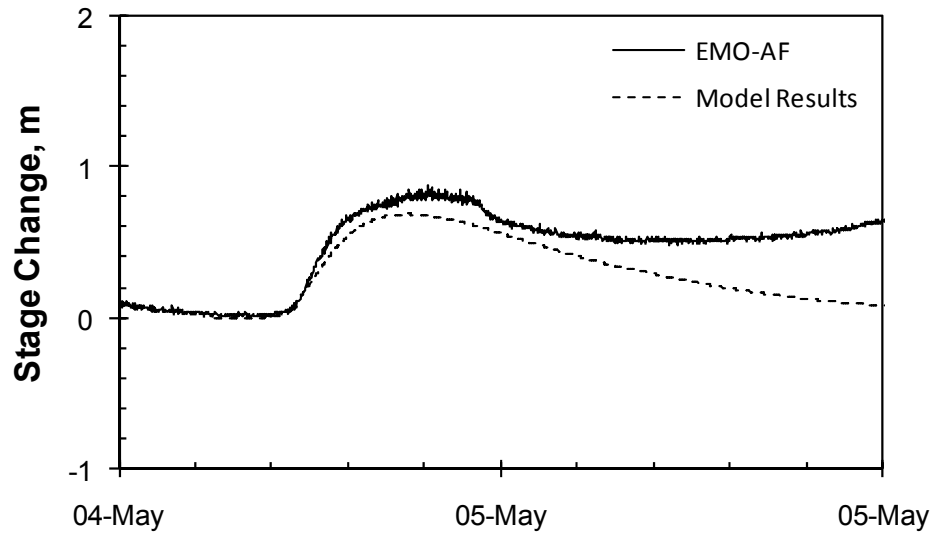


Figure 3.8, *River1D* simulation of released wave 'D' from Ice Jam Release Event 3.

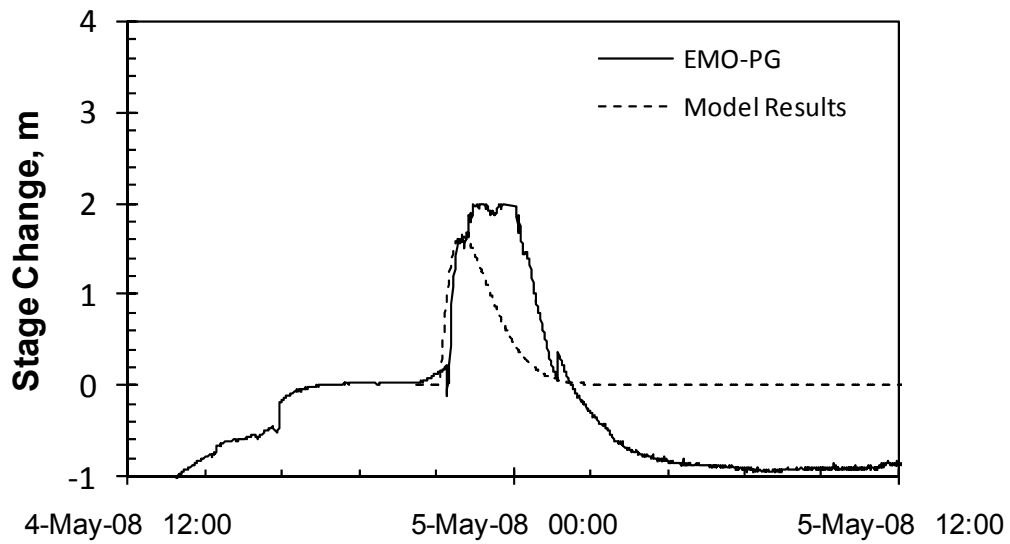


Figure 3.9, *River1D* simulation of released wave 'E' from Ice Jam Release Event 4.

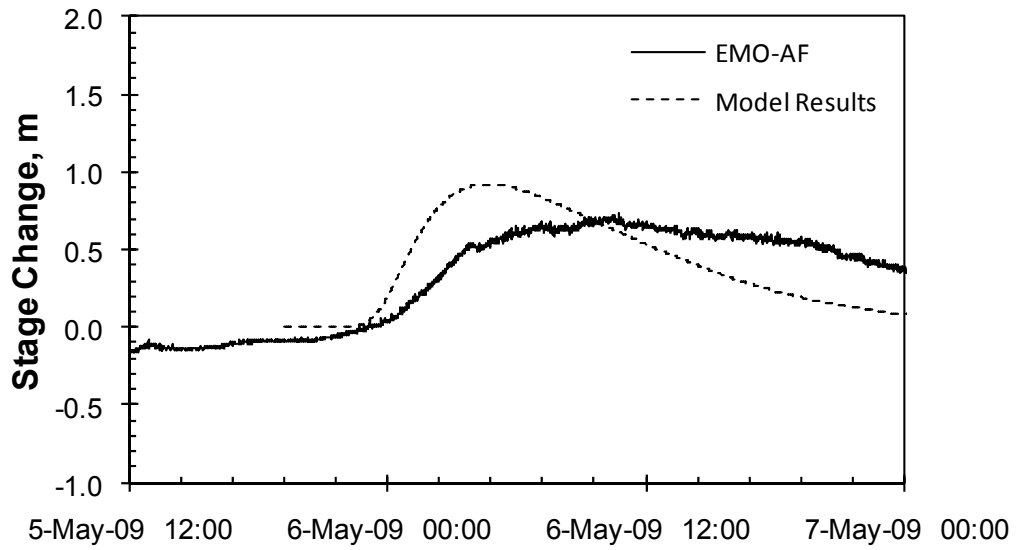


Figure 3.10, *RiverID* simulation of released wave 'G' from Ice Jam Release Event 5.

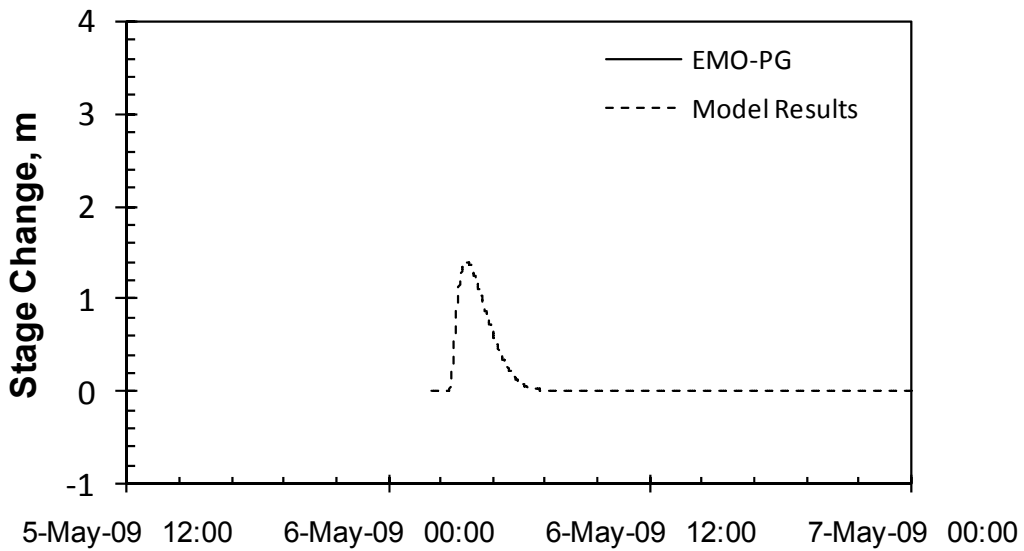


Figure 3.11, *RiverID* simulation of released wave 'H' from Ice Jam Release Event 6.

4.0 Summary

The Town of Hay River, situated at the Hay River delta on the south shore of Great Slave Lake, experiences annual risks to lives and property, due to flooding associated with breakup ice jams and ice jam release events. In particular, ice jam release events from upstream bring waves of ice and water to the town, which then jams against the ice in Great Slave Lake, often flooding the community. The town would benefit from the development of flood forecasting tools for such events; however, the small number of documented ice jam release events coupled with the absence of adequate ice transport data has limited researchers in the development of such forecasting tools. The situation at the Hay River provided an opportunity to study and document ice jam release events in sufficient detail so that a current ice jam release model (*RiverID*) could be tested as a forecasting tool.

Breakup monitoring was conducted on the Hay River during 2007, 2008 and 2009 to identify all possible features of ice jam release events, including observations of: the initial ice jam; the released water wave; and the released ice mass. Water waves were captured using multiple gauge stations on the Hay River and ice runs were observed using aerial reconnaissance flights and time-lapse camera stations setup at selected gauged stations along the reach. Analysing the data (which included ~80,000 photos) resulted in detailed information regarding the nature of ice jam release events along the Hay River.

Six ice jam release events were able to be identified during the three years of study. The documentation of these ice jam release events includes data on the propagation of the released ice mass, which has not previously been achieved with this level of detail .

Based on the observations of ice jam release events on the Hay River downstream of the NWT/AB border, it was found that ice jam release events often originate from the reach between Grumbler Rapids and the Alexandra Falls EMO gauge site (located about 2 km upstream of the falls). It was found that the height of the resulting water waves often did not attenuate, and sometimes even increased in magnitude between Alexandra Falls and Paradise Gardens. This means that it is highly likely that the associated ice runs were impeded in their travel through the river gorge between these two sites, enabling head to rebuild. Typical speeds of these waves were between 4 to 7 m/s. It was also observed that the ice runs associated with these ice jam release events travelled slower than the water wave front speeds, but the front of these ice runs always arrived before the peak of the water wave. Typical speeds of the ice runs were about 3 to 5 m/s, although the back of one ice run was documented moving at 7.4 m/s.

Sufficient details were captured for the six documented ice jam release events to enable the testing of the University of Alberta's *RiverID* hydrodynamic ice jam release model. It was particularly interesting to evaluate the model's performance in predicting the speed of the ice runs associated with ice jam release events, since these have not been previously documented in sufficient detail at any site to enable such testing. For all six ice jam release events simulated with *RiverID* it was found that the model did a reasonable job of predicting the time of arrival of the water wave – especially the fronts. However, it was found that the model's empirical parameters for accounting for the ice effects on the propagation water wave worked best when set to zero. That is, it does not seem that the ice had a significant effect in reducing the speed of the water wave, which perhaps is reasonable given the steep nature of the river in the reaches between observation points. It was definitely found that the modelled wave speeds were slower than the observed. That is, the model's assumption that the ice moves at the mean flow velocity

is wrong. The ice moves at a speed somewhere between the mean flow velocity and the water wave speed.

It is recommended that additional observations be conducted to observe the propagation of ice and water waves upstream of Alexandra Falls – this means that additional stations sensors would be needed. At present, the sparse network of cameras and water level stations along the river are too widely spaced to provide sufficient detail describing what happens to an ice jam release event sufficiently. It would be nice to do this between Alexandra Falls and Paradise Gardens, but this is not possible due to the inaccessibility of the river in the gorge at these times. In terms of the modelling, it is suggested that a new ‘model’ is needed to predict the ice run velocity for these types of events. However, additional data will be needed before that can be done.

5.0 References

- Ashton, G., 1986. River and lake ice engineering. Water Resources Publications, Littleton, Colorado, 485 p.
- Beltaos, S., 1983. Guidelines for extraction of ice-breakup data from hydrometric station records. National Research Council of Canada, Working Group on River Ice Jams.
- Beltaos, S., Burrell, B. and Ismail, S., 1994. Ice and sedimentation processes in the Saint John River, Canada. Proceedings of the IAHR Ice Symposium, 1994, p 11-21, Trondheim, Norway.
- Beltaos, S. and Burrell, B., 2005. Field measurements of ice-jam-release surges. Canadian Journal of Civil Engineering, 32(4), 699-711.
- Beltaos, S. and Burrell, B., 2005. Determining ice-jam surge characteristics from measured wave forms. Canadian Journal of Civil Engineering, 32(4), 687-698.
- Beltaos, S., and Krishnappan, B.G., 1982. Surges from ice jam releases: a case study. Can. J. Civil Eng. 9: 276–284.
- Blackburn, J. and Hicks, F., 2002. Suitability of Dynamic Modelling for Flood Forecasting During Ice Jam Release Surge Events. American Society of Civil Engineering: Journal of Cold Regions Engineering, 17(1): 18-36.
- Chow, (1959) V.T. Open Channel Hydraulics, McGraw Hill Book Co., New York, 680 p.
- Doyle, P.F. and Andres, D.D., 1979. 1979 Spring Breakup and Ice Jamming on the Athabasca River Near Fort McMurray. Internal Report SWE-70 05, Transportation and Surface Water Engineering Division, Alberta Research Council, Edmonton, Canada.

- Flato, G., and Gerard, R., 1986. Calculation of ice jam thickness profiles. Proc., 4th Workshop on Hydr. of River Ice, Subcommittee of Hydraulics of Ice Covered Rivers, National Research Council of Canada, Montreal.
- Gerard, R., Hicks, F., and Jasek, M., 1990b. Ice Jams and Flood Forecasting, Hay River, NWT – Phase 2 – ice jams and flood forecasting. Water Resources Engineering Report No. 90-4, Department of Civil Engineering, University of Alberta, Edmonton, Alta.
- Gerard, R. and Stanley, S. 1988. Documentation of Ice Regime of Hay River at Hay River NWT: Winter 1987-88. Report prepared for Indian and Northern Affairs Canada and Environment Canada, Edmonton, Alta.
- Healy, D. and Hicks, F., 1999. A Comparison of the ICEJAM and RIVJAM Ice Jam Profile Models, American Society of Civil Engineering: Journal of Cold Regions Engineering, 13(4): 180-198.
- Henderson, F., and Gerard, R., 1981. Flood Waves Caused by Ice Jam Formation and Failure. Proceedings of the 6th IAHR Symposium on Ice, Quebec City, Quebec, Volume 1, 277-287.
- Hicks, F., McKay, K., and Shabayek, S., 1997. Modelling an ice jam release surge on the Saint John River, New Brunswick. Proc. 9th CGU-HS CRIPE Workshop on River Ice, p 303-314. Fredericton, NB.
- Hicks, F., and Steffler, P., 1990. Finite element modeling of open channel flow. Water Resources Engineering Report No. 90-6. Department of Civil Engineering, University of Alberta, Edmonton, Alta.
- Hicks, F., and Steffler, P., 1992. A Characteristic-Dissipative-Galerkin Scheme for Open Channel Flow. ASCE Journal of Hydraulic Eng., 118(2): 337-352.
- Hicks, F., Steffler, P., Gerards, R., 1992. Finite element modelling of surge propagation and an application to the Hay River, N.W.T. Canadian Journal of Civil Engineering, 19, 454-462. Department of Civil Engineering, University of Alberta, Edmonton, Alta.
- Kowalczyk T. and Hicks, F., 2003. Observations of Dynamic Ice Jam Release on the Athabasca River at Fort McMurray, Alberta. Proc. 12th CGU-HS CRIPE Workshop on River Ice, Edmonton, Alta.

- Kowalczyk Hutchison, T. and Hicks, F., 2007. Observation of ice jam release waves on the Athabasca River near Fort McMurray, Alberta. *Canadian Journal of Civil Engineering*, 34 (4) 473-484.
- Krishnappan, B.G. and Snider, N., 1977. Mathematical modeling of sediment laden flows in natural streams. Scientific series No. 81, Inland Water Directorate, Canada Centre for Inland Waters, Burlington, Ontario, Canada.
- Liu, L.W. and Shen, H.T., 2004. Dynamics of ice jam release surges. *Proceedings of the 17th International Symposium of Ice*, St. Petersburg, Russia.
- She, Y. and F. Hicks, 2006. Modeling Ice Jam Release Waves with Consideration for Ice Effects. *Journal of Cold Regions Science and Technology*, 45:137-147.
- Shen, H.T., Su, J., and Liu, L., 2000. SPH simulation of river ice dynamics. *Journal of Computational Physics*, 165, 752-770.